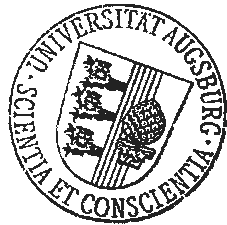

Density functional theory on a lattice

Zur Erlangung des akademischen Grades eines
Doktors der Naturwissenschaften
der Mathematisch-Naturwissenschaftlichen Fakultät
der Universität Augsburg

vorgelegte
Dissertation



von
Stefan Schenk

Augsburg, Mai 2009

Erstgutachter: Priv.-Doz. Dr. P. Schwab
Zweitgutachter: Prof. Dr. G.-L. Ingold

Tag der mündlichen Prüfung: 16. Juli 2009

Contents

1	Introduction	5
2	Spinless Fermions	9
2.1	Model	9
2.2	Ferromagnetic, antiferromagnetic and gapless phase	11
3	Static density functional theory	15
3.1	Density functional theory by Legendre transformation	15
3.2	Approximations	17
3.2.1	Local density approximation	17
3.2.2	Gradient approximations	19
3.2.3	Exact-exchange method	19
3.3	Practical applications	21
3.3.1	Charge gap in the spinless fermion model	22
3.3.2	Stability of the homogeneous system	24
3.3.3	Static susceptibility	27
3.3.4	Scattering from a single impurity	29
4	Time-dependent density functional theory	37
4.1	Time-dependent density functional theory by Legendre transformation	37
4.1.1	The Keldysh time-evolution	37
4.1.2	Action functional	39
4.1.3	Gauge invariance	40
4.1.4	Dynamical susceptibility and causality	41
4.2	Approximations	43
4.3	Dynamic Susceptibility	44
5	Transport through a quantum dot	49
5.1	Model	49
5.2	Effective potentials from exact diagonalization	51
5.3	Linear conductance	54
5.4	Results	57
5.4.1	General features	57
5.4.2	Local density approximation	58
5.4.3	Exact exchange approximation	61
5.4.4	Exchange-correlation potentials from exact diagonalization	62

6	Resumé	65
A	Some details of the spinless fermion model	69
A.1	Jordan-Wigner-Transformation	69
A.2	Bethe ansatz for spinless fermions	69
B	Hohenberg-Kohn theorem	73
C	Legendre transformations within DFT	75
C.1	Definition	75
C.2	Existence within the DFT context	75
C.3	V-representability	76
D	Properties of the dynamical susceptibility	77
E	Transparent boundaries	79
F	Potentials from exact diagonalizations for bulk systems	81
F.1	Applicability of the exact diagonalization procedure to bulk systems . . .	81
F.2	Constructing nonlocal potentials from the exact susceptibility	85

1 Introduction

Density functional theory (DFT) was formulated more than 40 years ago by Pierre Hohenberg, Walter Kohn and Lu Jeu Sham [1, 2]. Since then it has been continuously developed and extended and is now one of the most commonly used tools for the study of electronic structure in condensed matter physics and quantum chemistry. Its basic idea is to express the ground state energy in terms of the particle density and thereby providing a mapping between an interacting many-body system and a noninteracting single-particle Hamiltonian. Already in the first years DFT has been used not only for calculations of electron densities but also of spin densities [2, 3]. Other important extensions are the inclusion of vector potentials [3, 4, 5, 6] and time-dependent potentials [7, 8, 9, 10]. The former allows for calculations with magnetic fields and expresses the ground state energy as a functional of the density and the current-density, while the latter leads to time-dependent densities. Both extensions are needed for a fully gauge invariant formulation of density functional theory. Furthermore – while the static formulation allows only for ground state properties, e. g. the ground state energy – time-dependent density functional theory (TDDFT) gives also access to excitation energies via the singularities of the linear response function [11].

Contrary to these successes, one crucial ingredient for practical applications of density functional theory, the so-called exchange-correlation energy, is not known exactly. Often the interaction is split into two parts, the Hartree energy, which is easy to incorporate into the formalism, and the exchange-correlation energy. Unfortunately the construction of the theory makes approximations for this latter part quite intransparent. Identifying a well defined (explicit) expansion parameter, e. g. the interaction strength, and expanding up to a certain order in this parameter, is not that straightforward and obvious for DFT. Although known in principle for quite a long time [12, 13] this method has not been applied to DFT until the 90-ties [14, 15]. Especially the first order expansion in the interaction – the so-called exact-exchange method (EXX) – has received much attention since then and seems to give better results than older approximations [16], like the local density approximation (LDA) [1, 2] or the generalized gradient approximation (GGA) [17]. These are not derived from perturbation theory in the interaction strength but are constructed around the (nearly) homogeneous system, such that the homogeneous system is exact. In this case the exchange-correlation energy can be determined for example from Monte-Carlo simulations of the homogeneous system. Slow variations of the density can be taken into account by the use of density gradients. Although these approximations may be fully replaced by the exact-exchange method and higher order expansions at some point in the future, they are still heavily used, since the latter significantly increase the computational complexity.

Despite these problems with the exchange-correlation energy, density functional the-

ory became an important tool for the theoretical investigation of materials. On the other hand practical applications of DFT have further deficiencies even beyond the approximations for the exchange-correlation energy. For example, the Fermi surface and excitation energies are often extracted from the Kohn-Sham levels of static DFT – although it is not guaranteed that these quantities coincide with the real Fermi surface and excitations of the interacting system [18, 19]. In principle the band gap can be obtained from such a calculation [20], but it is often underestimated within the local density approximation. It was found that the discontinuities of the exact exchange-correlation potential, almost always not captured within LDA, contribute significantly to the gap [21, 22].

Do discrepancies between theory and experiment arise from insufficient exchange-correlation potentials or from the misuse of density functional theory? It is a promising approach to investigate such problems by means of simple lattice models [23, 24]. DFT results for one-dimensional lattices have been compared to exact diagonalizations of not too small systems [25, 26], quantum Monte Carlo simulations [27] and results from density matrix renormalization group (DMRG) calculations [28]. On the other hand one has to be careful when concluding from the quality of, for example, the local density approximation in one dimension to its performance in higher dimensions. The difference is that in the former case there is no Fermi surface but only two distinct Fermi points. Thus the description as a Fermi liquid is no longer valid and has to be replaced by the notion of a Luttinger liquid [29, 30, 31].

In this work we will study one-dimensional systems. Our main motivation for using such a model is the wealth of known properties to compare with. In addition, since a few years much work has been done to realize such systems in the laboratory. For example, nowadays it is possible to use single-wall carbon nanotubes [32, 33], ultra-cold atomic gases in optical lattices [34, 35, 36] or the edge states of a fractional quantum Hall fluid [37] to investigate a Luttinger liquid experimentally. These carbon nanotubes or other (almost) one-dimensional systems, like for example Indium phosphide nanowires, have some interesting applications as functional electronic devices on a molecular scale [38, 39]. Another approach uses organic molecules for building such a device [40]. In the experimental setup this organic molecule is usually contacted by two gold electrodes and the current voltage characteristics are measured [41, 42, 43, 44]. There are two distinct ways of modeling such systems theoretically: On one hand one can use simple phenomenological models [45], where additional effects, like e.g. driving with a laser field [46, 47] or some disorder [48], are comparably easy to incorporate. On the other hand one may use a realistic model of the experimental setup to calculate the transport properties [49, 50]. However, early experimental results and density functional calculations for such systems differed by several orders of magnitude. There has been much work done to understand and overcome the problems on the theoretical [51, 52, 53, 54] and the experimental side [55], and nowadays the difference is often less than an order of magnitude [55].

Despite these successes there are still open questions left. For example, there are still a few cases where density functional theory and experiment disagree. More important from a conceptual point of view is the question whether the use of exchange-correlation potentials which are calculated from equilibrium quantities is justified for such a non-equilibrium situation. Even in the linear response regime the behavior of DFT is not fully

understood. For example, it was found by comparing a DFT calculation on the basis of the exact exchange-correlation potential with results from DMRG [56] that it often is sufficient to use a naive approach for calculating the linear conductance, which neglects the so-called exchange-correlation kernel. Furthermore, as the previously mentioned (almost) one-dimensional systems are nowadays of great interest, it is necessary for the discussion of the results from density functional theory to understand the peculiarities of the approximations within this context.

In this thesis we investigate the successes and failures of the local density approximation and the exact-exchange approximation by comparison with exact results for transport properties, like the transmission through an impurity or the conductance through a small interacting system. In a further step we develop a scheme for calculating the exchange-correlation potential from exact diagonalizations of small systems, a procedure which is also feasible for strong interactions. In order to do so we use a one-dimensional model of spinless fermions with nearest-neighbor interaction. For this model the Bethe ansatz [57] is an efficient tool for determining the ground state energy or the Drude weight of the homogeneous system, thus providing the ingredients for the local density approximation. At half filling even some analytical results for the infinitely long system are known from bosonization [58]. Small systems – up to about 25 lattice sites – can be exactly diagonalized without any problem, and for larger systems one can also use the density matrix renormalization group formalism [59, 60] to obtain accurate results.

This work is organized as follows: In the next chapter we introduce the model of spinless fermions and we also recapitulate some known results. In the third chapter we introduce the static (current-) density functional theory. Usually this is done by proving the Hohenberg-Kohn theorem and then by a variation procedure to find the Kohn-Sham Hamiltonian. However we use an alternative approach which uses Legendre transformations to establish a mapping between the many-body and the single-particle Hamiltonian [61]. The advantage of this formulation is that it is easily extendable to other systems, like systems with a finite current or a time-dependent potential [62]. After introducing DFT and some of its approximations we reexamine some of the results by Schönhammer and Gunnarson [22, 23, 24] and add our own observations. The fourth chapter introduces the time-dependent DFT. To identify the successes and limits of the local density approximation we focus here on the dynamical susceptibility. In the fifth chapter we use a one-dimensional system consisting of noninteracting leads and a small interacting region to analyze DFT. We are especially interested in the results for the linear conductance through the interacting region. After showing the poor performance of LDA for this problem we use an exact diagonalization procedure to obtain improved exchange-correlation potentials, leading to a conductance which is close to the exact one. Finally in the last chapter we summarize our findings and propose some ideas for continuing these investigations.

2 Spinless Fermions

2.1 Model

We consider a tight-binding model of spinless fermions with nearest-neighbor interaction and periodic boundary conditions. In this work we restrict ourselves to one-dimensional models. For formal aspects such as the Hamiltonian or the formulation of (current-) density functional theory this is just for the sake of simplicity of notation. On the other hand we know numerous properties of this one-dimensional model, which we can use for the local density approximation or for comparison with results from density functional theory. The Hamiltonian can be written as

$$\hat{H} = \hat{T} + \hat{V} + \sum_l v_l \hat{n}_l \quad (2.1)$$

where

$$\hat{T} = -t \sum_l \left(e^{i\phi_l} \hat{c}_l^+ \hat{c}_{l+1} + e^{-i\phi_l} \hat{c}_{l+1}^+ \hat{c}_l \right) \quad (2.2)$$

is the kinetic energy ($\hbar = 1$) and

$$\hat{V} = V \sum_l \left(\hat{n}_l - \frac{1}{2} \right) \left(\hat{n}_{l+1} - \frac{1}{2} \right). \quad (2.3)$$

is the interaction. The local on-site potential is denoted by v_l and ϕ_l is a local phase which can be associated with a magnetic field. The hat denotes operator-valued quantities. \hat{c}_l^+ is a creation operator and \hat{c}_l annihilates a particle at site l and $\hat{n}_l = \hat{c}_l^+ \hat{c}_l$ is the occupation number operator. The system size is denoted by L and N stands for the number of particles on the lattice. The lattice constant is equal to one.

One immediately sees that

$$\hat{n}_l = \frac{\partial \hat{H}}{\partial v_l}. \quad (2.4)$$

Analogous we find the current operator

$$\hat{j}_l = \frac{\partial \hat{H}}{\partial \phi_l}, \quad (2.5)$$

where

$$\hat{j}_l = -it \left(e^{i\phi_l} \hat{c}_l^+ \hat{c}_{l+1} - e^{-i\phi_l} \hat{c}_{l+1}^+ \hat{c}_l \right) \quad (2.6)$$

is the local current between sites l and $l + 1$. An important relation that connects the densities and currents is the continuity equation. It can be found easily in the Heisenberg picture as

$$\frac{d}{dt} \hat{n}_l = i [\hat{H}, \hat{n}_l] = -(\hat{j}_l - \hat{j}_{l-1}). \quad (2.7)$$

This implies that, for time-independent systems, the current is constant throughout the whole ring. The currents $\langle \hat{j}_l \rangle$ and densities $\langle \hat{n}_l \rangle$ are observables and thus invariant under gauge transformations, which are described by the unitary operator

$$\hat{U} = \exp \left\{ i \sum_l \chi_l \hat{n}_l \right\}. \quad (2.8)$$

The Hamiltonian then transforms as

$$\hat{H} \longrightarrow \hat{U} \hat{H} \hat{U}^\dagger - \sum_l \dot{\chi}_l \hat{n}_l, \quad (2.9)$$

thereby implying the relations for the local phases and potentials:

$$\begin{aligned} \phi_l &\rightarrow \phi_l + \chi_l - \chi_{l+1} \\ v_l &\rightarrow v_l - \dot{\chi}_l. \end{aligned} \quad (2.10)$$

Invariants are then

$$e_l = \dot{\phi}_l - (v_{l+1} - v_l), \quad (2.11)$$

corresponding to the electric field in electrodynamics, and the total phase

$$\Phi = \sum_l \phi_l, \quad (2.12)$$

corresponding to the magnetic flux. Note that for a system of charged particles on a ring in a perpendicular magnetic field, Φ equals 2π times the magnetic flux in units of the flux quantum [63]. So for our system the local phase can be almost gauged away with only a remaining phase $\Phi = \sum_l \phi_l$ modulo 2π at the boundary.

The solution of the homogeneous system ($v_l = 0$) has been found by C. N. Yang and C. P. Yang using the Bethe ansatz technique [57, 64, 65]. In this series of papers they consider the Heisenberg XXZ model

$$\hat{H}^{\text{XXZ}} = -J \sum_l \left(\hat{\sigma}_x^{(l)} \hat{\sigma}_x^{(l+1)} + \hat{\sigma}_y^{(l)} \hat{\sigma}_y^{(l+1)} + \Delta \hat{\sigma}_z^{(l)} \hat{\sigma}_z^{(l+1)} \right). \quad (2.13)$$

which is equivalent to our model of spinless fermions with $J = \frac{t}{2}$ and $\Delta = -\frac{V}{2t}$. The relation between these two models can be seen by means of the Jordan-Wigner transformation [66]. Some of the details are shown in Appendix A.1. In a later chapter we employ the solution of the homogeneous system to obtain the exchange-correlation energies and potentials within the local density approximation. A short introduction to the Bethe ansatz is presented in Appendix A.2.

XXZ-model:	$\Delta > 1$	$-1 < \Delta < 1$	$\Delta < -1$
spinless fermions:	$V < -2t$	$-2t < V < 2t$	$V > 2t$
zero magnetization: (half filling)	ferromagnetic	gapless phase	antiferromagnetic
finite magnetization: (other fillings)	ferromagnetic	gapless phase	gapless phase

Figure 2.1: Short summary on the different phases of the Heisenberg XXZ model with anisotropy Δ and the corresponding spinless fermion model with interaction V .

2.2 Ferromagnetic, antiferromagnetic and gapless phase

So far we have only considered some general properties of the Hamiltonian (2.1). Now we turn our attention to the ground state of this model. By doing so we switch back and forth between the Heisenberg XXZ model and the spinless fermions, depending on which model gives a more intuitive explanation. An overview on the XXZ model is for example given by Hans-Jürgen Mikeska and Alexei K. Kolezhuk [67]. In general, one-dimensional systems are quite distinct from higher dimensional models [31, 29, 30]. In the following we will recapitulate some of the results for our model:

The Heisenberg XXZ model exhibits three phases – ferromagnetic, antiferromagnetic and the so-called gapless phase [68]. A short overview on these phases is given in Figure 2.1. For an anisotropy parameter $\Delta > 1$ it is in the ferromagnetic phase. Without an additional external field the ground state consists of the two degenerate states $|\uparrow\uparrow\uparrow \dots\rangle$ and $|\downarrow\downarrow\downarrow \dots\rangle$. An arbitrary small field leads to a collapse of the ground state to one of these two states and thus to a fully magnetized lattice. This phase corresponds to the spinless fermion model with attractive interaction $V < -2t$ and the states corresponding to the two ferromagnetic states above are the completely filled and the empty lattice.

The low lying excitations of the ferromagnetic Heisenberg model are magnons where the spin quantum number differs by one from the ground state values. In the language of spinless fermions these excitations would be states with one particle or hole on the lattice. Since the system is homogeneous, the kinetic energy of the excited state is determined by the plane wave dispersion $-2t \cos q$. Additionally we have to twist two interaction bonds, so that the dispersion of these low lying excitations is given by

$$\epsilon(q) = -2t \cos q - V. \quad (2.14)$$

The spectrum has a gap at $q = 0$ of magnitude $|V| - 2t$ which closes for $V \rightarrow -2t$.

The antiferromagnetic phase occurs for anisotropy $\Delta < -1$ and zero magnetization. However, since the antiferromagnetic state $\frac{1}{\sqrt{2}}(|\uparrow\downarrow\uparrow \dots\rangle + |\downarrow\uparrow\downarrow \dots\rangle)$ is an eigenstate of the Hamiltonian only in the limit $\Delta \rightarrow -\infty$, there are still quantum fluctuations present which prevents the order from being complete. In the spinless fermion model this phase appears at half filling for an interaction $V > 2t$. The excitation spectrum can be obtained in the strong interaction limit by perturbation theory [69]. It is given by

$$\epsilon(q) = \frac{V}{4} \left[1 - \frac{4t}{V} \cos(q) \cos(q + q') \right], \quad (2.15)$$

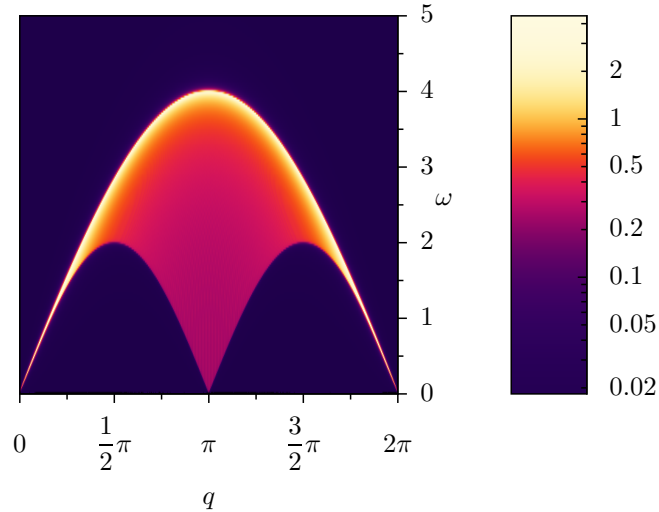


Figure 2.2: Imaginary part of the dynamical susceptibility $\text{Im}\chi(q, \omega)$ (in units of t^{-1}) at half filling and zero interaction.

where q' is an additional momentum with $-\pi < q' \leq \pi$. Technically we have here two momenta, because the excitations consists of two independently moving domain walls.

At zero magnetization for $-1 < \Delta < 1$ ($-2t < V < 2t$) and elsewhere for $\Delta < 1$ ($-2t < V$) one finds a phase with a gapless excitation spectrum. If the interaction is zero we have a simple dispersion law

$$\epsilon(k) = -2t \cos k, \quad (2.16)$$

and the ground state is just a Slater determinant of plane waves with wave-vectors smaller than the Fermi vector k_F . The excitation spectrum can be seen by means of the dynamical susceptibility as shown in Figure 2.2. There we have plotted the imaginary part of the dynamical susceptibility at half filling, giving the spectral weight of the charge excitations. The maxima and minima of the excitation continuum at interaction $V = \Delta = 0$ are easily found:

$$\Delta\epsilon_{\max} = \epsilon\left(k_F + \frac{q}{2}\right) - \epsilon\left(k_F - \frac{q}{2}\right) = 4t \sin \frac{q}{2}, \quad (2.17)$$

$$\Delta\epsilon_{\min} = \epsilon(k_F + q) - \epsilon(k_F) = 2t \sin q. \quad (2.18)$$

The long-wavelength low-frequency limit of the susceptibility is given by

$$\chi(q, \omega) = \chi_0 \frac{(v_F q)^2}{(v_F q)^2 - \omega^2}. \quad (2.19)$$

χ_0 is the static susceptibility and v_F the Fermi velocity.

In Figure 2.2 one clearly sees an unique feature of one-dimensional systems, the fact that no low-energy excitations exist apart from the points $q = 0$ and $q = 2k_F$. This can be easily understood by noting that there exists no Fermi surface in one dimension,

just two distinct points. The reduced phase space of the low lying excitations leads to a breakdown of the Fermi liquid theory for the interacting system and to a new concept, the so-called Luttinger liquid [58, 30]. One finds that the excitation spectrum from the susceptibility is qualitatively the same as in Figure 2.2. Yet there are differences, for example the Fermi velocity in (2.19) is renormalized with the interaction [70],

$$v = \frac{\pi t \sin(2\eta)}{\pi - 2\eta}, \quad (2.20)$$

where η is a parametrization of the interaction and is defined by

$$V = -2t \cos(2\eta). \quad (2.21)$$

The static susceptibility is also renormalized:

$$\chi_0 = \frac{\pi - 2\eta}{2\pi\eta \sin(2\eta)}. \quad (2.22)$$

The other relevant low energy limit is $q \rightarrow 2k_F$. In this case the susceptibility shows a power law divergence, given by [71]

$$\chi(q, \omega) \sim \frac{1}{[\omega^2 - v^2(q - 2k_F)^2]^{1 - \frac{1}{2\Theta}}}, \quad (2.23)$$

where Θ parametrizes the interaction according to $2\Theta = 1 - \frac{2}{\pi} \arcsin \Delta$.

3 Static density functional theory

In this chapter we examine density functional theory for static potentials and phases. Its basic idea is to express the ground state energy of an interacting many-body system as a functional of the densities. The existence of such a functional is provided by the Hohenberg-Kohn theorem [1], which we present in Appendix B. In a next step one uses the constrained search method [72, 73, 61] and a variational principle [2] to determine a single-particle Hamiltonian, the so-called Kohn-Sham Hamiltonian, whose eigenstates allow the calculation of the true ground state energy and density of the interacting Hamiltonian. An introduction to density functional theory can be found for example in [74, 75, 76]. However we take another point of view and present density functional theory in the context of Legendre transformations [62], which lies also at the heart of the constrained search method [61]. Besides a clear and insightful formulation of DFT, the approach using the Legendre transformation also gives a clear and precise way for extending density functional theory to more complex problems like the inclusion of vector-potentials, finite temperatures or systems, which are out of equilibrium. However, within this chapter we confine ourselves to models with static potentials v_l and vector-potentials, which only enter via the phases ϕ_l in the hopping term. After the formulation of density functional theory in the next section we introduce some approximations for an essential ingredient, the so-called exchange-correlation potential. Amongst them are the local density approximation and the exact-exchange method. Finally, in the last part of this chapter we investigate the quality of the approximations. The discussion on the local density approximation is also presented in [77].

3.1 Density functional theory by Legendre transformation

The principal idea behind current density functional theory is to establish a mapping between an interacting many-particle system \hat{H} with local potentials v_l and phases ϕ_l and a single-particle system \hat{H}^s with effective potentials v_l^s and phases ϕ_l^s . These Hamiltonian can be written as

$$\hat{H} = -t \sum_l \left(e^{i\phi_l} \hat{c}_l^\dagger \hat{c}_{l+1} + e^{-i\phi_l} \hat{c}_{l+1}^\dagger \hat{c}_l \right) + V \sum_l \hat{n}_l \hat{n}_{l+1} + \sum_l v_l \hat{n}_l \quad (3.1)$$

and

$$\hat{H}^s = -t \sum_l \left(e^{i\phi_l^s} \hat{c}_l^\dagger \hat{c}_{l+1} + e^{-i\phi_l^s} \hat{c}_{l+1}^\dagger \hat{c}_l \right) + \sum_l v_l^s \hat{n}_l. \quad (3.2)$$

The ground state energy of the Hamiltonian (3.1), $E = \langle \hat{H} \rangle$, is then a function of the potentials $\{v_l\}$ and the phases $\{\phi_l\}$. Their conjugated variables, the densities and currents

can then be found as

$$n_l = \langle \hat{n}_l \rangle = \frac{\partial E}{\partial v_l}, \quad j_l = \langle \hat{j}_l \rangle = \frac{\partial E}{\partial \phi_l}. \quad (3.3)$$

Now we introduce the Legendre transform F of the ground state energy which transforms from the potentials and phases to the new variables $\{n_l\}$ and $\{j_l\}$ according to the relation

$$F[n, j] = E - \sum_l v_l n_l - \sum_l \phi_l j_l. \quad (3.4)$$

Here n and j is a shorthand notation for the sets $\{n_l\}$ and $\{j_l\}$. The local potentials and phases can be recovered by

$$v_l = -\frac{\partial F}{\partial n_l}, \quad \phi_l = -\frac{\partial F}{\partial j_l}. \quad (3.5)$$

In order to establish the mapping between the interacting and the single-particle system, the ground state energy of the latter is transformed analogously,

$$F^s[n^s, j^s] = E^s - \sum_l v_l^s n_l^s - \sum_l \phi_l^s j_l^s. \quad (3.6)$$

Considering the single-particle system at the same densities as the interacting system, $n_l^s = n_l$ and $j_l^s = j_l$, rewriting F as $F^s + (F - F^s)$ and using the back-transformation (3.5) gives a relation between the single-particle and many-body potentials,

$$v_l^s = v_l + \frac{\partial E^{\text{HXC}}}{\partial n_l}, \quad \phi_l^s = \phi_l + \frac{\partial E^{\text{HXC}}}{\partial j_l}. \quad (3.7)$$

Here we have defined the Hartree-Exchange-Correlation energy as $E^{\text{HXC}} \equiv F - F^s$. The difference

$$v_l^s - v_l = \frac{\partial E^{\text{HXC}}}{\partial n_l} = v_l^{\text{HXC}} \quad (3.8)$$

is then the so-called Hartree-exchange-correlation potential. In the traditional formulation of DFT the mapping between the interacting and the single-particle system is provided by the Hohenberg-Kohn theorem and the so-called v -representability of the interacting density. In our context these theorems ensure the existence of the Legendre transformation and the back-transformation. The Hohenberg-Kohn theorem can be found in Appendix B and the relation between these theorems and Legendre transforms is discussed in more detail in Appendix C.

The ground state energy of the interacting system can be found by the reversed transformation, $F \rightarrow E$, which can be expressed in terms of single-particle quantities as

$$\begin{aligned} E &= F + \sum_l v_l n_l + \sum_l \phi_l j_l \\ &= F^s + (F - F^s) + \sum_l [v_l^s + (v_l - v_l^s)] n_l + \sum_l [\phi_l^s + (\phi_l - \phi_l^s)] j_l \\ &= E^s + E^{\text{HXC}} + \sum_l (v_l - v_l^s) n_l + \sum_l (\phi_l - \phi_l^s) j_l. \end{aligned} \quad (3.9)$$

E^s can be evaluated as the sum over the N lowest eigenvalues of the single-particle system

$$E^s = \sum_{j=1}^N \epsilon_j. \quad (3.10)$$

Clearly, the ground state energy is not only the sum of eigenvalues of the noninteracting Hamiltonian, but one also has to take the correction $E^{\text{HXC}} - \sum_l v_l^{\text{HXC}} n_l$ into account. As we will see later these corrections are quite important and should not be neglected. Introducing explicitly the Hartree contribution, E^{H} , through

$$E^{\text{HXC}} = E^{\text{H}} + E^{\text{XC}} \quad (3.11)$$

with $E^{\text{H}} = V \sum_l n_l n_{l+1}$, we arrive at the standard relation

$$v_l^s = v_l + v_l^{\text{H}} + v_l^{\text{XC}}. \quad (3.12)$$

The Hartree potential is apparently $v_l^{\text{H}} = V(n_{l-1} + n_{l+1})$ and the exchange-correlation potential is given by

$$v_l^{\text{XC}} = \frac{\partial E^{\text{XC}}}{\partial n_l}. \quad (3.13)$$

In addition we get for the single-particle phases

$$\phi_l^s = \phi_l + \phi_l^{\text{XC}}, \quad \phi_l^{\text{XC}} = \frac{\partial E^{\text{XC}}}{\partial j_l} \quad (3.14)$$

since the Hartree energy depends on the densities only. Please note that the single-particle potentials and phases depend, by construction, on the densities and the currents. Therefore the auxiliary system has to be determined self-consistently with respect to the densities and currents. The exchange correlation energy can be formally written as

$$E^{\text{XC}} = \langle 0 | \hat{T} + \hat{V} | 0 \rangle - \langle 0_s | \hat{T}^s | 0_s \rangle - E^{\text{H}} + \sum_l \phi_l^{\text{XC}} j_l, \quad (3.15)$$

where $|0\rangle$ and $|0_s\rangle$ are the ground state wave functions of the interacting and the single-particle system, respectively. Up to now we have been avoiding the problem of determining the exchange-correlation energy explicitly. Since this is a hard problem we have to make some approximations. Some of the possible approximations are presented in the next sections.

3.2 Approximations

3.2.1 Local density approximation

A simple approximation for the exchange-correlation energy is the so-called local density approximation (LDA). There the exchange-correlation energy is written as

$$E^{\text{XC}}[n, j] = \sum_l \epsilon^{\text{XC}}(n_l, j_l). \quad (3.16)$$

Thus the exchange-correlation potentials and phases

$$v_l^{\text{XC}} = \frac{\partial E^{\text{XC}}}{\partial n_l} = \frac{\partial \epsilon^{\text{XC}}}{\partial n_l} \quad \text{and} \quad \Phi_l^{\text{XC}} = \frac{\partial E^{\text{XC}}}{\partial j_l} = \frac{\partial \epsilon^{\text{XC}}}{\partial j_l}. \quad (3.17)$$

are functions of the local density and current-density only. This local energy ϵ^{XC} can be determined from the exact exchange-correlation energy of the static homogeneous system for given density n and current j ,

$$\epsilon^{\text{XC}} = \frac{E^{\text{XC}}}{L}, \quad (3.18)$$

where E^{XC} is calculated from the exact ground state energy according to equation (3.15). For the three-dimensional electron gas this energy is usually obtained by analytical calculations for certain limiting cases and quantum monte carlo simulations followed by a interpolation procedure [78, 79]. For our system of spinless fermions this can efficiently be done with the Bethe ansatz [57], hence we call the exact ground state energy $E^{\text{BA}}(n, j)$. A detailed presentation of the Bethe ansatz is shown in the Appendix A.2. Admittedly the Bethe ansatz solution is found as a function of n and ϕ . Thus the phase variable has to be eliminated from this expression in favor of the current, using the relation

$$j = \frac{1}{L} \frac{\partial E^{\text{BA}}(n, \phi)}{\partial \phi} \quad (3.19)$$

for the homogeneous system. The second term in (3.15), which we denote $E^0(\phi)$, is given by the single-particle result ($-\pi/L < \phi < \pi/L$)

$$E^0(\phi) = E^0 \cdot \cos \phi, \quad E^0 \simeq -\frac{2t}{\pi} L \sin(\pi n), \quad (3.20)$$

where the latter relation holds for large L . Since $\phi \sim 1/L$, we may expand for small ϕ ; in particular, the Drude weights, D^{BA} and D^0 , are defined according to the following relations ($\phi \rightarrow 0$):

$$E^{\text{BA}}(\phi) - E^{\text{BA}}(0) = D^{\text{BA}} L \phi^2 \quad (3.21)$$

$$E^0(\phi) - E^0(0) = D^0 L \phi^2 \quad (3.22)$$

Note that D^{BA} and D^0 are functions of the density, and D^{BA} depends on the interaction V . For example, $D^0 = (t/\pi) \sin(n\pi) = v_F/2\pi$, where v_F is the bare Fermi velocity, and $D^{\text{BA}} = \pi t \sin \mu / [4\mu(\pi - \mu)]$ for half filling ($n = 1/2$), where V (in the range $-2t \dots 2t$) is related to μ by $V = -2t \cos \mu$ [80].

Combining the above relations, we obtain

$$\epsilon^{\text{XC}}(n, j) = \frac{1}{L} (E^{\text{BA}}(n, 0) - E^0(n, 0)) - V n^2 + \frac{1}{2} \lambda^{\text{XC}} j^2, \quad (3.23)$$

where

$$\lambda^{\text{XC}}(n) = \frac{1}{2} \left(\frac{1}{D^0(n)} - \frac{1}{D^{\text{BA}}(n)} \right). \quad (3.24)$$

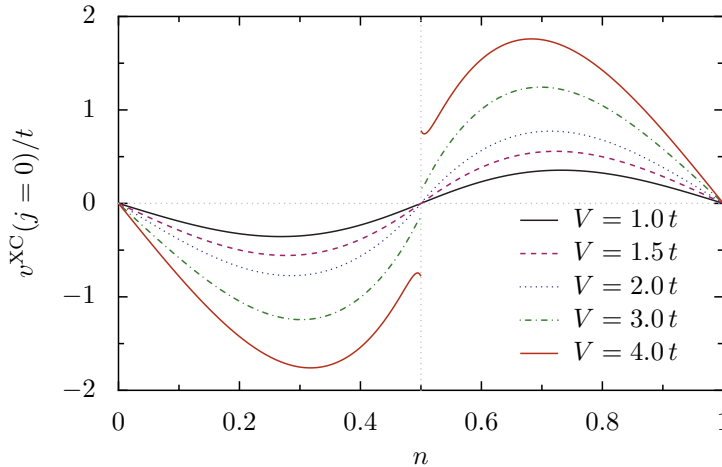


Figure 3.1: Exchange-correlation potential as function of the density at $j = 0$ for various interactions. Potentials with $V > 2$ have a jump at $n = 0.5$.

Note that $\lambda^{\text{XC}}(n) \leq 0$ since $D^{\text{BA}}(n) \leq D^0(n)$. The resulting approximation may be called *current-LDA* (C-LDA) and is obviously exact if the system is homogeneous. The exchange-correlation potential for current j equal to zero and the second-order contribution λ^{XC} are depicted in Figures 3.1 and 3.2, respectively. The validity of the approximation for other than the homogeneous system will be examined later.

3.2.2 Gradient approximations

In contrast to e.g. the Hartree-Fock approximation, density functional theory within the local density approximation is a local theory. This has the advantage that the computational costs are significantly lower in DFT+LDA. A way to improve LDA is to take not only the local densities but also its gradients into account

$$E^{\text{XC}}[n] = \sum_l \epsilon^{\text{XC}}(n_l, \nabla n_l). \quad (3.25)$$

This definition leads to the so-called generalized gradient approximation (GGA). A short overview on GGA and earlier gradient approximations can be found for example in [74] and a variety of different functionals in use are shown in [75]. The construction of a modern GGA, based on a number of exact conditions, can be found in [81]. However, within this work we will not investigate the gradient approximations, so we do not go into more detail.

3.2.3 Exact-exchange method

Another way of approximating the exchange-correlation energy is the exact-exchange method (EXX) which is exact up to first order in the interaction [14, 82]. It shows some similarities with the Hartree-Fock approximation, but retains some of the computational simplicity of the density functional formalism, which is especially relevant

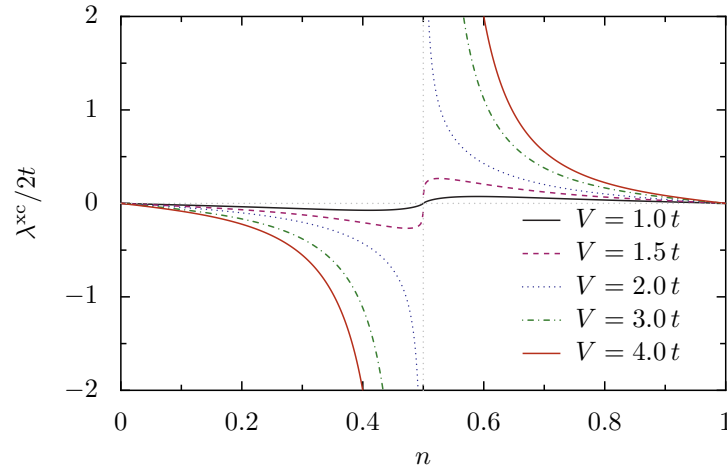


Figure 3.2: Second order correction to the exchange-correlation potential for currents $j \neq 0$ as a function of the density.

for systems with long-range interaction. For our one-dimensional artificial system with nearest-neighbor interaction Hartree-Fock calculations are faster since it only modifies the secondary diagonals of the Hamiltonian while the exact-exchange method needs a complicated calculation scheme, as we will see in the following.

In principle the exact-exchange approximation, also known as the optimized effective potential approach [12, 13, 15], even allows higher order approximations. Basically this scheme expands the ground state energy in orders of the interaction just as in usual perturbation theory. The first order contributions are the Hartree and the exchange energy,

$$E^{\text{HXC}}[n] \approx E^{\text{H}}[n] + E^{\text{X}}[n], \quad (3.26)$$

where $E^{\text{H}}[n] = V \sum_l n_l n_{l+1}$. The exchange energy is given by

$$E^{\text{X}} = -V \sum_l \left[\sum_j^{\text{occ.}} \varphi_j^*[n](l) \varphi_j[n](l+1) \right] \left[\sum_k^{\text{occ.}} \varphi_k^*[n](l+1) \varphi_k[n](l) \right], \quad (3.27)$$

where the sums over j and k go over the occupied states φ of the single-particle Hamiltonian, i. e. the lowest N eigenstates. The main difference to the usual perturbation theory is that the orbitals $\varphi_j[n]$ depend on the densities and are eigenstates of the Kohn-Sham Hamiltonian but not of an arbitrary single-particle Hamiltonian, as the Hartree-Fock orbitals would be. The corresponding potential is then obtained by taking the derivative

$$v_l^{\text{X}} = \frac{\partial E^{\text{X}}}{\partial n_l} = \sum_{l', l''} \sum_i^{\text{occ.}} \frac{\partial E^{\text{X}}}{\partial \varphi_i(l'')} \frac{\partial \varphi_i(l'')}{\partial v_{l'}} \frac{\partial v_{l'}}{\partial n_l} + \frac{\partial E^{\text{X}}}{\partial \varphi_i^*(l'')} \frac{\partial \varphi_i^*(l'')}{\partial v_{l'}} \frac{\partial v_{l'}}{\partial n_l}. \quad (3.28)$$

The indices l' and l'' go over the lattice ($1 \dots L$) while the sum over i again goes over the occupied states. The first term of both summands on the right hand side is simple to

determine from (3.27) and we have for example:

$$\frac{\partial E^X}{\partial \varphi_i(l'')} = -V \sum_j^{\text{occ.}} (\varphi_j^*(l'') \varphi_j(l''+1) \varphi_i^*(l''+1) + \varphi_i^*(l''-1) \varphi_j^*(l'') \varphi_j(l''-1)). \quad (3.29)$$

The second terms in (3.28) can be found by first order perturbation theory. Consider the Hamiltonian \hat{H}^s which corresponds to the eigenstates φ_j and perturb it with a small potential term $\delta v_{l'} \hat{n}_{l'}$. Then the derivative is

$$\frac{\partial \varphi_i(l'')}{\partial v_{l'}} = \lim_{\delta v_{l'} \rightarrow 0} \frac{\varphi_i^{v_{l'} + \delta v_{l'}}(l'') - \varphi_i^{v_{l'}}(l'')}{\delta v_{l'}} = \sum_{k \neq i} \varphi_k(l'') \frac{\varphi_k^*(l') \varphi_i(l')}{\epsilon_i - \epsilon_k}. \quad (3.30)$$

The $\epsilon_{l'}$ are the eigenenergies of the single-particle Hamiltonian. The sum over k includes all eigenstates of the Hamiltonian except the i -th. Finally, the last expression of (3.28) is the inverse of the susceptibility and can be derived by applying (3.30) to the relation $n_l = \sum_j^{\text{occ.}} \varphi_j^*(l) \varphi_j(l)$:

$$\chi_{ll'} = \frac{\partial n_l}{\partial v_{l'}} = \sum_i^{\text{occ.}} \sum_{j \neq i} \frac{\varphi_i^*(l) \varphi_j(l) \varphi_j^*(l') \varphi_i(l')}{\epsilon_i - \epsilon_j} + \text{c.c.} \quad (3.31)$$

Combining the results and inserting into (3.28) one gets an expression for the exchange potential

$$v_l^x = -2V \sum_{l', l''} \sum_{i, j}^{\text{occ.}} \sum_{k \neq i} \left\{ \frac{\varphi_j^*(l'') \varphi_j(l''+1) \varphi_i^*(l''+1) \varphi_k(l'') \varphi_k^*(l') \varphi_i(l')}{\epsilon_i - \epsilon_k} + \text{c.c.} \right\} \chi_{ll'}^{-1}. \quad (3.32)$$

Note that the susceptibility χ has an eigenvalue which is zero. This eigenvalue corresponds to a homogeneous change of the density and thus is not particle number conserving. So we have to exclude it before inverting χ .

The calculation of this exchange-potential is already numerically expensive. So, although possible, the inclusion of higher order terms is not feasible. However, the correlation energy can be approximated analogous to the local density approximation (3.16),

$$E^{\text{HXC}}[n] = E^{\text{H}}[n] + E^{\text{X}}[n] + \sum_l \epsilon^{\text{C}}(n_l), \quad (3.33)$$

where ϵ^{C} can be determined from the exact solution of the homogeneous system. In the following we denote the resulting approximation by EXX+LDA.

3.3 Practical applications

We have seen that density functional theory provides a way of mapping many-body properties onto a single-particle problem. Unfortunately therefore one has to make two sacrifices. First, one cannot extract every many-particle quantity from a density functional

calculation. For example the excitation energies or the density of states are concepts that lie outside the static formalism. The second sacrifice is the approximation of the exchange-correlation potential. So there are certainly limitations to density functional theory and it is the aim of this section to investigate them. A thorough review of the quality of the local density approximation when applied to realistic materials can be found for example in [83].

3.3.1 Charge gap in the spinless fermion model

An important quantity to distinguish metals from insulators and to characterize the insulator is the band gap (see for example [84]). It is common knowledge in the DFT community that usually the local density approximation underestimates the band gap while the Hartree-Fock theory would overestimate it. So sometimes a material is found to be a metal in density functional calculations while experiments show it to be a semiconductor or insulator. The band gap problem has been studied intensively in the literature, in particular it has been pointed out that a discontinuity in the exchange-correlation potential is crucial [19, 21, 85]. Lattice models are quite useful for the understanding of such problems [22, 23, 24]. We now repeat some of the work done for our model of spinless fermions. The charge gap can be defined as the difference

$$\Delta = \mu_{N+1} - \mu_N, \quad (3.34)$$

where μ_N is the chemical potential of a N -particle system and, according to [20], can be calculated as $\mu_N = E_N - E_{N-1}$. The Kohn-Sham gap is defined as the difference of the *lowest unoccupied (molecular) orbital* (LUMO) and the *highest occupied (molecular) orbital* (HOMO),

$$\Delta^{\text{KS}} = \epsilon_{N+1} - \epsilon_N. \quad (3.35)$$

If the exchange-correlation energy has no discontinuities as a function of the particle number [21], the two quantities are identical in the thermodynamic limit. Please note that we need to solve three self-consistent calculations for particle numbers $N - 1$, N and $N + 1$ to obtain Δ , while Δ^{KS} only uses results from a N -particle calculation.

For the investigation of the charge gap we first look at the homogeneous system. There a gap opens for strong interactions $V > 2t$. In this case the local density approximation gives the correct ground state energies E_N . Thus the gap Δ obtained from the homogeneous system is obviously exact. On the other hand, since the system is homogeneous, the Hartree potential and the exchange-correlation potential also have to be homogeneous. Therefore the potentials contribute only by a global energy shift. The eigenstates of this Hamiltonian are then just plain waves with a cosine dispersion and no gap at all. So we see that in this case the Kohn-Sham gap Δ^{KS} is always zero for arbitrary interaction strength, whereas $\Delta \neq 0$ for $V > 2t$. We can now conclude that the exchange-correlation potential is discontinuous, as seen also in Figure 3.1. So in this case the band gap is completely due to the discontinuity of the exchange-correlation potential.

Next we investigate the gap in a weakly interacting system, i. e. within the gapless phase with $|V| < 2$. There we open a gap by inserting the potential $v_l = u \cos 2k_F l$,

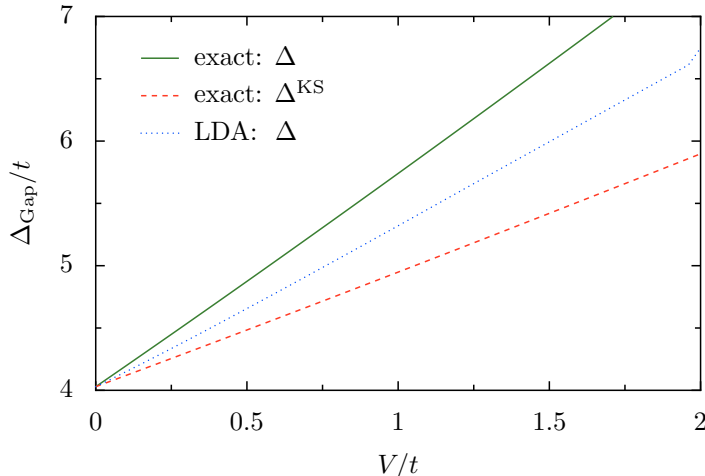


Figure 3.3: Charge gap of a system with a staggered potential ($u = 2t$) as a function of the interaction at half filling. We compare three different gaps: The exact gap (solid green line) and the LDA gap (dotted blue line), both obtained as the difference of the chemical potentials, the LUMO-HOMO gap (dashed red line) as obtained from a DFT calculation with the exact exchange-correlation potential. The system size is $L = 26$.

where k_F is the Fermi vector and u is the strength of the potential. In case of half filling this leads to a staggered potential

$$v_l = \begin{cases} u & \text{if } l \text{ is even,} \\ -u & \text{if } l \text{ is odd.} \end{cases} \quad (3.36)$$

The calculation of the gap with various methods gives the results shown in Figures 3.3 to 3.6. In Figure 3.3 we use a half filled system to compare the exact charge gap, as obtained from exact diagonalizations, to the LUMO-HOMO gap from a density functional calculation with the exact exchange-correlation potential and the DFT+LDA gap. We see that for a noninteracting system the band gap is of the size of the potential ($2u = 4t$) and increases with interaction. In contrast to the homogeneous system the Kohn-Sham gap is now not equal to zero. However both, the full gap with the local density approximation and the LUMO-HOMO gap with the exact exchange-correlation potential, are far too low compared to the real size of the gap. To substantiate this finding we show some results at quarter filling in Figure 3.4. Again we see that, while the real gap is growing with increasing interaction, the gap predicted by the LUMO-HOMO value of exact density functional theory is almost constant and the LDA gap is even decreasing.

This behavior coincides with the common knowledge that LDA usually underestimates the band gaps. On the other hand it is found that within Hartree-Fock theory the predicted band gap is often overestimated compared to experimental data. Since for weak interactions the exact-exchange approximation is equivalent to Hartree-Fock theory we expect an oversized band gap from the former. If we look again at the two situations, half and quarter filling, we find the results depicted in Figures 3.5 and 3.6 meet these

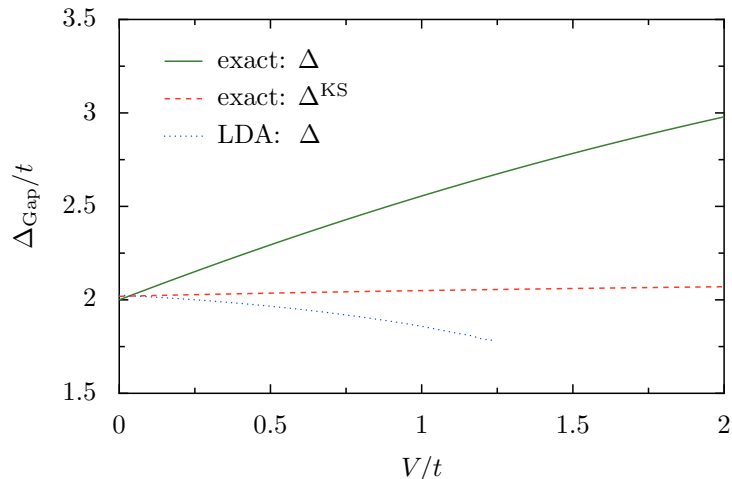


Figure 3.4: Charge gap of a system with a staggered potential ($u = 2t$) as a function of the interaction at quarter filling. We compare three different gaps: The exact gap (solid green line) and the LDA gap (dotted blue line), both obtained as the difference of the chemical potentials, the LUMO-HOMO gap (dashed red line) as obtained from a DFT calculation with the exact exchange-correlation potential. The system size is $L = 28$. The LDA calculations did not converge for $V > 1.2t$.

expectations. Furthermore we see that at half filling the exact-exchange method is quite good for all considered interactions and in both cases tremendously better than the LDA. However, these results can still be improved quite easily by using the exact-exchange approximation together with a local density approximation for the correlation energy (EXX+LDA).

3.3.2 Stability of the homogeneous system

In Section 2.2 we discussed the phase diagram of the interacting spinless fermions. For repulsive interactions, $V > 0$, the system exhibits a ordered phase for $V > 2t$ at half filling and is gapless elsewhere. In the case of the ordered phase the homogeneous system is unstable with respect to small perturbations, thus an infinite small perturbation leads to a staggered density profile. In the gapless phase on the other hand the homogeneous system is stable against such perturbations.

In this section we follow our results in [86] and investigate the stability of the homogeneous system within the local density approximation. This is done by means of the charge susceptibility $\chi(q)$, which is defined via the relation

$$\delta n_q = -\chi(q) \delta v_q. \quad (3.37)$$

δn_q and δv_q are the Fourier transforms of the on-site densities n_l and the potentials v_l , respectively. Analogous we can define a single-particle susceptibility $\chi^s(q)$ through the change of the density by a change of the (effective) single-particle potential

$$\delta n_q = -\chi^s(q) \delta v_q^s. \quad (3.38)$$

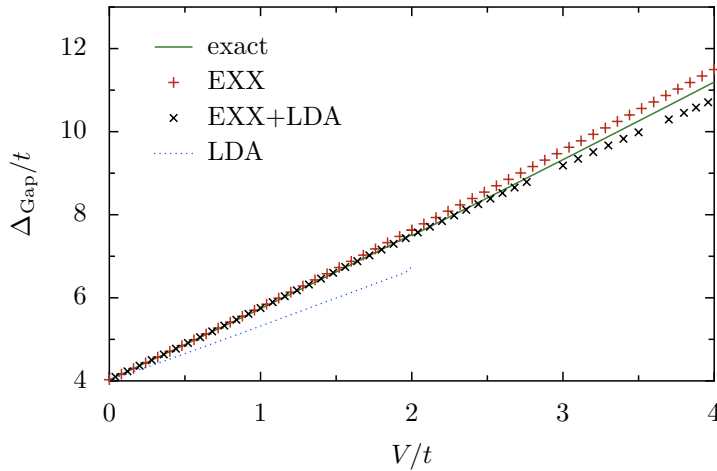


Figure 3.5: Charge gap of a system of size $L = 26$ with a staggered potential ($u = 2t$) as function of the interaction at half filling. We compare the exact result (solid green line) with density functional results obtained within the local density approximation (dotted blue line), the exact-exchange approximation (red +) and a combination of both, where the correlation energy is approximated by a local approximation (black \times).

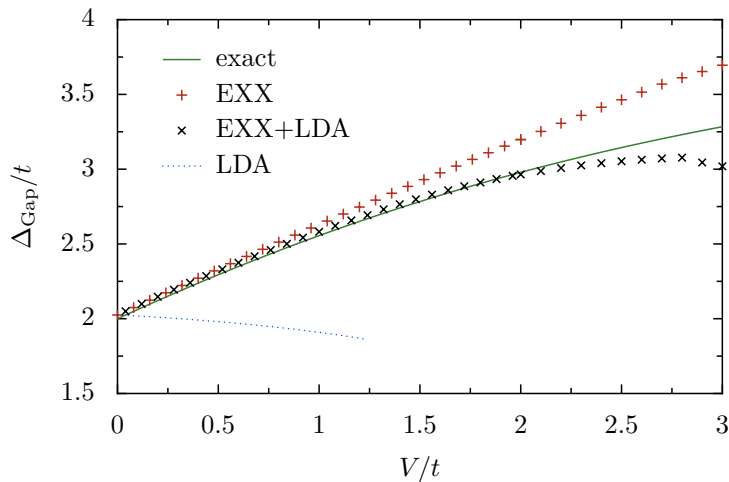


Figure 3.6: Charge gap of a system of size $L = 28$ with a staggered potential ($u = 2t$) as function of the interaction at quarter filling. We compare the exact result (solid green line) with density functional results obtained within the local density approximation (dotted blue line), the exact-exchange approximation (red +) and a combination of both, where the correlation energy is approximated by a local approximation (black \times).

Using equation (3.12), $\delta v_q^H/\delta n_{q'} = \delta_{qq'} \delta v_q^H/\delta n_q$ and the analogous result for $\delta v_q^{\text{XC}}/\delta n_{q'}$ we rewrite δv_q^s as

$$\delta v_q^s = \delta v_q + \delta v_q^H + \delta v_q^{\text{XC}} = \delta v_q + \left(\frac{\delta v_q^H}{\delta n_q} + \frac{\delta v_q^{\text{XC}}}{\delta n_q} \right) \delta n_q. \quad (3.39)$$

Inserting (3.37) into this expression and equating (3.37) and (3.38) gives then a relation between $\chi(q)$ and $\chi^s(q)$,

$$\chi(q) = \chi^s(q) \{1 + [2V \cos(q) + f^{\text{XC}}(q)] \chi(q)\} \quad (3.40)$$

or

$$\chi(q) = \frac{\chi^s(q)}{1 + [2V \cos(q) + f^{\text{XC}}(q)] \chi^s(q)}. \quad (3.41)$$

Here, $2V \cos(q)$ is the Hartree term from (3.39) and f^{XC} is the derivative of the exchange-correlation potential with respect to the density. In the thermodynamic limit ($L \rightarrow \infty$) the susceptibility of the auxiliary system is given by

$$\chi^s(q) = \frac{1}{4\pi t \sin(q/2)} \ln \left| \frac{\sin(q/2) + \sin k_F}{\sin(q/2) - \sin k_F} \right| \quad (3.42)$$

with the Fermi wave vector k_F . Equation (3.41) is exact if one knows the exact expression of the exchange-correlation kernel $f^{\text{XC}}(q)$. In case of the local density approximation this kernel is independent of q and only depends on the filling.

The stability boundary of the homogeneous system is determined by the condition that the static susceptibility becomes infinite and changes sign, i. e. if

$$\frac{1}{\chi^s(q)} + V(q) + f^{\text{XC}}(q) = 0. \quad (3.43)$$

Due to the logarithmic divergence of $\chi^s(q)$ for $q \rightarrow 2k_F$ this is equivalent to the condition that $V(q) + f^{\text{XC}}(q)$ changes sign. Figure 3.7 shows the region of stability for the local density approximation in the n - V -plane for the infinite system and for finite systems of length $L = 10^3$ and $L = 10^4$, respectively. If we investigate the weak interacting case in more detail we find

$$f_{\text{LDA}}^{\text{XC}} = \frac{\partial^2}{\partial n^2} (\epsilon^{\text{BA}} - \epsilon^{\text{H}}) = -V(2k_F) + \mathcal{O}(V^2), \quad (3.44)$$

which cancels the $V(q)$ -part of the denominator for $q \rightarrow 2k_F$. So in first order in the interaction we cannot draw a conclusion about the stability of the homogeneous system. Numerically one finds that the second order correction of $f_{\text{LDA}}^{\text{XC}}$ changes sign at $n_c \approx 0.331$, thus limiting the range of stability to $n_c < N < 1 - n_c$ at weak coupling. In contrast, the Hartree approximation is stable only for $V(2k_F) > 0$, i. e. below quarter and above three quarter filling, while the exact ground state is unstable only at half filling for interactions $V > 2t$.

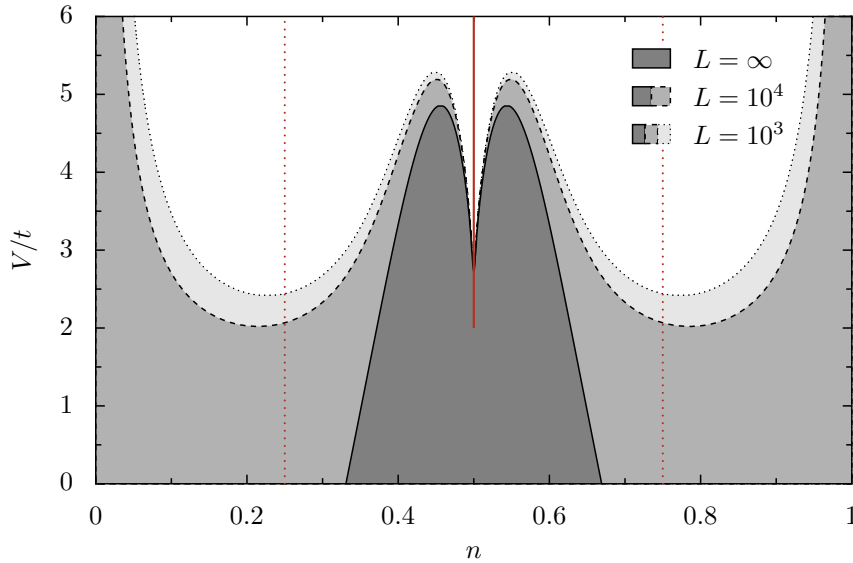


Figure 3.7: Region of stability as a function of the density and interaction for a homogeneous system. The shaded areas show the stable regions of the local density approximation for different system sizes. The solid red line at $n = 0.5$ depicts the charge instability obtained from the exact ground states. The dotted red line marks the border of the stable region of the Hartree approximation ($n < 0.25$ and $n > 0.75$).

Since the single-particle susceptibility at $2k_F$ diverges only logarithmically with system size L there are pronounced finite size effects that strongly enlarge the region of stability within the local density approximation. As a consequence within LDA finite homogeneous systems are stable for all densities from weak to intermediate interaction strength, as can be seen in Figure 3.7 for $L = 10^3$ and $L = 10^4$.

We did not study the stability of the exact-exchange method. In principle the exchange-correlation kernel is known for this approximation [87, 88], but in order to use condition (3.43) for finding the stability boundary one has to evaluate a quite complex expression. Another way to address this issue is to investigate whether, starting with an inhomogeneous system, the self-consistency procedure for solving the single-particle Hamiltonian leads to an homogeneous or inhomogeneous density profile. However, due to finite size effects and finite numerical accuracy the results for the boundary are inconclusive. On the other hand it seems that the region of stability is strongly reduced within this method, at least near half filling. There the homogeneous system is definitely unstable for interaction $V = t$, maybe also for weaker interactions.

3.3.3 Static susceptibility

Here we investigate the static density-density response function in more detail, at first for the local density approximation, later within the exact-exchange formalism. In Figures 3.8 and 3.9 we compare $\chi^{\text{LDA}}(q)$ with exact susceptibilities obtained from exact diagonalization of small systems. As to be expected, in the long wavelength limit,

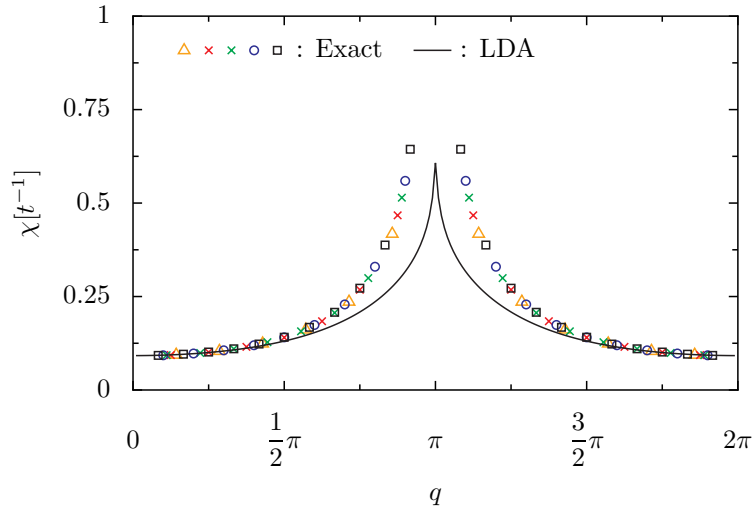


Figure 3.8: Static susceptibility at half filling for interaction $V = t$. The symbols are results from exact diagonalizations at system sizes $L = 14, 16, 18, 20, 24$. The line is the result from a LDA calculation at $L = 202$.

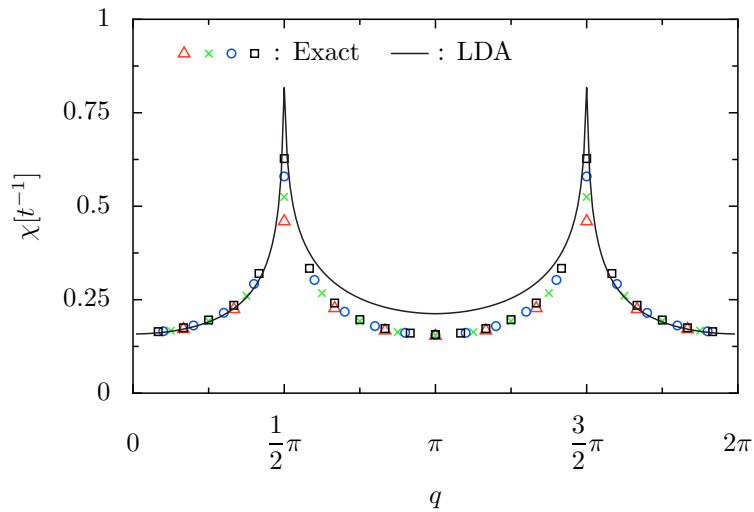


Figure 3.9: Static susceptibility at quarter filling for interaction $V = t$. The symbols are results from exact diagonalizations at system sizes $L = 12, 16, 20, 24$. The line is the result from a LDA calculation at $L = 204$.

$q \rightarrow 0$, perfect agreement is found. Technically, there is a cancellation between the susceptibility $1/\chi^s(0) = 2\pi t \sin k_F$ and the second derivative of the Hartree energy $\epsilon^H = -(2t/\pi) \sin k_F + Vn^2$ with respect to $n = k_F/\pi$. Therefore

$$\chi^{\text{LDA}}(q \rightarrow 0) = \left(\frac{\partial^2 \epsilon^{\text{BA}}}{\partial n^2} \right)^{-1} = \frac{1}{L} \frac{\partial N}{\partial \mu} \quad (3.45)$$

which is the exact uniform susceptibility of the interacting system. Unfortunately already the next to leading contribution, $\sim q^2$, is not obtained correctly within LDA. At half filling the discrepancy between the LDA susceptibility and the exact one becomes more and more pronounced for $q \rightarrow 2k_F = \pi$. At $q = 2k_F$ the exact susceptibility diverges with the power law (2.23), while in LDA there is only a cusp. The cusp value itself remains finite and approaches $\chi^{\text{LDA}}(\pi) = 1.668/t$ for $L \rightarrow \infty$. At quarter filling $\chi^{\text{LDA}}(q)$ is very close to the exact susceptibility for $q < 2k_F$, while for $q > 2k_F$ there is a clear discrepancy. For $q = 2k_F = \pi/2$ the exact result again is strongly size-dependent but finite whereas the LDA result diverges already at finite system size, since at quarter filling one is already outside the range of stability of the local density approximation. In order to obtain the next to leading contribution correctly we could use a gradient approximation. In general, higher orders could be obtained by using the exact results for the susceptibility to reconstruct the exchange-correlation potential. For a short overview on this problem we refer to Appendix F.2.

Let us now turn our attention to the exact-exchange approximation. If we repeat our investigation of the static susceptibility we find Figures 3.10 and 3.11. Additionally we show results where we have improved the exact-exchange approximation by including the correlation energy within a local approximation. If we focus on the pure exact-exchange approximation we see that it agrees far better with exact results than the LDA for a wide range of q -values. However, in the long-wavelength limit where the local density approximation is (almost) exact we see a sudden decrease which does not reflect the true result. This result can be connected to our previous discussion of the stability of the homogeneous system as follows: To obtain the static susceptibility, we explicitly calculated the density response to a small perturbation. The decrease of the susceptibility at small q implies that the calculation converged to an ordered phase. Thus we find that the exact-exchange method predicts the homogeneous system to be unstable even for the weak interaction $V = t$. However, looking at the results for the exact-exchange approximation where the correlation energy has been treated with a local density approximation, it seems that this instability can easily be cured. For the sake of completeness we also show Figure 3.11 where we compare these two approximations with exact results at quarter filling. Again we see that a better treatment of the exchange part gives far better results at higher q -values than the local density approximation.

3.3.4 Scattering from a single impurity

To elaborate more on the problem of the $2k_F$ divergence we now investigate a model with non-zero potential v_l . An important example of such a model is the case of a single impurity, i. e. $v_l = v_{\text{imp}}$ at the impurity site and $v_l = 0$ elsewhere. In particular, we take

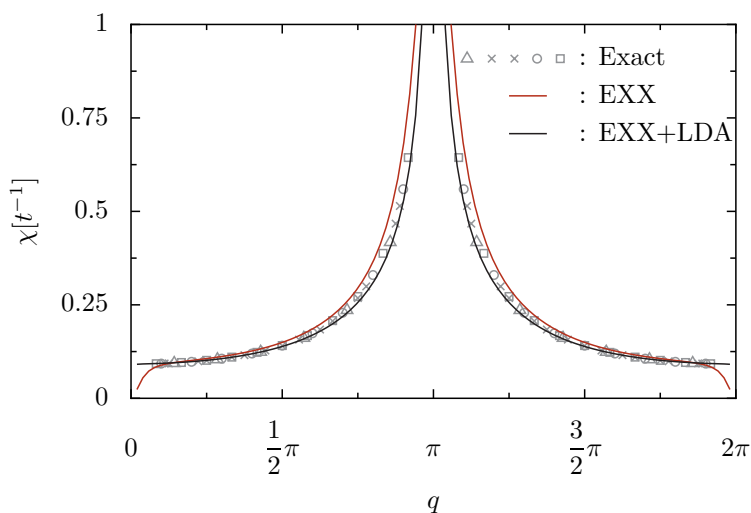


Figure 3.10: Static susceptibility for a homogeneous system at half filling for interaction $V = t$. The symbols are results from exact diagonalizations at system sizes $L = 12, 16, 20, 24$. The red line is the result from a DFT calculation at $L = 102$ within the exact-exchange approximation. The black line stems from a similar calculation where additionally the correlation-part of the energy was approximated using the local density approximation.

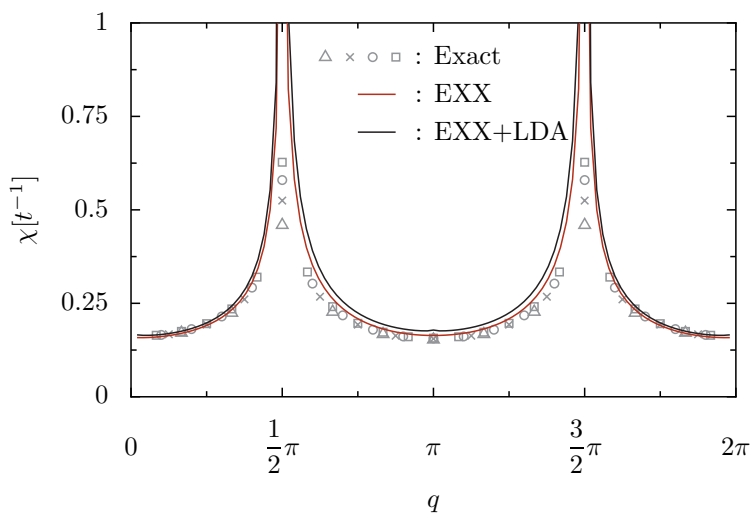


Figure 3.11: Static susceptibility for a homogeneous system at quarter filling for interaction $V = t$. The symbols are results from diagonalizations. The red line is the result from a DFT calculation at $L = 100$ within the exact-exchange approximation. The black line stems from a similar calculation where additionally the correlation-part of the energy was approximated using the local density approximation.

a look onto the scattering at such an impurity, where, in one dimension, the reflection and transmission coefficients are strongly renormalized by the interaction [89, 90, 91].

This renormalization can be understood by a simple picture developed by Matveev et al. [91]. Without interaction an impurity leads to modulations of the density (known as Friedel oscillations) which decay as $1/r$ with the distance r to the impurity. The presence of electron-electron interaction leads to additional scattering at these density oscillations. For wave vector q close to k_F the correction to the bare transmission \mathcal{T}_0 up to linear order in the interaction is given by [91]

$$\delta\mathcal{T} = -2\alpha\mathcal{T}_0(1 - \mathcal{T}_0) \ln\left(\frac{1}{|q - k_F|d}\right). \quad (3.46)$$

The parameter d characterizes the typical length scale of the interaction, i. e. it is equal to one for nearest-neighbor interaction. The prefactor α takes the interaction strength into account. It is given by the sum of the Hartree and exchange contributions, $\alpha = \alpha_H + \alpha_x$, with $\alpha_H = -V(2k_F)/2\pi v_F$ and $\alpha_x = V(0)/2\pi v_F$. Please note that equation (3.46) is valid as long as $\delta\mathcal{T} \ll 1$, thereby implying

$$\alpha \ln(1/|q - k_F|d) \ll 1. \quad (3.47)$$

Because of this condition we cannot use equation (3.46) for arbitrarily small $|q - k_F|$. In order to obtain the transmission within this limit we have to sum the leading divergences to all orders in the interaction. This can be done by using a renormalization group approach [91]:

According to equation (3.46), a small change dq of a wave vector q ($q > k_F$) leads to a renormalization of the transmission,

$$\mathcal{T}(q) - \mathcal{T}(q - dq) = -2\alpha\mathcal{T}_0(1 - \mathcal{T}_0) \ln\frac{(q - dq - k_F)d}{(q - k_F)d}. \quad (3.48)$$

Using this renormalized transmission $\mathcal{T}(q - dq)$ instead of \mathcal{T}_0 as new initial value we repeat the renormalization procedure. Thus the change of the transmission due to a change of the wave vector is given by

$$d\mathcal{T} = 2\alpha\mathcal{T}(1 - \mathcal{T}) \frac{dq d}{(q - k_F)d} = 2\alpha\mathcal{T}(1 - \mathcal{T}) \cdot d \ln\{(q - k_F)d\}. \quad (3.49)$$

We now repeat this renormalization step by step until we reach the finite size limit $q - k_F = 2\pi/L$. The total renormalization of the transmission is then found as the solution to the differential equation (3.49). The typical scale of the initial value is $q_0 - k_F \propto 1/d$ and corresponds to the bare transmission $\mathcal{T} = \mathcal{T}_0$. The solution of this equation at $q - k_F = 2\pi/L$ is then given by

$$\mathcal{T} = \frac{\mathcal{T}_0 (2\pi/[q_0 - k_F]L)^{2\alpha}}{\mathcal{R}_0 + \mathcal{T}_0 (2\pi/[q_0 - k_F]L)^{2\alpha}}, \quad (3.50)$$

where $\mathcal{R}_0 = 1 - \mathcal{T}_0$ is the bare reflection probability. Thus it is found that the transmission at $q \rightarrow k_F$ renormalizes algebraically with the system size and approaches zero in the thermodynamic limit, even for a weak defect (repulsive interaction).

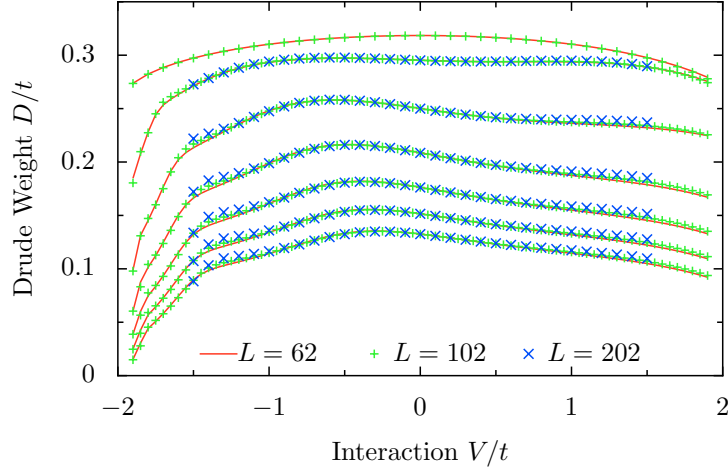


Figure 3.12: LDA results for the Drude weight of a half filled system with a single impurity as function of the interaction strength, for several values of the impurity strength $v_{\text{imp}} = 0, t, 2t, 3t, 4t, 5t, 6t$ (from top to bottom), and different system sizes. In contrast to the exact results, within LDA the Drude weight is practically independent of the system size.

Repeating the previous arguments within the density functional formalism, thereby rewriting the exchange-correlation potential as $v_l^{\text{XC}} = \sum_{l'} f_{ll'}^{\text{XC}} \delta n_{l'}$, we find the interaction parameter $\alpha = -[V(2k_F) + f^{\text{XC}}(2k_F)]/2\pi v_F$. As before the first term of this expression is the Hartree contribution. However, within the local density approximation the second term is $f_{\text{LDA}}^{\text{XC}} = -V(2k_F) + \mathcal{O}(V^2)$ which cancels the Hartree term. Therefore the transmission is *not* renormalized in DFT+LDA up to first order in the interaction.

To substantiate this finding numerically we calculate the Drude weight D for a system with a single impurity. It is defined as the response of the system to a change of boundary conditions according to

$$D = \frac{L}{2} \left. \frac{d^2 E}{d\Phi^2} \right|_{\Phi=0}, \quad (3.51)$$

where $E(\Phi)$ is the ground state energy. Φ can be interpreted as the magnetic flux through the one-dimensional ring or a twist in the boundary conditions, such that $\Phi = 0$ corresponds to periodic and $\Phi = \pi$ to antiperiodic boundary conditions [63, 89].

We choose the Drude weight for characterizing the transmission through the impurity for several reasons: First, it is calculated from the Φ -dependence of the ground state energy and thus much simpler to obtain than the transmission which is a property of the wave function. Second, unlike the wave function the ground state energy is a well defined quantity within the density functional formalism and its dependence on the magnetic flux is also justified by means of CDFT. On the other hand the Drude weight is closely related to the transmission through the defect [92, 93, 94]. In the noninteracting system – where \mathcal{T} is not renormalized – the size dependence of D is negligible. In the interacting system, on the other hand, the transmission coefficient for $(q - k_F) \approx v_F/L$ is relevant as discussed above. Correspondingly, the Drude weight increases (decreases) algebraically with system size for repulsive (attractive) interaction [90, 91, 89].

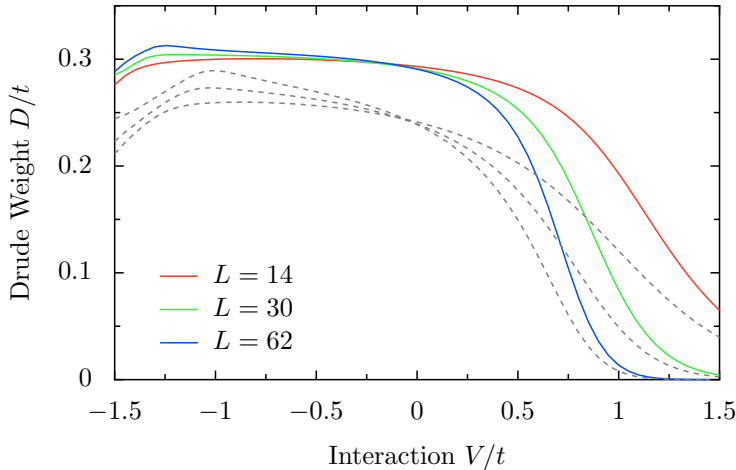


Figure 3.13: Exact exchange results for the Drude weight of a half filled system with a single impurity as function of the interaction strength. The colored lines are calculated at impurity strength $v_{\text{imp}} = t$ for different system sizes. The dashed gray lines are the corresponding results for $v_{\text{imp}} = 2t$.

In Figure 3.12 we present our LDA results for the Drude weight at half filling, for different system sizes ($L = 62, 102, 202$) and different values of the impurity strength ($v_{\text{imp}} = 0, t, 2t, 3t, 4t, 5t, 6t$). Unlike the (numerically) exact results [89], we do not observe any dependence on system size within the local density approximation, which is in agreement with the perturbative argument given after equation (3.50). On the other hand, if we use the exact-exchange method we do find a renormalization with system size. In Figure 3.13 we present the Drude weight for three different system sizes as function of the interaction. For clarity we restrict ourselves to two impurity strengths ($v_{\text{imp}} = t, 2t$). If we investigate the size dependency more closely at different interactions, we find the results depicted in Figure 3.14. There we have plotted the Drude weight as function of the system size. One clearly sees an exponential decrease of the Drude weight with increasing system size, in contrast to the algebraic decrease predicted by (3.50). Recall that the exact-exchange method predicts an ordered ground state, and thus a gapped system. In this context the exponential decrease of the Drude weight is no surprise.

Since in Chapter 3.3.3 we could cure this problem of the exact-exchange method by including the correlation term within a local approximation, it is interesting, how EXX+LDA affects the renormalization of the Drude weight. In order to investigate this, we shortly repeat our discussion on the basis of the two Figures 3.15 and 3.16. In the first figure, 3.15, we show again the Drude weight as a function of the interaction for different system sizes and impurity strengths. Again we find a renormalization with the system size. In addition, the comparison with Figure 3.14 shows that the renormalization is not as strong as within the pure exact-exchange method. Studying the dependence of the Drude weight on the system size we find Figure 3.16. There we plot the behavior of the Drude weight for several interactions V . As one can see, for interaction $V = t$ we still see the exponential behavior, which indicates a gap, albeit a much smaller one than in EXX. For weaker interactions the limit of large system size also can be described by an

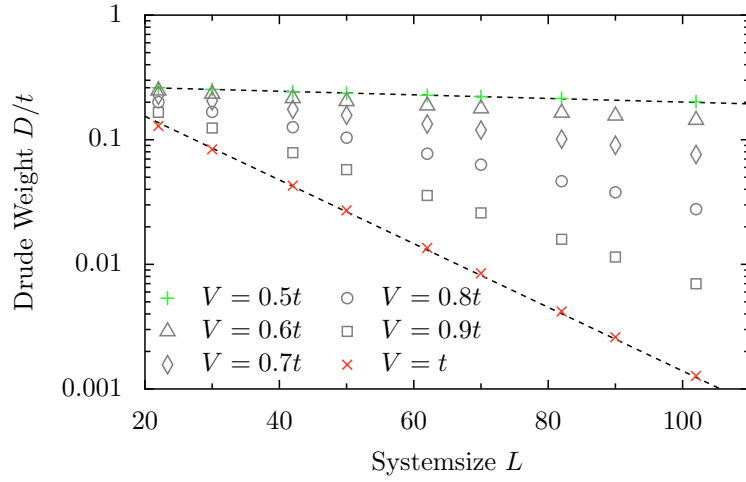


Figure 3.14: Exact exchange results for the Drude weight of a half filled system with a single impurity ($v_{\text{imp}} = t$) as function of the system size at different interactions. The dashed lines are fits with exponential functions.

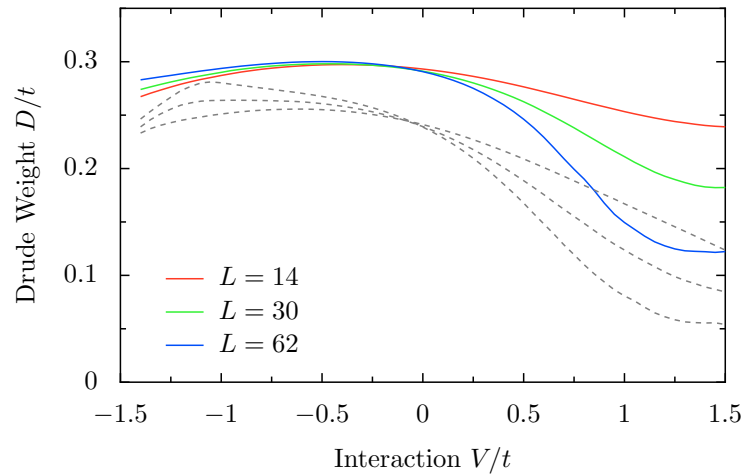


Figure 3.15: Results for the Drude weight of a half filled system with a single impurity as function of the interaction strength within the EXX+LDA approximation. The colored lines are calculated at impurity strength $v_{\text{imp}} = t$ for different system sizes. The dashed gray lines are the corresponding results for $v_{\text{imp}} = 2t$.

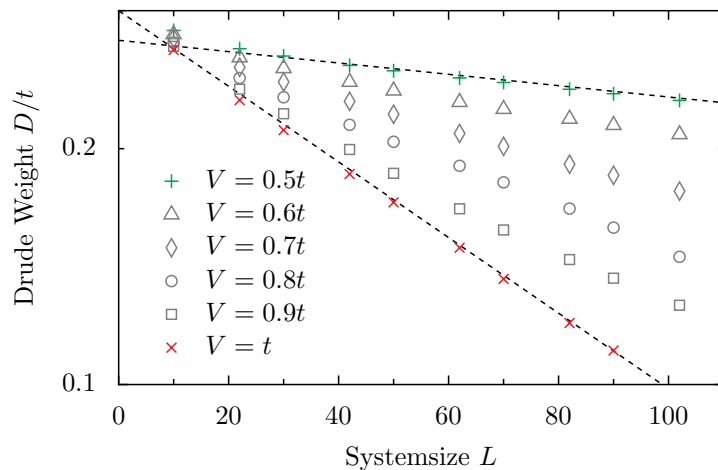


Figure 3.16: Results for the Drude weight of a half filled system with a single impurity ($v_{\text{imp}} = t$) as function of the system size at different interactions within the EXX+LDA approximation. The upward axis uses a logarithmic scale. The dashed lines are fits with exponential functions. So for large size L the system renormalizes exponentially.

exponential function, although we see differences for small systems. In any case, even EXX+LDA does not reproduce the algebraic dependence on the system size as expected from equation (3.50).

4 Time-dependent density functional theory

In the last section we analyzed static density functional theory together with two approximations, the local density approximation and the exact-exchange method. We have seen that one can extract the ground state energy and density from such a calculation. However, often one is also interested in excitation energies or the dynamical response to some applied field. Access to these quantities can be gained via the time-dependent density functional theory introduced by E. Runge and E. K. U. Gross [7] and put on a more formal basis by R. van Leeuwen [10]. A comprehensive treatment of this topic can be found for example in [95, 96].

4.1 Time-dependent density functional theory by Legendre transformation

As we have seen in the last chapter the basic idea of static density functional theory is the mapping of an interacting Hamiltonian onto a noninteracting one. In the case of a time-dependent system the idea is the same, to provide a mapping from the interacting Hamiltonian \hat{H} onto an effective single-particle system \hat{H}^s . Thus, one has to map the time evolution of the interacting system, given by the time-dependent Schrödinger equation,

$$i \frac{d}{dt} |\Psi(t)\rangle = \hat{H}(t) |\Psi(t)\rangle, \quad (4.1)$$

onto the evolution of a single-particle system. An important ingredient for the existence of the mapping within the static formalism is the Rayleigh-Ritz principle, i. e. the minimal property of the ground state energy. For time-dependent systems this principle is no longer applicable. The role of the ground state energy can, however, be played by the quantum mechanical action, which shall be introduced in the following. Thereby we follow the reasoning in [10] or the third chapter of [95], which is based on the Keldysh technique [97, 98]. We consider here a system at finite temperature T since it is easy to incorporate into the formalism. Of course, the limit $T \rightarrow 0$ is no challenge.

4.1.1 The Keldysh time-evolution

First we introduce the time-evolution operator $\hat{S}(t, t')$ which is defined by the relation $|\Psi(t)\rangle = \hat{S}(t, t') |\Psi(t')\rangle$. Inserting this into the time-dependent Schrödinger equation and its complex conjugate we find

$$i \frac{d}{dt} \hat{S}(t, t') = \hat{H}(t) \hat{S}(t, t') \quad \text{and} \quad i \frac{d}{dt'} \hat{S}(t, t') = -\hat{S}(t, t') \hat{H}(t'). \quad (4.2)$$

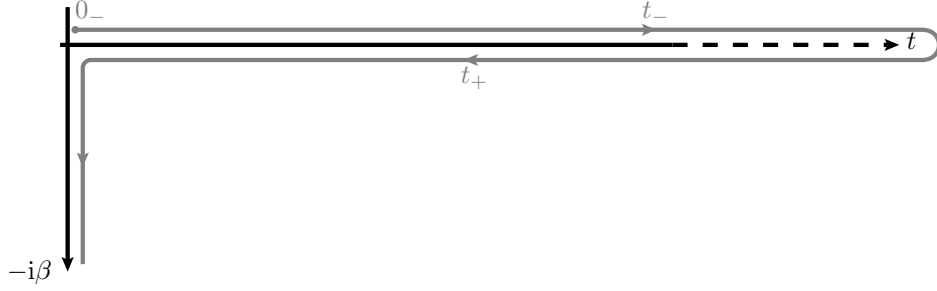


Figure 4.1: Keldysh contour for the pseudo-time τ .

The solution to these equations is formally found as

$$\hat{S}(t, t') = \begin{cases} \mathbb{T} \left[e^{-i \int_{t'}^t dt_1 \hat{H}(t_1)} \right] & t > t' \\ \bar{\mathbb{T}} \left[e^{-i \int_{t'}^t dt_1 \hat{H}(t_1)} \right] & t < t' \end{cases}, \quad (4.3)$$

where \mathbb{T} is the chronological time-ordering operator which orders operators with later times to the left and $\bar{\mathbb{T}}$ is the anti-chronological time-ordering operator.

The expectation value of an observable \hat{O} at some time t can then be evaluated as $O(t) = \text{Tr}\{\hat{\rho}_0 \hat{S}(0, t) \hat{O} \hat{S}(t, 0)\}$ where $\hat{\rho}_0$ is the density operator at $t = 0$. If the system is in equilibrium for $t \leq 0$, the density operator can be written as

$$\hat{\rho}_0 = \frac{e^{-\beta(\hat{H}_0 - \mu \hat{N})}}{\text{Tr}\{e^{-\beta(\hat{H}_0 - \mu \hat{N})}\}} = \frac{e^{\beta \mu \hat{N}} \hat{S}(-i\beta, 0)}{\text{Tr}\{e^{\beta \mu \hat{N}} \hat{S}(-i\beta, 0)\}}, \quad (4.4)$$

where $\beta = 1/k_B T$ is the inverse temperature and μ is the chemical potential. The expectation value of \hat{O} is then found as

$$O(t) = \frac{\text{Tr}\{e^{\beta \mu \hat{N}} \hat{S}(-i\beta, 0) \hat{S}(0, t) \hat{O} \hat{S}(t, 0)\}}{\text{Tr}\{e^{\beta \mu \hat{N}} \hat{S}(-i\beta, 0)\}}. \quad (4.5)$$

We can interpret this result as an evolution along a contour from zero to time t , back to zero and then along the imaginary axis up to $-i\beta$ as depicted in Figure 4.1. In the following we denote the evolution along this contour by the pseudo-time τ .

Before we can formulate the time-dependent version of density functional theory we need one more property of the time-evolution operator. Introducing a small perturbation $\delta\hat{V}(\tau)$ into the Hamiltonian \hat{H} we get

$$i \frac{d}{d\tau} \delta\hat{S}(\tau, \tau') = \delta\hat{V}(\tau) \hat{S}(\tau, \tau') + \hat{H}(\tau) \delta\hat{S}(\tau, \tau') \quad (4.6)$$

for the change of the evolution operator. Using (4.2) and the boundary condition $\delta\hat{S}(\tau, \tau) = 0$ we can solve this equation and we find for the change of the time-evolution operator:

$$\delta\hat{S}(\tau, \tau') = -i \int_{\tau'}^{\tau} d\tau_1 \hat{S}(\tau, \tau_1) \delta\hat{V}(\tau_1) \hat{S}(\tau_1, \tau'). \quad (4.7)$$

4.1.2 Action functional

The role of the ground state energy in static density functional theory is now played by the functional

$$\tilde{A}[v, \phi] = i \ln \text{Tr} \left\{ e^{\beta \mu \hat{N}} \hat{S}(-i\beta; 0_-) \right\}. \quad (4.8)$$

Please note that v and ϕ are contour variables, i.e. they may take different values on the forward and the backward branch, and \hat{S} is the time-evolution operator along the contour in Figure 4.1. Physical potentials can be recovered by requiring $v(t_+) = v(t_-)$ after the calculation, where t_+ and t_- indicate equal times on the backward and forward contour, respectively. Since we want to use a Legendre transformation to transform from the potentials to their conjugate variables, the densities, and thus obtaining the effective single-particle potential we need to check that for \tilde{A} equations analogous to (3.3) hold. By using (4.7) we find for a variation in the potential

$$\frac{\delta \tilde{A}}{\delta v_l(\tau)} = \frac{\text{Tr} \left\{ e^{\beta \mu \hat{N}} \hat{S}(-i\beta, 0) \hat{S}(0, \tau) \hat{n}_l \hat{S}(\tau, 0_-) \right\}}{\text{Tr} \left\{ e^{\beta \mu \hat{N}} \hat{S}(-i\beta, 0_-) \right\}} = n_l(\tau). \quad (4.9)$$

Similarly we find for a variation in the phase

$$\frac{\delta \tilde{A}}{\delta \phi_l(\tau)} = j_l(\tau). \quad (4.10)$$

In the next step we perform the Legendre transformation from the potentials and phases to the densities and currents,

$$A[n, j] = \tilde{A}[v, \phi] - \int_C d\tau \sum_l n_l(\tau) v_l(\tau) - \int_C d\tau \sum_l j_l(\tau) \phi_l(\tau). \quad (4.11)$$

The subscript C implies integration over the whole contour. As usual one recovers the local potentials and phases by

$$\frac{\delta A}{\delta n_l(\tau)} = -v_l(\tau) \quad \text{and} \quad \frac{\delta A}{\delta j_l(\tau)} = -\phi_l(\tau). \quad (4.12)$$

If we follow the same procedure for a noninteracting system \hat{H}^s , i.e. by defining a time-evolution operator $\hat{S}^s(t, t')$ and then introducing the functional \tilde{A}^s similar to (4.8), we can again perform a Legendre transformation from the single-particle potentials and phases to their conjugate variables

$$A^s[n, j] = \tilde{A}^s[v^s, \phi^s] - \int_C d\tau \sum_l n_l(\tau) v_l^s(\tau) - \int_C d\tau \sum_l j_l(\tau) \phi_l^s(\tau). \quad (4.13)$$

Since we want our auxiliary system \hat{H}^s to yield the same densities and currents as the interacting system \hat{H} we relate A and A^s through the identity

$$A[n, j] = A^s[n, j] + (A[n, j] - A^s[n, j]) = A^s[n, j] + A^{\text{HXC}}[n, j]. \quad (4.14)$$

The last equality is simply the definition of the Hartree-exchange-correlation functional $A^{\text{HXC}}[n, j]$. Using (4.12) we find the following rule for determining the effective single-particle quantities,

$$\begin{aligned} v_l(\tau) &= v_l^s(\tau) - v_l^{\text{HXC}}(\tau), \\ \phi_l(\tau) &= \phi_l^s(\tau) - \phi_l^{\text{XC}}(\tau), \end{aligned} \quad (4.15)$$

where the Hartree-exchange-correlation potential $v_l^{\text{HXC}}(\tau)$ is defined as

$$v_l^{\text{HXC}}(\tau) = \frac{\delta A^{\text{HXC}}}{\delta n_l(\tau)}. \quad (4.16)$$

Since the Hartree term does not depend on the currents, we find

$$\phi_l^{\text{XC}}(\tau) = \frac{\delta A^{\text{XC}}}{\delta j_l(\tau)}, \quad (4.17)$$

which also depends on all densities and currents. Please remember that all these quantities depend on the contour-time variable τ instead of the physical time t . Thus the variation of the potentials (phases) in positive t -direction is independent of the variation in negative t -direction. Physical potentials can be recovered by requiring physical densities, i. e. they are the same on the forward and the backward branch of the contour. Then we have

$$v_l^{\text{HXC}}(t) = \left. \frac{\delta A^{\text{HXC}}}{\delta n_l(\tau)} \right|_{n=n_l(t), j=j_l(t)} \quad \text{and} \quad \phi_l^{\text{XC}}(t) = \left. \frac{\delta A^{\text{XC}}}{\delta j_l(\tau)} \right|_{n=n_l(t), j=j_l(t)}. \quad (4.18)$$

4.1.3 Gauge invariance

An important point we have neglected up to now is the gauge invariance of our system. The influence of gauge invariance on density functional theory is twofold: On one hand it is desirable that not only the interacting system but also the single-particle system is gauge-invariant. On the other hand the gauge invariance affects the Legendre transform, because the transform (4.11) is no longer unique. So the question arises, if this non-uniqueness affects physical quantities.

We begin by shortly repeating how a gauge transformation (2.8) affects the potentials and phases:

$$\begin{aligned} \phi'_l &= \phi_l + \chi_l - \chi_{l+1} \\ v'_l &= v_l - \dot{\chi}_l \end{aligned} \quad (4.19)$$

Thus, if we variate the generating functional \tilde{A} in the direction of these gauge transformations, we get

$$\delta \tilde{A} = \tilde{A}[v', \phi'] - \tilde{A}[v, \phi] = - \int_C d\tau \sum_l [\dot{\chi}_l(\tau) n_l(\tau) + (\chi_{l+1}(\tau) - \chi_l(\tau)) j_l(\tau)]. \quad (4.20)$$

Partial integration of the first term and resummation of the second term leads to

$$\delta\tilde{A} = - \int_C d\tau \sum_l \chi_l(\tau) [\dot{n}_l(\tau) + j_l(\tau) - j_{l-1}(\tau)]. \quad (4.21)$$

Since \tilde{A} is gauge invariant, it follows that $\delta\tilde{A} = 0$ for all $\chi_l(\tau)$, thereby implying the continuity equation (2.7). Thus our question from above has to be answered with: yes, the gauge invariance does affect physical quantities, but in a completely desirable way, since it enforces the continuity equation.

Of course, the gauge transformation is recovered by the back-transformation from the densities to the potentials, $A[n, j] \rightarrow \tilde{A}[v, \phi]$. In this case one can exploit that the Legendre transform uses an extremal condition (cf. Appendix C) and calculate the extremum under the constraint that the continuity equation is fulfilled,

$$\tilde{A}[v, \phi] = \text{ext}_{n, j} \left\{ A[n, j] - \int_C d\tau \sum_l \chi_l(\tau) [\dot{n}_l(\tau) + j_l(\tau) - j_{l-1}(\tau)] \right\}. \quad (4.22)$$

Here the $\chi_l(\tau)$ are the Lagrange parameters. Invoking, as before, a partial integration of the first term and a resummation of the second, the extremum is now given by

$$\frac{\delta A}{\delta n_l(\tau)} + \dot{\chi}_l(\tau) = -v_l(\tau) \quad (4.23)$$

and

$$\frac{\delta A}{\delta j_l(\tau)} + \chi_{l+1}(\tau) - \chi_l(\tau) = -\phi_l(\tau). \quad (4.24)$$

Comparing this expressions with (4.12) we find the original gauge transformation (4.19).

4.1.4 Dynamical susceptibility and causality

After this introduction of time-dependent density functional theory we now turn our attention to an important quantity which is accessible within this framework, the dynamical susceptibility. For example, the explicit evaluation on the contour of the density-density response function gives

$$\chi_{nn}(l, \tau, l', \tau') = - \frac{\delta n_l(\tau)}{\delta v_{l'}(\tau')} = i \langle \text{T}_C [\Delta \hat{n}_l(\tau) \Delta \hat{n}_{l'}(\tau')] \rangle. \quad (4.25)$$

Here $\Delta \hat{n}_l(\tau)$ is a density fluctuation operator $\Delta \hat{n}_l(\tau) = \hat{n}_l(\tau) - \langle \hat{n}_l(\tau) \rangle$ in the Heisenberg picture. Switching back to physical potentials, where $\delta v(t) = \delta v(t_+) = \delta v(t_-)$, we find

$$\delta n_l(t) = - \int dt' \sum_{l'} \left[\chi(l, \tau, l', \tau') \Big|_{\tau=t, \tau'=t'_-} - \chi(l, \tau, l', \tau') \Big|_{\tau=t, \tau'=t'_+} \right] \delta v_{l'}(t'), \quad (4.26)$$

where the change of sign in the second term comes from the integration on the backwards branch of the contour. Inserting (4.25) gives

$$\delta n_l(t) = - \int dt' \sum_{l'} \chi_{nn}^R(l, t, l', t') \delta v_{l'}(t'), \quad (4.27)$$

with the definition $\chi_{nn}^R(l, t, l', t') = i\Theta(t - t') \langle [\hat{n}_l(t), \hat{n}_{l'}(t')] \rangle$ for the retarded density-density correlation function. The step function Θ originates from the cancellation of terms for $t' > t$.

If we repeat the whole argument for the single-particle functional A^s we find accordingly the single-particle susceptibility χ_{nn}^s . Since the solution of our single-particle system provides us with χ_{nn}^s and we are interested in the response χ_{nn} of the interacting system, we need a relation between the two. This can be found by noticing that the Legendre transformation provides also a relation between $A[n, j]$ and the susceptibility,

$$[\chi_{nn}(l, \tau, l', \tau')]^{-1} = \frac{\delta^2 A}{\delta n_l(\tau) \delta n_{l'}(\tau')}. \quad (4.28)$$

Then, using this relation together with (4.14) we find

$$[\chi_{nn}]^{-1} = [\chi_{nn}^s]^{-1} + f_{nn}^{\text{HXC}}, \quad (4.29)$$

where we defined the so-called Hartree-exchange-correlation kernel as

$$f_{nn}^{\text{HXC}}(l, \tau, l', \tau') = \frac{\delta v_l^{\text{HXC}}(\tau)}{\delta n_{l'}(\tau')}. \quad (4.30)$$

Please note that it is defined as functional derivative on the contour. Applying the same procedure as for the susceptibilities when going back from the pseudo-times on the Keldysh contour to physical times gives a retarded Hartree-exchange-correlation kernel, which therefore introduces a source of memory into the calculation. This causality crucially depends on the fact that the variations of the potential along the forward and the backward part of the contour are independent. If we would use physical potentials in the definition of the susceptibility, for example,

$$\frac{\delta^2 \tilde{A}}{\delta v_l(t) \delta v_{l'}(t')} = \frac{\delta n_l(t)}{\delta v_{l'}(t')} = -\chi_{nn}(l, t, l', t'), \quad (4.31)$$

the left-hand side would be symmetric under exchange of (l, t) and (l', t') . Thus the response function χ would not be zero for $t' > t$, i. e. not causal [99, 100, 96].

In the preceding discussion we used χ_{nn} to illustrate the principle of the Keldysh formalism, but similarly we may consider the density-current- or the current-current correlation functions (χ_{nj} , χ_{jn} and χ_{jj}). Hence we will use a matrix notation to denote the susceptibility in the following,

$$\tilde{\chi} = \begin{pmatrix} \chi_{nn}^R & \chi_{nj}^R \\ \chi_{jn}^R & \chi_{jj}^R \end{pmatrix}. \quad (4.32)$$

Accordingly the Hartree-exchange-correlation kernel has a similar structure,

$$f^{\text{HXC}} = \begin{pmatrix} f_{nn,R}^{\text{HXC}} & f_{nj,R}^{\text{HXC}} \\ f_{jn,R}^{\text{HXC}} & f_{jj,R}^{\text{HXC}} \end{pmatrix}, \quad (4.33)$$

where the elements $f_{\mu\nu,R}^{\text{HXC}}$ are the retarded versions of

$$f_{\mu\nu}^{\text{HXC}}(l, \tau, l', \tau') = \frac{\delta^2 A^{\text{HXC}}}{\delta\mu_l(\tau) \delta\nu_{l'}(\tau')}. \quad (4.34)$$

Thus (4.29) can be written in the form

$$[\tilde{\chi}]^{-1} = [\tilde{\chi}^s]^{-1} + \tilde{f}^{\text{HXC}} \quad \text{or} \quad \tilde{\chi} = [1 + \tilde{\chi}^s \tilde{f}^{\text{HXC}}]^{-1} \tilde{\chi}^s. \quad (4.35)$$

The components of the matrix (4.32) are related via the continuity equation or gauge transformations. A short summary of these relations and a few symmetries can be found in Appendix D.

4.2 Approximations

Clearly, similar to the static formalism, we have avoided the problem of solving the time-dependent many-body Schrödinger equation by putting all interaction effects into the Hartree-exchange-correlation potential. However, since we do not know this quantity, we have to use some approximations. As already discussed in Chapter 3, we separate the Hartree potential from the exchange-correlation potential. Since in the Hartree potential the interaction is instantaneous there is no further complication within the time-dependent formalism. So we have $v^{\text{HXC}} = v^{\text{H}} + v^{\text{XC}}$ and the kernel of the susceptibility becomes $\tilde{f}^{\text{HXC}} = \tilde{f}^{\text{H}} + \tilde{f}^{\text{XC}}$. Therefore the susceptibility (4.35) reduces to the standard RPA expression if $\tilde{f}^{\text{XC}} = 0$. Note that \tilde{f}^{H} only has an nn -entry, in Fourier representation given by $V(q) = 2V \cos q$. However, as we saw in Section 4.1.4, the exchange-correlation potential does in principle have a memory, i. e. it depends on all previous densities. The simplest approximation is then to assume that the system evolves adiabatically, which means that it is completely determined by the densities (and currents) at the considered time. In this case we can just reuse the exchange-correlation potentials and phases calculated from the static exchange-correlation energy (3.23).

It does, however, make an essential difference if we consider charge densities only or together with the current-densities. In the first case this assumption, together with the local density approximation, gives the so-called adiabatic LDA, also known as ALDA, while we denote the second case with C-ALDA where the C stands for the current. The main difference between these two is that the ALDA is a truly local approximation both in space and in time while the inclusion of currents takes some nonlocal effects, again both in space and in time, into account [9]. The reason for this is simply particle conservation as can be seen from the continuity equation for our one-dimensional lattice model,

$$-\omega n(q, \omega) + 2 \sin \frac{q}{2} j(q, \omega) = 0 \quad (4.36)$$

or in real space

$$\dot{n}_l(t) = j_{l-1}(t) - j_l(t). \quad (4.37)$$

A more thorough investigation of nonlocal exchange-correlation potentials, that can be constructed with help of currents, can be found in [9, 101] and the resulting functional has

been tested for example by P. L. de Boeij [102]. The adiabatic LDA has been compared with exact results in [103, 104]. For the calculation of the exchange-correlation kernel within the exact-exchange approximation we refer to [87, 88]. It has already been applied in [105, 106, 107, 108].

4.3 Dynamic Susceptibility

Now we investigate the dynamical susceptibility within C-ALDA in more detail. In particular, we consider a homogeneous system with total flux $\Phi \rightarrow 0$. In this limit, the current also vanishes, $j \rightarrow 0$. In this case we find that the off-diagonal elements of the Hartree-exchange-correlation kernel (4.33), f_{jn}^{HXC} and f_{nj}^{HXC} , both vanish, because the expansion of the ground state energy with respect to the current has no first order term. Thus \tilde{f}^{HXC} contains only the two terms f_{nn}^{HXC} and f_{jj}^{HXC} , and the χ_{nn} -element of (4.35) is given by

$$\chi_{nn}(q, \omega) = \chi_{nn}^s(q, \omega) - \chi_{nn}^s(q, \omega) f_{nn}^{\text{HXC}} \chi_{nn}(q, \omega) - \chi_{nj}^s(q, \omega) f_{jj}^{\text{HXC}} \chi_{jn}(q, \omega). \quad (4.38)$$

Employing particle conservation (D.5) we rewrite the density-current correlators in terms of the density-density response. Solving then for χ_{nn} we get

$$\chi_{nn}(q, \omega) = \frac{\chi_{nn}^s(q, \omega)}{1 + \chi_{nn}^s(q, \omega) \left[f_{nn}^{\text{HXC}} + \frac{\omega^2}{4 \sin^2(q/2)} f_{jj}^{\text{HXC}} \right]}, \quad (4.39)$$

where f_{nn}^{HXC} and f_{jj}^{HXC} are, due to the local adiabatic approximation, independent of q and ω . If $f_{jj}^{\text{HXC}} = 0$ we recover the approximation known as ALDA.

In order to discuss this result in more detail, recall that in the long-wavelength low-frequency limit the density response of the single-particle system is given by

$$\chi_{nn}^s(q, \omega) \simeq \chi_{\text{stat}}^s \frac{(qv_F)^2}{(qv_F)^2 - (\omega + i0)^2}, \quad (4.40)$$

where v_F is the Fermi-velocity and the static susceptibility is given by $\chi_{\text{stat}}^s = 1/\pi v_F$. Considering the limit $\omega = 0, q \rightarrow 0$, and noting that

$$f_{nn}^{\text{XC}} = \frac{1}{L} \left(\frac{\partial^2 E^{\text{BA}}}{\partial n^2} - \frac{\partial^2 E^0}{\partial n^2} - 2LV \right) \quad (4.41)$$

it is straightforward to verify that the density response of the interacting system is

$$\chi_{\text{stat}} = \left(\frac{1}{L} \frac{\partial^2 E^{\text{BA}}}{\partial n^2} \right)^{-1}. \quad (4.42)$$

On the other hand, taking $q \rightarrow 0$ first, we find

$$\chi_{jj}(q = 0, \omega \rightarrow 0) = -2D^{\text{BA}}, \quad (4.43)$$

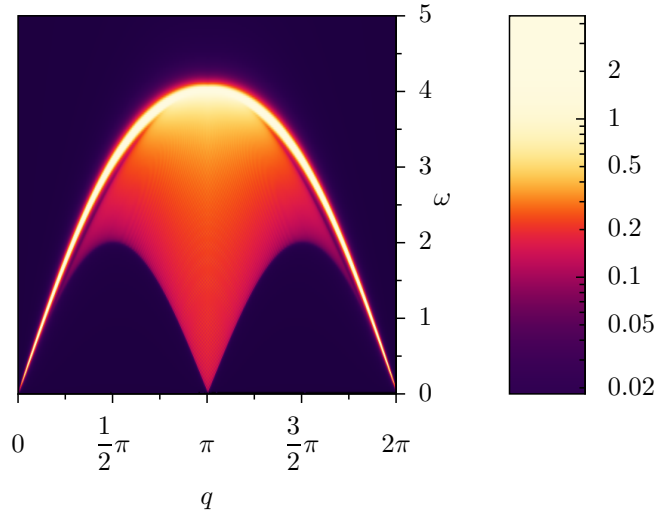


Figure 4.2: Imaginary part of the dynamical susceptibility $\text{Im}\chi_{nn}(q, \omega)$ in units of t^{-1} for half filling and $V = 1.0t$. ω is given in units of t obtained within the C-ALDA. For the plot we replace the imaginary part of the denominator in (D.3) by a finite value, η , which we choose here to be $0.005t$.

i. e. in both limits we recover the exact result. The minus here is due to our definition of the response function. Inserting (4.40) into (4.39) we find for small q, ω

$$\chi_{nn}(q, \omega) \simeq \chi_{\text{stat}} \frac{(qv)^2}{(qv)^2 - (\omega + i0)^2}, \quad (4.44)$$

where

$$v^2 = v_F^2 \frac{1 + \frac{f_{nn}^{\text{HXC}}}{\pi v_F}}{1 - \frac{f_{jj}^{\text{HXC}} v_F}{\pi}} = \frac{2D^{\text{BA}}}{\chi_{\text{stat}}}. \quad (4.45)$$

This is exactly the susceptibility of a Luttinger liquid. So, C-ALDA gives the correct values of the static susceptibility χ_{stat} and the velocity v of the collective modes.

To complete our analysis of the dynamical susceptibility we present some numerical results. In Figure 4.2 we plot the imaginary part of $\chi_{nn}(q, \omega)$ for half filling and interaction $V = t$. The continuum has the same boundaries as in the noninteracting case (cf. Fig. 2.2), but now its spectral weight vanishes in the long-wavelength limit. Above the continuum there is a well-defined branch of collective excitations. As discussed above, the corresponding velocity for $q \rightarrow 0$ has the exact value. However the contour plot is almost indistinguishable from the corresponding one obtained within ALDA. This can be seen for example by means of Figures 4.3 and 4.4 where the profile in ω -direction of the imaginary part of $\chi_{nn}(q, \omega)$ at $q = \pi/2$ is shown. These two figures use a much higher system size and a lower value for the broadening η . The blue line corresponds to the single-particle system which has a divergence at the higher end of the spectrum. The green and red lines depict the susceptibilities within the ALDA and C-ALDA, respectively. As one sees, the spectral weight of the quasi-particle continuum is diminished compared to χ^s , while there is a single peak above the continuum. This peak corresponds to the branch

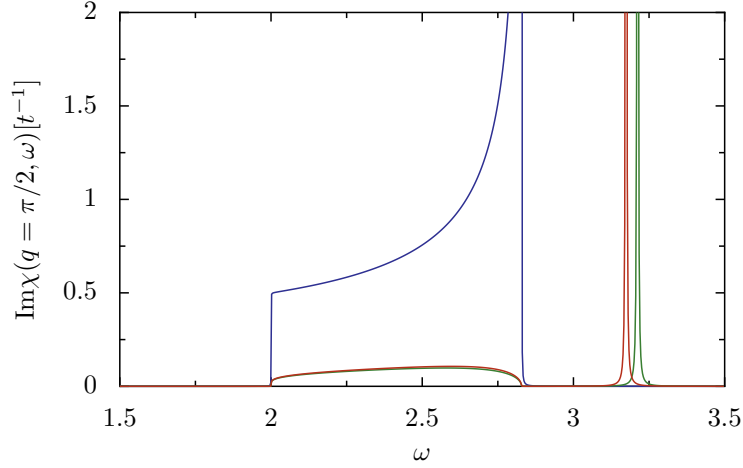


Figure 4.3: Imaginary part of the dynamic susceptibility $\text{Im}\chi_{nn}(q, \omega)$ (in units of t^{-1}) as a function of the frequency ω at $q = \pi/2$ and interaction $V = t$. The system was chosen to be of size $L = 10^6$ and at half filling. The red curve corresponds to the single-particle susceptibility χ^s whereas the green line is obtained within the standard adiabatic LDA while the red line is for C-ALDA. ($\eta = 10^{-4}t$)

of collective excitations in Figure 4.2 and clearly there is only a minor difference when including the current.

However, these results have some shortcomings. In [109] Rodrigo G. Pereira, Steven R. White and Ian Affleck investigated the dynamical structure factor for the Heisenberg XXZ model, which corresponds to the density-density correlation function in the spinless fermion model. Amongst others they used the DMRG approach which gives (numerically) accurate results. These DMRG results differ in various ways from Figures 4.3 and 4.4. First, contrary to the adiabatic approximation the whole continuum and not only one branch is shifted by the interaction. A second qualitative difference is that in the DFT+ALDA approach the singularity lies above the continuum while the exact results show that it is shifted by the interaction to the lower edge of the continuum. Thus, as with the static susceptibility, the local density approximation only gives reasonable results in the long-wavelength limit, $q \rightarrow 0$.

In the previous discussion we used the linear response function as a means to investigate the validity of the adiabatic approximations. Now we can reverse this argument and ask what can we learn from our results for the real exchange-correlation kernel and therefore for the corresponding potential. So let us first investigate what happens technically in the adiabatic local density approximation. This can be seen in Figure 4.5, where we have plotted the real part of the dynamic susceptibility as function of the frequency ω at $q = \pi/2$ for a system of 50 lattice sites at half filling. The dashed black line depicts the single-particle susceptibility. One can see due to the finite size of our system a few singularities which become a continuum in the thermodynamic limit, $L \rightarrow \infty$. The constant red line is equivalent to the inverse of the Hartree-exchange-correlation kernel,

$$\frac{1}{2V \cos(q) + f_{nn}^{\text{HXC}}}, \quad (4.46)$$

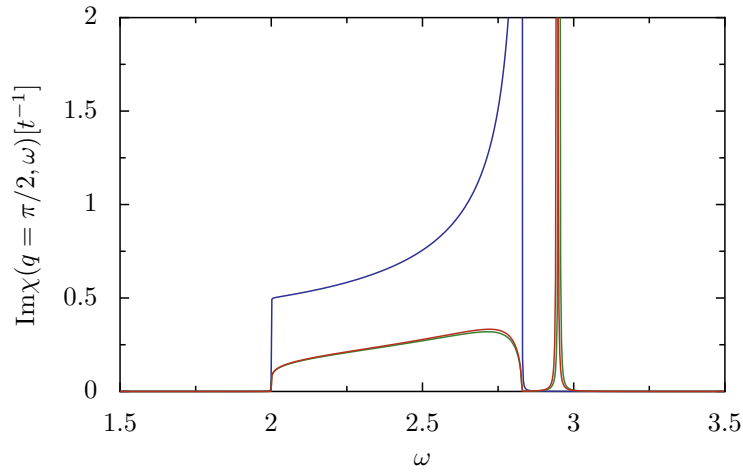


Figure 4.4: Same as Figure 4.3, for $V = 0.5t$

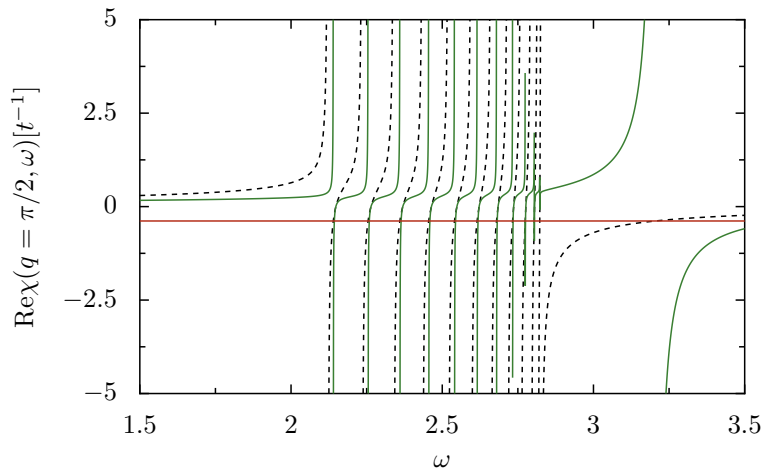


Figure 4.5: Real part of the dynamic susceptibility $\text{Re}\chi_{nm}(q, \omega)$ (in units of t^{-1}) as a function of the frequency ω at $q = \pi/2$. The system was chosen to be of size $L = 50$ and at half filling. The dashed black curve corresponds to the single-particle susceptibility χ^s whereas the green line is obtained within ALDA. The constant red line shows the value of f^{HXC} .

such that the points, where the red and black lines intersect, determine the singularities of the susceptibility within the adiabatic local density approximation which is plotted as a green line. Including the f_{jj}^{HXC} term does not change the picture qualitatively since this term is an analytical function in ω and the prefactor is rather small. As one sees from this picture the highest singularity is shifted by the ALDA denominator but all other poles can only be shifted in the small region between the neighboring singularities that is by zero in the thermodynamic limit.

Thus, the quasi-particle continuum has to stay at the same position with an analytic exchange-correlation kernel, whereas in the exact susceptibility the boundaries of the continuum do depend on the interaction strength. To capture this kind of physics within DFT one has to find and use a highly non-analytic function for $\check{f}^{\text{HXC}}(q, \omega)$.

5 Transport through a quantum dot

As already said before, DFT is an important tool for determining the electronic structure of materials. In recent years the application of density functional theory to the electronic transport through interfaces between two materials or through nanocontacts between two leads became more and more important. In the following we concentrate on the latter. As an application they can be used for electronics of molecular size while from a theoretical point of view they consist of open systems out of equilibrium. Both features, the open system and the non-equilibrium are very difficult to treat theoretically. In order to investigate the quality of density functional theory when applied to such a problem, one needs to decide whether discrepancies to the experiment or other theoretical approaches arise because of an insufficient modeling of said features or because of the underlying approximation for the exchange-correlation potential. In the following we focus on the latter question and study the conductance through a quantum dot by means of the linear conductance which only depends on equilibrium quantities. Moreover we employ a model which has already been investigated using the density-matrix renormalization group approach (DMRG). Thus we are able to assess the quality of different approximations even for strong interactions.

5.1 Model

In this chapter we modify our model of spinless fermions. We follow [56], where the authors used DMRG to calculate the exact conductance of a quantum dot attached to leads. Figure 5.1 is a schematic picture of this model. The Hamiltonian can be written as

$$\hat{H} = \hat{H}_C + \hat{H}_L + \hat{H}_R + \hat{H}_{C \leftrightarrow L} + \hat{H}_{C \leftrightarrow R} \quad (5.1)$$

where \hat{H}_C is the Hamiltonian for the central system. \hat{H}_L and \hat{H}_R stand for the left and right lead, respectively, while $\hat{H}_{C \leftrightarrow L}$ and $\hat{H}_{C \leftrightarrow R}$ are the couplings between the leads and the system. The central system \hat{H}_C consists of ten real-space sites. The first two sites are noninteracting, whereas the next five sites, the (quantum) dot, are interacting and can also be tuned by a gate voltage v_{gate} . The last three sites are again noninteracting. Therefore the corresponding Hamiltonian can be written as

$$\hat{H}_C = - \sum_{l=1}^9 t_{l,l+1} (\hat{c}_l^\dagger \hat{c}_{l+1} + \hat{c}_{l+1}^\dagger \hat{c}_l) + V \sum_{l=3}^6 \left(\hat{n}_l - \frac{1}{2} \right) \left(\hat{n}_{l+1} - \frac{1}{2} \right) + \sum_{l=3}^7 v_{\text{gate}} \hat{n}_l. \quad (5.2)$$

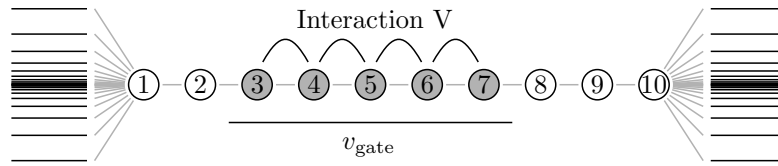


Figure 5.1: The model used throughout Chapter 5. At the center we have five interacting sites which can be tuned by the gate voltage. These sites are coupled to a few noninteracting real-space sites (empty circles) and at both sides we have noninteracting leads which are modelled in k -space. For clarity the different hopping parameters have been omitted in this picture.

As in the previous sections V is the interaction strength. The hopping amplitude $t_{l,l+1}$ takes several values

$$t_{l,l+1} = \begin{cases} t & l = 1, 8, 9 \\ t' & l = 2, 7 \\ t_{\text{dot}} & l = 3 \dots 6 \end{cases}, \quad (5.3)$$

such that the hopping between interacting sites is given by t_{dot} , the hopping between noninteracting sites by t and the coupling between interacting and noninteracting sites by t' . The numerical values of these parameters are in the following chosen to be: $t = 1$, $t_{\text{dot}} = 0.5$ and $t' = 0.2$. The leads are modelled by a series of discrete energy levels,

$$\hat{H}_{L/R} = \sum_k \epsilon_k \hat{c}_k^+ \hat{c}_k, \quad (5.4)$$

such that the number of levels near the Fermi energy for half filled leads is exponentially dense,

$$\epsilon_k = \frac{\sinh(\Gamma k)}{\sinh(\Gamma L_{L/R})}. \quad (5.5)$$

Here $L_{L/R}$ is the size of the left/right lead. The index k goes from $-\frac{1}{2}L_{L/R}$ to $\frac{1}{2}L_{L/R}$ and the parameter Γ has the value $\Gamma = 0.2$ for our calculations. This choice for the levels of the leads has the advantage that there are enough levels near the Fermi energy, i. e. the resolution is high enough, to observe the resonances when tuning the gate voltage, while at the same time keeping the size of the leads sufficiently small for efficient numerical calculations. The couplings between system and leads can be written as

$$\hat{H}_{C \leftrightarrow L} = \sum_k t_k (c_k^+ c_1 + c_1^+ c_k) \quad \text{and} \quad \hat{H}_{C \leftrightarrow R} = \sum_k t_k (c_k^+ c_{10} + c_{10}^+ c_k), \quad (5.6)$$

where the energy levels ϵ_k are coupled directly to the outermost real-space sites. This coupling is modelled in a way to resemble an open system as close as possible. A detailed derivation of the coupling strength can be found in Appendix E. We find that

$$t_k = \frac{1}{\sqrt{\pi \mathcal{N}(\epsilon_k)}}, \quad (5.7)$$

where $\mathcal{N}(\epsilon)$ is the density of states in the leads at energy ϵ .

5.2 Effective potentials from exact diagonalization

In this chapter we are looking at a situation, which is in some respect fundamentally different to the situation in earlier chapters: we study a system where the interaction is confined to a small region, the quantum dot. Thus we are able to use not only the LDA and the exact-exchange method to investigate this model, but the small size of the quantum dot also enables us to calculate a good exchange-correlation potential by using exact diagonalizations of the central system \hat{H}_C , which contains the dot and a few neighboring sites.

In this case we approximate the Hartree-exchange-correlation energy for the complete Hamiltonian (5.1),

$$E^{\text{HXC}} = F[n] - F^s[n] \quad \text{where} \quad v_l^{\text{HXC}} = \frac{\partial}{\partial n_l}(F[n] - F^s[n]), \quad (5.8)$$

by the Hartree-exchange-correlation energy of the central region without the leads,

$$E^{\text{HXC}} = F_C[n] - F_C^s[n] \quad \text{where} \quad v_l^{\text{HXC}} = \frac{\partial}{\partial n_l}(F_C[n] - F_C^s[n]). \quad (5.9)$$

Here $F_C[n]$ is the Legendre-transform of the ground state energy of the central region \hat{H}_C without the leads (compare to the definition of F in Chapter 3). Accordingly $F_C^s[n]$ is its noninteracting pendant, corresponding to an effective noninteracting Hamiltonian \hat{H}_C^s for this region. Please note that $F_C[n]$ and $F_C^s[n]$ depend on all densities of the central system. Thus, within this approximation, we are able to calculate a nonlocal Hartree-exchange-correlation potential for the central region.

The remaining task is now to calculate $F_C[n]$, $F_C^s[n]$ and their derivatives. In order to do so, we introduce an potential $\sum_l v_{C,l} \hat{n}_l$ into the Hamiltonian of the central region (5.2) and an analogous potential $\sum_l v_{C,l}^s \hat{n}_l$ into the single-particle Hamiltonian \hat{H}_C^s . By adjusting these potentials we are able to reproduce the density profile, given by the complete single-particle Hamiltonian \hat{H}^s , at the central region. Then (at this profile) with the definitions (3.4) and (3.5) of the Legendre transformation we find

$$E^{\text{HXC}} = E_C - E_C^s + \sum_l v_l^{\text{HXC}} n_l \quad \text{and} \quad v_l^{\text{HXC}} = v_{C,l}^s - v_{C,l}. \quad (5.10)$$

Since the extended interacting region contains only a few lattice sites – 10 in our model – an exact diagonalization of the Hamiltonian or, even better, a simple iteration method like the Lanczos algorithm to calculate the ground state of the interacting Hamiltonian \hat{H}_C is still quite fast. Thus, even if we have to take the iteration process for finding the correct density profile into account, this procedure is still feasible for calculations. A schematic of the self-consistent procedure is depicted in Figure 5.2.

However, we still have to deal with another complication. If we look at the Hamiltonian \hat{H}_C then the eigenstates contain only an integer number of particles. Calculations of the total system on the other hand may give a fractional number of particles, \mathcal{N} , at the extended interacting region. So, instead of only one ground state, we have to use a

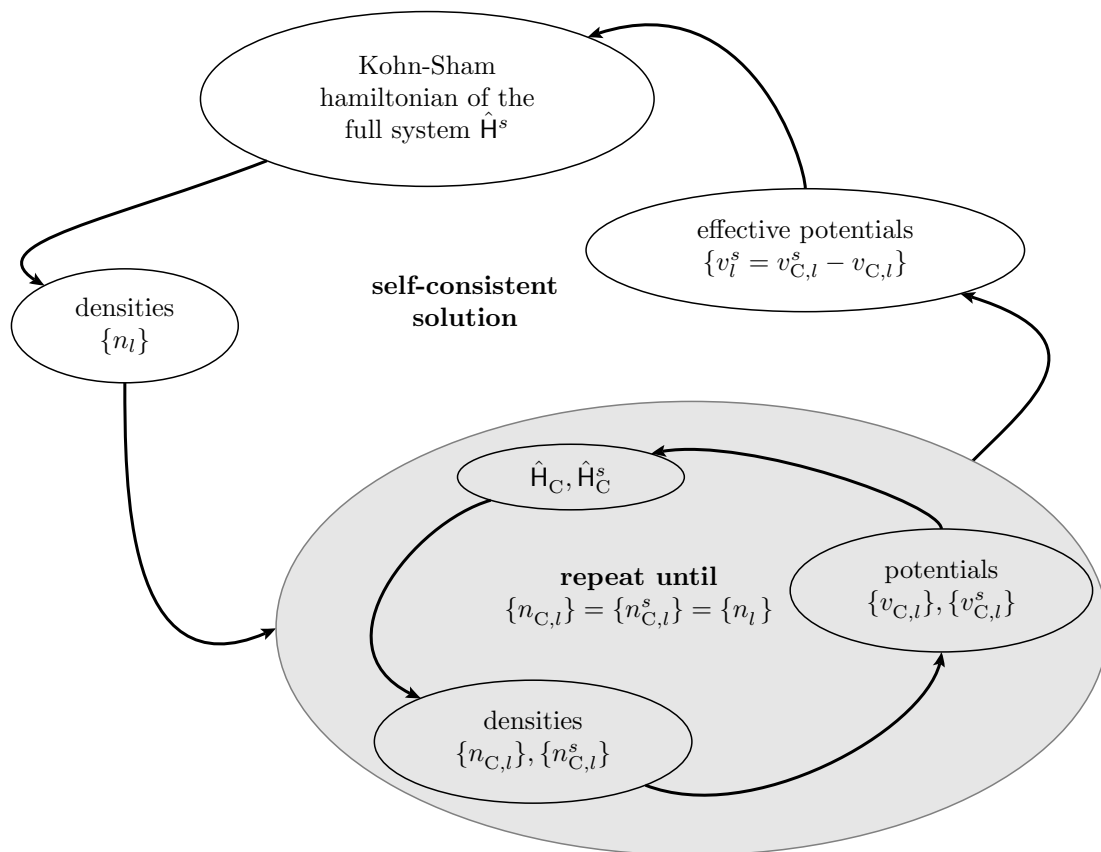


Figure 5.2: Schematic of the self-consistent procedure that is used to obtain the nonlocal exchange-correlation potential. Within this scheme we have two self-consistent cycles. The inner cycle (greyed out) consists of a three-step procedure. It begins with diagonalization of the interacting Hamiltonian \hat{H}_C of the central region and the corresponding single-particle Hamiltonian \hat{H}_C^s to obtain the ground state. In the next step we determine the densities $n_{C,l}^s, n_{C,l}$ of both systems. If these densities differ from the density of the complete single-particle system \hat{H}^s we determine new potentials $v_{C,l}^s, v_{C,l}$ and repeat this cycle. If the ground state densities of \hat{H}_C and \hat{H}_C^s agree with n_l the inner self-consistency cycle terminates and we can calculate the effective single-particle potential for the complete system. The outer cycle is the same as for other density functional calculations, where we diagonalize the Kohn-Sham Hamiltonian, calculate the density and then calculate the exchange-correlation potential until we reach self-consistency.

superposition of states with different particle numbers. The most simple superposition is described by the density operator

$$\hat{\rho} = \alpha |N, 0\rangle \langle N, 0| + (1 - \alpha) |N + 1, 0\rangle \langle N + 1, 0|, \quad (5.11)$$

where $|N, 0\rangle$ denotes the N -particle ground state. \mathcal{N} lies between the integer numbers N and $N + 1$ and $\alpha = N + 1 - \mathcal{N}$ is chosen, such that $\text{Tr}\{\hat{\rho}\hat{N}\} = \mathcal{N}$. We can motivate this ansatz by considering the density operator for the grand canonical ensemble

$$\hat{\rho} = \frac{1}{Z} e^{-\beta(\hat{H}_C - \mu\hat{N})}. \quad (5.12)$$

The partition function is defined as $Z = \text{Tr}\{e^{-\beta(\hat{H}_C - \mu\hat{N})}\}$, β is the inverse temperature, μ the chemical potential and \hat{N} the particle number operator of the system. The zero temperature limit $\beta \rightarrow \infty$ gives a projector to a single state $\hat{\rho} = |N, 0\rangle \langle N, 0|$ and the number of particles as a function of the chemical potential is a step-function. If we choose $\mu = E_{N+1} - E_N$, where E_N is the energy of the N -particle ground state, the system is exactly in between the N - and the $N + 1$ -particle ground state,

$$\hat{\rho} = \frac{1}{2} (|N, 0\rangle \langle N, 0| + |N + 1, 0\rangle \langle N + 1, 0|). \quad (5.13)$$

Any slight deviation of this value gives again a pure state with an integer number of particles. However if we use an arbitrary small but finite temperature the steps between the particle numbers are broadened and we can adjust μ to give any fractional particle number. In this case the dominant part of the density operator reads:

$$\hat{\rho} = \frac{1}{Z} \left[|N, 0\rangle \langle N, 0| e^{-\beta(E_N - \mu N)} + |N + 1, 0\rangle \langle N + 1, 0| e^{-\beta(E_{N+1} - \mu(N+1))} \right]. \quad (5.14)$$

One then finds the relation

$$\mu = E_{N+1} - E_N + \frac{1}{\beta} \ln \left(\frac{1}{\alpha} - 1 \right). \quad (5.15)$$

between μ and α . Considering only discrete systems (and neglecting degeneracies) we can always choose the temperature small enough so that only the two states $|N, 0\rangle$ and $|N + 1, 0\rangle$ contribute significantly. This was also found in [110] for the ground state energy of a system with fractional particle number. In the following we abbreviate this approximation with ED (*exact diagonalization*). In Figure 5.3 we show an example for the Hartree-exchange-correlation potential at the central region obtained with DFT+ED compared to the potential from the exact-exchange method.

The exact diagonalization procedure, as discussed in this section, is by construction not applicable to long chains of interacting fermions. However, one may ask, if we can generalize this procedure to such systems. A straightforward generalization is to look at site l and calculate the exchange-correlation energy for this site from exact diagonalization of this site together with its neighbors. By studying the static susceptibility with this generalization we find two inherent artifacts that render this method useless. The corresponding discussion can be found in Appendix F.1.

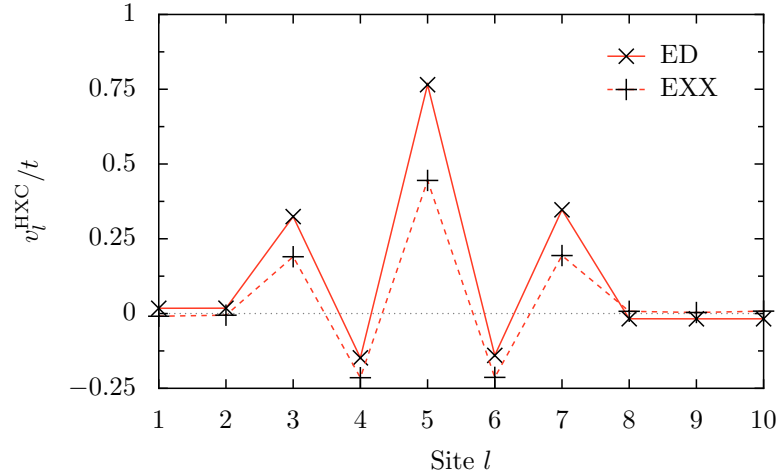


Figure 5.3: Hartree-exchange-correlation potential at the central region. We compare the exact-exchange approximation to our exact diagonalization procedure. The interaction strength was set to $V = t = 2t_{\text{dot}}$; the gate voltage was $V_{\text{gate}} = 0.5t$.

5.3 Linear conductance

The linear conductance G is determined from the response of a system to an applied bias voltage U , i. e. as the ratio of the induced current and the bias voltage,

$$G = \frac{I}{U}. \quad (5.16)$$

Since we consider only one-dimensional systems the current is simply given by the current-density, $j = \langle \hat{j} \rangle$. The bias voltage can be modelled as a difference in the chemical potentials of the left and right lead. In the following we choose a symmetric model where the left and right lead are shifted by $+\frac{U}{2}$ and $-\frac{U}{2}$, respectively. If U is small we can use linear response theory to calculate the change of the current by means of the current-density response function,

$$\delta j_l = - \sum_{l' \in \text{L,R}} \chi_{jn}(l, l', \omega) \delta v_{l'}, \quad (5.17)$$

where $\delta v_{l'} = \frac{U}{2}$ on the left and $\delta v_{l'} = -\frac{U}{2}$ on the right lead (denoted by L and R respectively). In the dc-limit $\omega \rightarrow 0$ the current j is, due to current conservation in one-dimension, constant throughout the system. Therefore the conductance in the linear response limit is given by

$$G = -\pi \frac{e^2}{\hbar} \lim_{\omega \rightarrow 0} \text{Re} \left[\sum_{l' \in \text{L}} \chi_{jn}(l, l', \omega) - \sum_{l' \in \text{R}} \chi_{jn}(l, l', \omega) \right] \quad (5.18)$$

where the site l can be chosen arbitrarily. Here we put back the physical units e and \hbar . There are also other, equivalent, possibilities to calculate the conductance, e. g.

$$\delta j_l = \sum_{l'} \sigma(l, l', \omega) \delta e(l', \omega), \quad (5.19)$$

where $e(l, \omega) = i\omega\phi_l - v_{l+1} + v_l$ corresponds to the electric field and σ is the nonlocal conductivity. In a gauge where the electric field is put into the local phase one finds

$$G = \pi \frac{e^2}{h} \lim_{\omega \rightarrow 0} \text{Re} \frac{1}{i\omega} (\chi_{jj}(l, l_{L \leftrightarrow C}, \omega) + \chi_{jj}(l, l_{C \leftrightarrow R}, \omega)). \quad (5.20)$$

Here the indices $l_{L \leftrightarrow C}$ and $l_{C \leftrightarrow R}$ denote the sites of the system coupled to the left and right lead, respectively. All other elements of the sums vanish because of the constant potential. Using a static gauge transformation we can shift these two indices to any position on the central region. For practical application of equation (5.20) it is favorable to evaluate the current-current correlation function not at the bonds to the leads but at the first bonds within the central region ($l_{1 \rightarrow 2}$ and $l_{9 \rightarrow 10}$ with the notation of fig. 5.1). The reason simply is that in the former case we have to evaluate the current from every energy level of the leads to the central region while the latter only needs the current between two sites. Since the exact result does not depend on l one may also choose l as $l_{1 \leftrightarrow 2}$ and as $l_{9 \leftrightarrow 10}$ and again average over this two values, so that the conductance of the single-particle system becomes

$$\begin{aligned} G^s &= \pi \frac{e^2}{h} \lim_{\omega \rightarrow 0} \text{Re} \frac{1}{2i\omega} \sum_{k,p} \frac{|\langle k | \hat{j}_{l_{1 \leftrightarrow 2}} + \hat{j}_{l_{9 \leftrightarrow 10}} | p \rangle|^2 (f_k - f_p)}{\omega + \epsilon_p - \epsilon_k + i\eta} \\ &= \pi \frac{e^2}{h} \lim_{\omega \rightarrow 0} \frac{-\eta}{2\omega} \sum_{k,p} \frac{|\langle k | \hat{j}_{l_{1 \leftrightarrow 2}} + \hat{j}_{l_{9 \leftrightarrow 10}} | p \rangle|^2 (f_k - f_p)}{(\omega + \epsilon_p - \epsilon_k)^2 + \eta^2} \\ &= \pi \frac{e^2}{h} \eta \sum_{k,p} \frac{|\langle k | \hat{j}_{l_{1 \leftrightarrow 2}} + \hat{j}_{l_{9 \leftrightarrow 10}} | p \rangle|^2 (f_k - f_p)}{[(\epsilon_p - \epsilon_k)^2 + \eta^2]^2} (\epsilon_k - \epsilon_p). \end{aligned} \quad (5.21)$$

Since we are dealing with a finite system the parameter η is kept bigger than zero. This leads to a broadening of the energy levels and to an additional source/drain in the continuity equation for the leads,

$$\partial_t n_l + \eta n_l + j_l - j_{l-1} = 0. \quad (5.22)$$

η must be chosen large enough, so that enough particles are created/annihilated in the leads to sustain the current through the system. On the other hand if it is too large, too much details of the conductance are smeared out. A sensible choice for our system is found to be $\eta = 0.4 \cdot 10^{-4}$. Due to the relations between the current-current, current-density and density-density correlator one can also use χ_{nn} to calculate the conductance. Beginning with (5.18) and using the continuity equation (5.22), one finds

$$G^s = \frac{\pi e^2 \eta}{2h} \sum_{k,p} \frac{|\langle k | \hat{N}_L + \hat{N}_R | p \rangle|^2 (f_k - f_p)}{(\epsilon_p - \epsilon_k)^2 + \eta^2} (\epsilon_k - \epsilon_p). \quad (5.23)$$

Here \hat{N}_L and \hat{N}_R are the occupation number operator for the left and the right lead, respectively. Using the same argument as before we symmetrized the expression with respect to exchanging $L \leftrightarrow R$.

As already stated during the discussion of the susceptibilities in Chapters 3 and 4 the susceptibility of the interacting system is given by the single-particle susceptibility modified by a denominator similar to the random-phase approximation (RPA). Therefore we also have to modify the conductance. If we use, for example, the density-density correlator to calculate the conductance (5.23),

$$G = \pi \frac{e^2}{2h} \lim_{\omega \rightarrow 0} \text{Re} \sum_{l, l' \in \text{L,R}} (i\omega + \eta) \chi_{nn}(l, l', \omega) = \pi \frac{e^2 \eta}{2h} \text{Re} \sum_{l, l' \in \text{L,R}} \chi_{nn}(l, l', 0), \quad (5.24)$$

with L and R denoting the left and the right lead, the correction to the single-particle susceptibility is given by the matrix equation

$$\check{\chi}_{nn} = [1 - \check{\chi}_{nn}^s \check{f}_{nn}^{\text{HXC}}]^{-1} \check{\chi}_{nn}^s. \quad (5.25)$$

The elements of the matrix $\check{\chi}_{nn}$ are given by $[\check{\chi}_{nn}]_{ll'} = \chi_{nn}(l, l', 0)$. We will see soon that the Hartree-exchange-correlation kernel $\check{f}_{nn}^{\text{HXC}}$ is irrelevant for the model and approximations of the present study. Nevertheless we complete here the general discussion. We analyze equation (5.25) under the assumption that $\check{f}_{nn}^{\text{HXC}}$ can be truncated in real space for positions that are far from the interacting region. Clearly this assumption holds for the ALDA, where $\check{f}_{nn}^{\text{HXC}}$ is confined to the interacting region. In this case it is given by

$$[\check{f}_{nn}^{\text{HXC}}]_{ll'} = \begin{cases} f_{\text{ALDA}}^{\text{XC}}(n_l) & \text{if } l = l' \text{ and } l, l' \text{ interacting} \\ V & \text{if } l = l' + 1, l' - 1 \text{ and } l, l' \text{ interacting} \\ 0 & \text{otherwise} \end{cases}, \quad (5.26)$$

where l and l' are interacting sites. Please remember that $f_{\text{LDA}}^{\text{XC}}(n_l) = \partial v^{\text{XC}}(n_l) / \partial n_l$. V is the interaction strength and the elements on the secondary diagonal are derived from the Hartree potentials. Since we need only the double sum of the susceptibilities (5.24) and $\check{f}_{nn}^{\text{HXC}}$ is confined to the interacting region, we do not have to solve the matrix equation (5.25) but the simpler equations

$$\sum_{i, j \in \text{L,R}} [\check{\chi}_{nn}]_{ij} = \sum_{i, j \in \text{L,R}} [\check{\chi}_{nn}^s]_{ij} + \sum_{l, m \in \text{C}} \left(\sum_{i \in \text{L,R}} [\check{\chi}_{nn}^s]_{il} \right) [\check{f}_{nn}^{\text{HXC}}]_{lm} \left(\sum_{j \in \text{L,R}} [\check{\chi}_{nn}]_{mj} \right) \quad (5.27)$$

and

$$\sum_{j \in \text{L,R}} [\check{\chi}_{nn}]_{lj} = \sum_{j \in \text{L,R}} [\check{\chi}_{nn}^s]_{lj} + \sum_{l', m \in \text{C}} [\check{\chi}_{nn}^s]_{ll'} [\check{f}_{nn}^{\text{HXC}}]_{l'm} \left(\sum_{j \in \text{L,R}} [\check{\chi}_{nn}]_{mj} \right). \quad (5.28)$$

Here C denotes the sites of the central region. The second equation is needed to calculate the last term of the first equation. Therefore the index l only denotes sites of the interacting system and the second equation can be solved self-consistently. Thus in a more compact syntax the conductance can be written as

$$G = G^s + \frac{\pi e^2 \eta}{2h} \text{Re} \{ \underline{\chi}^s \check{f}_{nn}^{\text{HXC}} \underline{\chi} \} \quad (5.29)$$

$$\underline{\chi} = \underline{\chi}^s + \check{\chi}_{\text{red}}^s \check{f}_{nn}^{\text{HXC}} \underline{\chi},$$

with the vectors $\underline{\chi} = \sum_{j \in L, R} [\check{\chi}_{nn}]_{lj}$ and $\underline{\chi}^s = \sum_{j \in L, R} [\check{\chi}_{nn}^s]_{lj}$. $\check{\chi}_{\text{red}}^s$ is a ‘reduced’ susceptibility of the single-particle system, which only takes into account changes of the density in the interacting system due to variations of the potential at the interacting system. The solution of this reduced form of the matrix equation does in our case (ALDA for five interacting sites) only need the inversion of a 5×5 -matrix instead of a $L \times L$ -matrix as in (5.25) and is thus numerically quite efficient.

As already stated before the exchange-correlation kernel is irrelevant for the calculation of the linear conductance within our model. Rewriting equation 5.19 as

$$\delta j_l = \sum_{l'} \sigma^s(l, l') [\delta e(l') + \delta e^{\text{HXC}}(l')], \quad (5.30)$$

where σ^s is the single-particle conductivity and $\delta e^{\text{HXC}} = -v_{l+1}^{\text{HXC}} + v_l^{\text{HXC}}$, we can rephrase the above statement as: The internal field δe^{HXC} does not contribute to the conductivity. This can be easily seen in one dimension: Particle conservation implies the current is constant throughout the system, i. e. σ^s does not depend on the position l . Additionally we have the symmetry $\sigma^s(l, l') = \sigma^s(l', l)$, thus it also does not depend on l' . Then the current through our dot becomes

$$\delta j = \sigma^s \sum_{l'} [\delta e(l') + \delta e^{\text{HXC}}(l')]. \quad (5.31)$$

Inserting the explicit expression for the internal field we see that most terms of the sum cancel and only the two Hartree-exchange-correlation potentials at the interfaces to the leads contribute. If they are small, as to be expected for our system where the interaction is confined to a small region, we may neglect them and find that $\sigma^s = \sigma$.

5.4 Results

Calculating the conductance for our model system with various approximations for different interaction strengths gives a number of interesting results. With figures 5.4 to 5.11 we show a representative overview of these results. In the previous section we have already argued that the Hartree-exchange-correlation kernel is negligible. In fact, within the local density approximation the contribution of this kernel is zero, because the exchange-correlation potential is confined to the interacting region. Thus we use $G = G^s$ in the following discussion.

5.4.1 General features

The first figure, 5.4, shows the conductance as function of the gate voltage for the non-interacting system (grey line) and for a relatively weak interaction, $V = 0.5t = t_{\text{dot}}$ (red line). The results in this graph were obtained with LDA. The first, trivial, observations are that there are five resonances and the conductance at each of the resonances is equal to one. The number of the resonances is just the number of energy levels of our dot and occur whenever, by tuning v_{gate} , one of the levels is at the Fermi energy. The height of

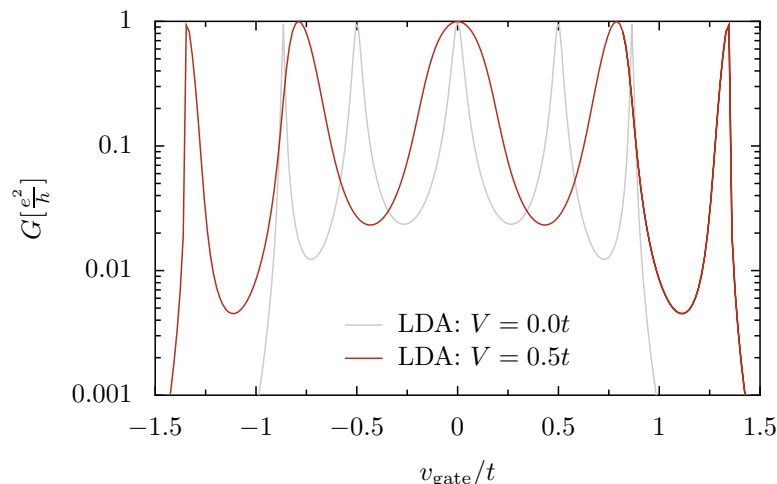


Figure 5.4: Conductance through the small interacting region calculated within the local density approximation for interactions $V = 0$ (grey) and $V = 0.5t = t_{\text{dot}}$ (red).

the maximum of G is determined by the fact that we are dealing with a one-dimensional model without spin and thus have only one transport channel, so that $G = e^2/h$ for resonant scattering. The next observation is the symmetry with respect to $v_{\text{gate}} = 0$ which is caused by the particle-hole symmetry of our model (5.2). If we now compare the interacting with the noninteracting result we see that the resonance peaks are shifted. This shift is equally easy understood. So let us look at the outermost peaks. They occur at the transition from five to four particles or from one to zero particles on the dot. Thus there is no interaction between particles on the dot. However, since the interaction of our system (5.2) is symmetrized,

$$\hat{V} = V \sum_{l=3}^6 \left(\hat{n}_l - \frac{1}{2} \right) \left(\hat{n}_{l+1} - \frac{1}{2} \right) = V \sum_{l=3}^6 \hat{n}_l \hat{n}_{l+1} - V \sum_{l=3}^6 \frac{1}{2} (\hat{n}_l + \hat{n}_{l+1}) + V \cdot \hat{1}, \quad (5.32)$$

we have an additional potential causing this shift. A rough estimate, assuming that the particle is in the potential minimum at the three inner sites, predicts an interaction dependent shift of the resonances by V . This is about the value we find in Figure 5.4. The second peak is not shifted as much since now particle-particle interaction (the first term in (5.32)) cancels part of the potential felt by the second particle or hole.

5.4.2 Local density approximation

In the next two figures we compare the LDA-calculations with more accurate results. In Figure 5.5 we show the number of particles on the quantum dot as a function of the gate voltage at interaction $V = 0.5t = t_{\text{dot}}$. Since this interaction is relatively weak, a self-consistent Hartree-Fock calculation, which we present also in this figure, is still reasonable. The number of particles on the dot carries similar information as the conductance. For example, the positions of the conductance peaks are given by the

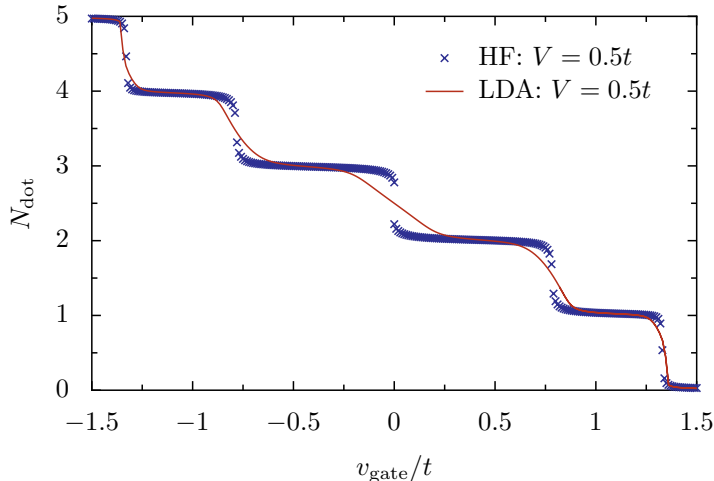


Figure 5.5: Number of particles in the interacting region at interaction $V = 0.5t = t_{\text{dot}}$. We compare results from the local density approximation to a Hartree-Fock calculation.

transitions of the particle number, and the width of the former correspond to the width of the latter. We already see that, although the local density approximation reproduces the positions of the resonances quite well, the width of the inner resonances is far too big. This property of the LDA can be seen more drastically in Figure 5.6, where we set the interaction to $V = 2t = 4t_{\text{dot}}$. For comparison with exact results we have also plotted DMRG results, which we extracted from Figure 3 of [56]. Another problem of the local density approximation at this interaction strength is that the convergence of the calculation is somewhere between rather poor and nonexistent.

How can we explain this extraordinary broadening in LDA? Let us begin with the resonance at $v_{\text{gate}} = 0$. Since our system is particle-hole symmetric it yields a homogeneous half-filled density distribution at exactly this value. If we tune the gate voltage we effectively shift the energy levels of the dot such that the central level is no longer at the Fermi energy and therefore the conductance decreases. Furthermore the central energy level is now either fully occupied or empty. If we are using the local density approximation, an essential ingredient is the exchange-correlation energy which has a minimum at half filling (cf. Fig. 5.7). So, within LDA, the system gains more energy by staying at half filling, compared to the loss of half a particle and the shift by v_{gate} . Thus the local density approximation keeps the central level at the Fermi edge and one expects that the system stays at the resonance condition as long as the gate voltage is smaller than the difference of the exchange-correlation energies at half filling and $\frac{2}{5}$ filling. To corroborate this explanation let us take a look at Figure 5.7. There we have plotted the exchange-correlation energy for the homogeneous interacting system as a function of the density n as it is used for LDA. The black line corresponds to interaction strength $V = 4t_{\text{dot}}$, as in Figure 5.5, while the red line corresponds to Figure 5.6. If we compare the exchange-correlation energies for half and $\frac{2}{5}$ filling, as indicated by the grey dotted lines, we find that the systems energy gain per lattice site is about $\Delta\epsilon^{\text{XC}} = 0.012t_{\text{dot}}$ for

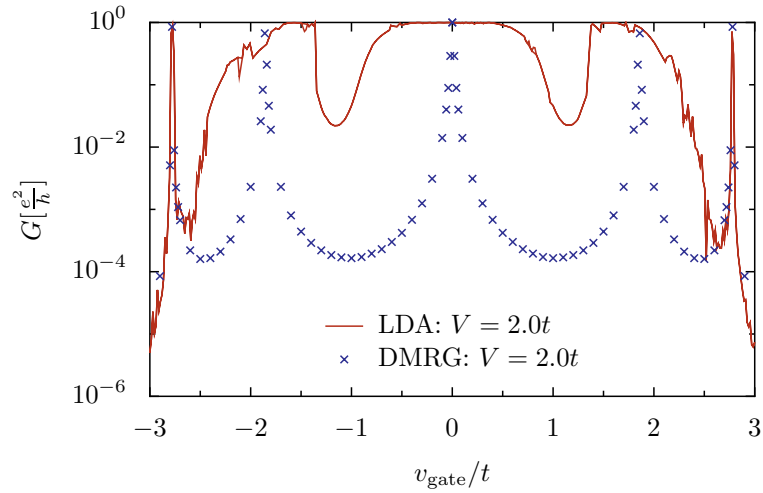


Figure 5.6: Conductance through the small interacting region calculated within the local density approximation for interaction $V = 2t = 4t_{\text{dot}}$. The exact results from DMRG calculations are extracted from Fig. 3 of [56]. Due to convergence problems the quality of the LDA data is rather poor.

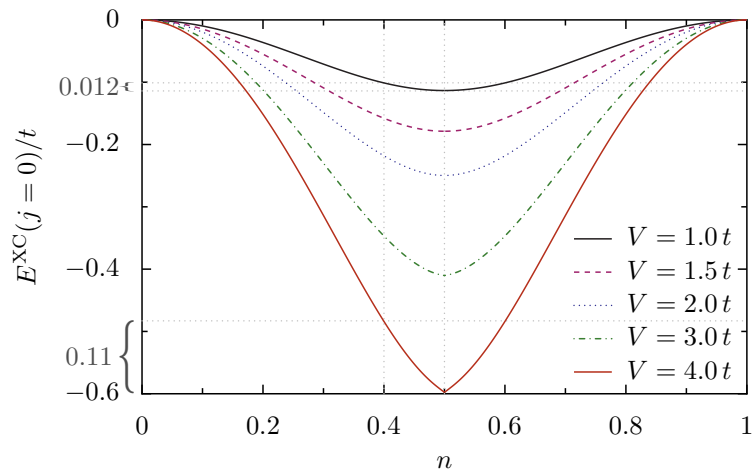


Figure 5.7: Exchange-correlation energy of the homogeneous system, calculated with Bethe ansatz for various interactions. The dotted lines show the differences of the energy between half and $\frac{2}{5}$ filling.

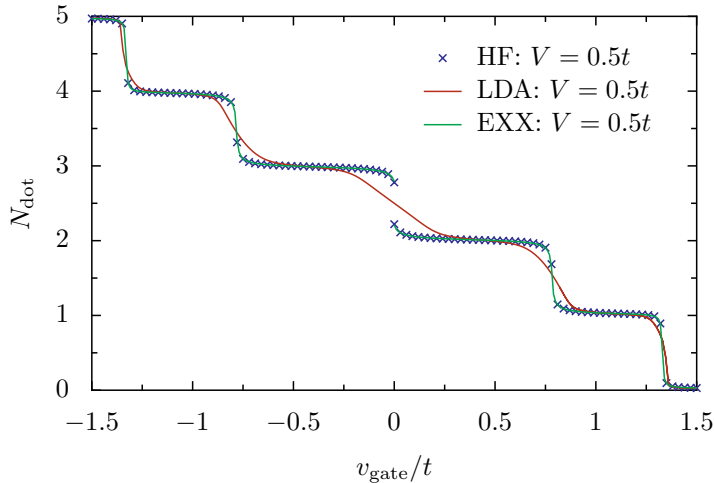


Figure 5.8: Number of particles in the interacting region calculated within the exact-exchange approximation for interaction $V = 0.5t = t_{\text{dot}}$. For comparison results from LDA and Hartree-Fock are included.

$V = t_{\text{dot}}$ and $\Delta\epsilon^{\text{XC}} = 0.11t_{\text{dot}}$ for $V = 4t_{\text{dot}}$. Thus in the latter case the total energy gain for staying at half filling is about $\Delta E^{\text{XC}} = 0.55t_{\text{dot}}$ which gives approximately the half the width of the plateau at $v_{\text{gate}} = 0$. The outer peaks are unaffected by the local density approximation, since in their case there is at maximum only one particle in the interacting region and therefore there is no interaction.

5.4.3 Exact exchange approximation

Having analyzed the deficiencies of the local density approximation we can ask ourselves how to improve the results. In the following we present two ways for improvement: In the next section we use the exact diagonalization procedure, introduced in Chapter 5.2, to determine an exchange-correlation potential which depends non-locally on the densities. Another way to generate such a potential is to use the exact-exchange approximation (3.32), which should be valid for weak interactions. The results can be seen in Figure 5.8. One finds that the steps in occupation are reproduced as good as within the Hartree-Fock approximation.

As the Hartree-Fock approximation the exact-exchange method suffers from a problem when going to higher interactions. If we look at the number of particles on the dot one finds a hysteresis when increasing and decreasing the gate voltage around one of the steps, i. e. the jump from one particle number to another is not occurring at the correct value of v_{gate} , but at lower values when decreasing and at higher values when increasing the gate voltage. In Figure 5.9 we show such a hysteresis, which was obtained from a Hartree-Fock calculation.

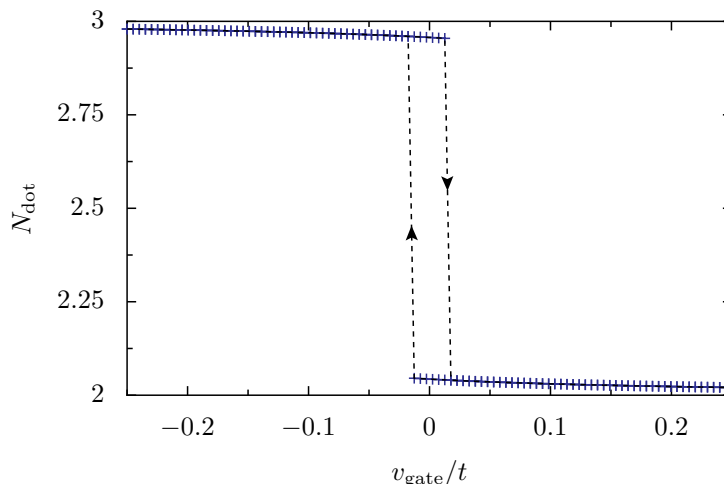


Figure 5.9: Hysteresis in the number of particles as function of the gate voltage as it is seen from a Hartree-Fock calculation. The symbols are the results from the calculation, the dashed lines indicate the hysteresis. The interaction was set to $V = t = 2t_{\text{dot}}$.

5.4.4 Exchange-correlation potentials from exact diagonalization

To evaluate the quality of the exchange-correlation potentials obtained from our exact diagonalization procedure 5.2 we calculate the conductance for relatively weak and strong interactions. The result for the conductance through a weakly interacting system can be seen in Figure 5.10. We see that the widths of the resonances are much closer to the Hartree-Fock result than within the local density approximation. The discrepancies between DFT+ED and Hartree-Fock can be traced back to the following: Though the chosen interaction $V = 0.5t = t_{\text{dot}}$ is relatively weak compared to the value in Figure 5.11, $V = 4t_{\text{dot}}$, it is already strong enough that higher than first order contributions to the Hamiltonian become important. This can be seen from the hysteresis in the conductance or the particle number on the dot when increasing and decreasing the gate voltage, which is absent in an exact calculation. Although it is small this hysteresis is already present for $V = t_{\text{dot}}$ and becomes stronger for stronger interactions.

If we examine the conductance using this method at a strong interaction $V = 4t_{\text{dot}}$ we find Figure 5.11. For comparison we have also included the exact results from a DMRG calculation. We see that the conductance near the resonances is reproduced really good by our nonlocal exchange-correlation potential. Thus we see that it is indeed sufficient to calculate the exchange-correlation potential for the central region and to neglect it at the leads. Since it is also justified to neglect the exchange-correlation kernel in the calculation of the linear conductance for such a system, we may conclude that our exact-diagonalization procedure for the exchange-correlation potential is a suitable method for calculating the transport through a small interacting region even at strong interactions.

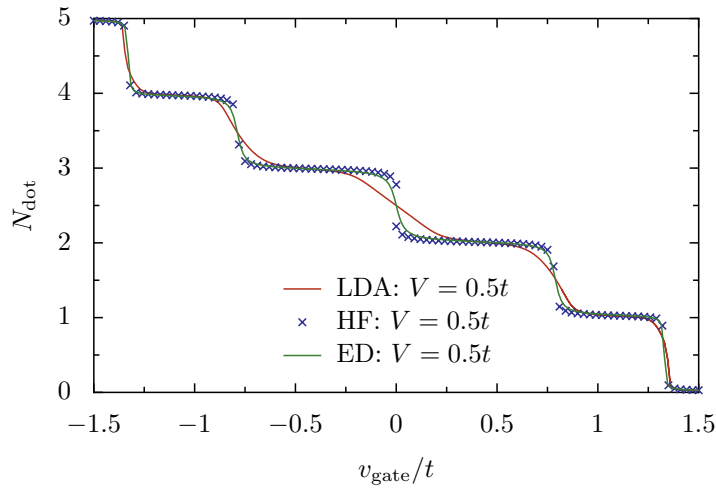


Figure 5.10: Number of particles in the interacting region calculated within DFT+ED for interaction $V = 0.5t = t_{\text{dot}}$. For comparison results from LDA and Hartree-Fock are included.

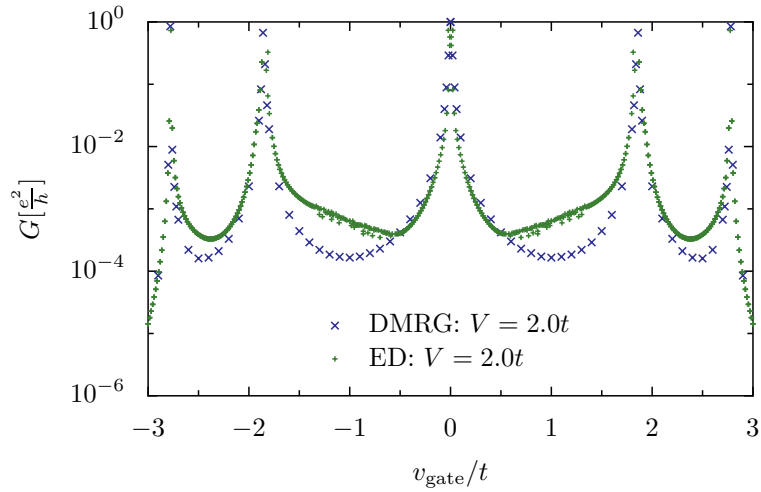


Figure 5.11: Conductance through the small interacting region calculated for interaction $V = 4t_{\text{dot}} = 2t$. The DMRG data was extracted from Fig. 3 of [56].

6 Resumé

In this work we studied one-dimensional lattice models in order to investigate the applicability and accuracy of density functional theory. We focused on the local density approximation (LDA) but also discussed the exact-exchange method, and a new method introduced by us which employs exact diagonalizations of small systems to determine the exchange-correlation potential which depends non-locally on the densities.

In particular, we first studied the static theory and extended it by formulating the current density functional theory (CDFT) on a lattice: CDFT takes not only the potentials but also phase factors in the hopping term into account. Using Legendre transformations we learned how the interaction gives rise to effective single-particle potentials and phases. Within the local density approximation these potentials can efficiently be determined by means of the Bethe ansatz. Using this formalism we recapitulated the band gap problem. We established that derivative discontinuities of the exchange-correlation potential always contribute significantly to the gap. As commonly known we confirmed that LDA underestimates the gap, whereas the exact-exchange method, especially together with a local approximation of the correlation energy, gives quite good results.

Next we studied the phase diagram of the spinless fermion model within the local density approximation. We found that the parameter range where the homogeneous system is unstable is strongly enlarged within LDA compared to the exact solution. Analyzing the density-density correlation function we saw that, as to be expected, LDA becomes exact in the long-wavelength limit but fails near the singularity at $2k_F$, where k_F is the Fermi wave vector. This singularity is important to describe backscattering processes, and accordingly the description of the transmission through a weak impurity fails completely within the local density approximation. This situation is again improved by using the exact-exchange method. We found that this approximation gives a better treatment of the $2k_F$ -singularity, but has an inherent stability problem. This instability gives rise to an exponential renormalization of the Drude weight, while the exact result is an algebraic decrease.

In the next step we introduced the time-dependent version of current density functional theory on the lattice by use of the Keldysh formalism. This formulation allows the treatment of problems with time-dependent potentials and phases. After extending the local density approximation to the adiabatic LDA (ALDA), we turned our attention to the dynamic susceptibility. We found that the inclusion of the current densities into the theory gives rise to a frequency-dependent exchange-correlation kernel. With this new part the dynamic susceptibility becomes exact in the long-wavelength low-frequency limit. In other words, in the long-wavelength limit not only the static susceptibility but also the velocity of the collective excitations is exactly reproduced by C-ALDA. However, we also found that the boundaries of the quasi-particle continuum do not change as a

function of the interaction strength, which does not reflect the true situation.

In the fifth chapter we studied a model consisting of a small interacting region coupled to two leads and calculated the linear conductance through this ‘quantum dot’. To assess the quality of the results obtained from density functional theory, we checked them against results calculated within the Hartree-Fock approximation and with the density matrix renormalization group algorithm. We realized that even for weak interactions the local density approximation dramatically overestimates the width of the resonance peaks. For stronger interactions this leads to a conductance which is several orders of magnitude higher than the true result. The reason for this problem is that the LDA not only favors a homogeneous density profile, but also keeps the quantum dot near half filling. We also found that the exact-exchange approximation gives reasonable results for weak interactions. Another interesting property of this model is that we do not have to take the exchange-correlation kernel into account for the calculation of the conductance, i. e. the internal field due to the interaction can be neglected. This can be done whenever the system has only one transport channel and the Hartree-exchange-correlation potential is negligible at the contacts to the leads.

Since the local density approximation gave poor results, we looked for a way to determine improved exchange-correlation potentials, depending not only on the local density but on all densities of the central region. This can be done by using exact diagonalizations of the central region for the interacting and the single-particle case evaluated at the same densities as the full system. We found that such an exchange-correlation potential improves the conductance dramatically.

Naturally we were not able to answer all open questions, so this work can be extended in several ways: For example, up to now we have considered only systems with one transport channel. One could simply add another channel by including the spin of a particle, which would lead to the Hubbard model. In this case we could still use the Bethe ansatz to determine the exchange-correlation potential within the local density approximation [111]. If we calculate the conductance through a small interacting region within this model we will probably encounter situations where the exchange-correlation kernel cannot be neglected.

The exchange-correlation kernel was discussed in this work only within the adiabatic LDA and the C-ALDA. So in order to generalize the calculation of the conductance to systems with a larger number of channels, where the local density approximation probably still fails, we need for example to evaluate this kernel within the exact-exchange approximation. In this case we could investigate the influence of the exchange-correlation kernel on the conductance. We would also be able to answer the question whether the exact-exchange approximation improves the results for dynamical susceptibility.

So far we have considered only the linear conductance through a quantum dot. A next step would be to go beyond this linear regime and calculate the full I - V -characteristics. This is nowadays often done using the so-called ‘non-equilibrium Green’s functions’ together with the Landauer-Büttiker formalism [49, 50]. However, this approach has two problems: First, it uses the eigenfunctions of the Kohn-Sham Hamiltonian to calculate the Green’s functions, which is not justified within density functional theory. A second difficulty is that the transport through an interacting region is in principle a non-equilibrium

situation. Thus also a non-equilibrium exchange-correlation potential is required. In contrast, recent calculations of the I - V -characteristics use equilibrium potentials only. Therefore it would be most interesting to see how the exchange-correlation potential for a non-equilibrium situation could be determined and how it affects the results.

A Some details of the spinless fermion model

A.1 Jordan-Wigner-Transformation

The Jordan-Wigner transformation [66] is a way to transform a Heisenberg XXZ model

$$-J \sum_l \left(\hat{\sigma}_x^{(l)} \hat{\sigma}_x^{(l+1)} + \hat{\sigma}_y^{(l)} \hat{\sigma}_y^{(l+1)} + \Delta \hat{\sigma}_z^{(l)} \hat{\sigma}_z^{(l+1)} \right) \quad (\text{A.1})$$

into a model of spinless fermions with nearest-neighbor interaction. The relation between the spin- and particle-operators are

$$\begin{aligned} \hat{\sigma}_z^{(l)} &= 2\hat{n}_l - 1 \\ \hat{\sigma}_-^{(l)} &= \exp \left\{ -i\pi \sum_{i=1}^{l-1} \hat{n}_i \right\} \hat{c}_l \end{aligned} \quad (\text{A.2})$$

where $\hat{\sigma}_-^{(l)} = \frac{1}{2}(\hat{\sigma}_x^{(l)} - i\hat{\sigma}_y^{(l)})$. Using this the Heisenberg model can be written as

$$- \underbrace{2J}_t \sum_l (\hat{c}_l^+ \hat{c}_{l+1} + \hat{c}_{l+1}^+ \hat{c}_l) - \underbrace{4J\Delta}_V \sum_l \left(\hat{n}_l - \frac{1}{2} \right) \left(\hat{n}_{l+1} - \frac{1}{2} \right), \quad (\text{A.3})$$

where N is the particle number and L is the lattice size. So we have $J = \frac{t}{2}$ and $\Delta = -\frac{V}{2t}$ where t and V are our usual spinless fermion parameters.

A.2 Bethe ansatz for spinless fermions

A useful and quite general tool for solving one-dimensional systems is the ansatz introduced by Bethe [112]. Some models that have been solved with this ‘Bethe ansatz’ are for example the one-dimensional Bose gas [113, 114], the Heisenberg XXZ magnet [57, 64, 65], the Heisenberg XYZ chain [115] and the Hubbard model [111]. A comprehensive work on this subject and related problems is the book by Korepin, Bogoliubov and Izergin [70].

Since we are basically working with a Heisenberg XXZ model we follow closely Yang and Yang [57] and only translate it into the spinless fermion language. Consider the homogeneous spinless fermion model with nearest-neighbor interaction

$$\hat{H} = -t \sum_l (\hat{c}_l^+ \hat{c}_{l+1} + \hat{c}_{l+1}^+ \hat{c}_l) + V \sum_l \hat{n}_l \hat{n}_{l+1}. \quad (\text{A.4})$$

We are looking for the ground state solution $|\Psi\rangle$ of this Hamiltonian,

$$\hat{H}|\Psi\rangle = E|\Psi\rangle, \quad (\text{A.5})$$

where $|\Psi\rangle$ can be written as

$$|\Psi\rangle = \sum_{x_1, \dots, x_N} \psi(x_1 \dots x_N) \hat{c}_{x_1}^+ \hat{c}_{x_2}^+ \dots \hat{c}_{x_N}^+ |0\rangle. \quad (\text{A.6})$$

Here $|0\rangle$ is the vacuum state and x_1, \dots, x_N are the positions of the N particles. Now look onto an ordered sector of the configuration space with $x_1 < x_2 < \dots < x_N$. Consider a configuration $\langle \text{config} |$ with N particles at positions x_1, \dots, x_N where no pair of particles is located at neighboring sites. Then applying $\langle \text{config} |$ from the left to (A.5) gives

$$-t \sum_{j=1}^N \psi(\dots x_j - 1 \dots) + \psi(\dots x_j + 1 \dots) = E\psi(x_1 \dots x_N). \quad (\text{A.7})$$

If two particles are neighboring, $x_{m+1} = x_m + 1$, we get the equation

$$\begin{aligned} & -t \sum_{\substack{j \neq m \\ j \neq m+1}} [\psi(\dots x_j - 1 \dots) + \psi(\dots x_j + 1 \dots)] + \\ & -t [\psi(\dots x_m - 1, x_m + 1 \dots) + \psi(\dots x_m, x_m + 2 \dots)] \\ & = (E - V)\psi(x_1 \dots x_N). \end{aligned} \quad (\text{A.8})$$

Now we make a plane-wave ansatz for the wave-function:

$$\psi(x_1 \dots x_N) = \sum_{\text{Perm.}} A_{\text{Perm.}} \exp \left\{ i \sum_{j=1}^N p_{\text{Perm}(j)} x_j \right\}. \quad (\text{A.9})$$

The sum goes over all possible permutations of the momenta $\{p_i\}_{i=1 \dots N}$. $A_{\text{Perm.}}$ is a prefactor that depends on the permutation. Inserting this ansatz into (A.7) we get a relation for the energy as in the noninteracting case,

$$E = -2t \sum_{j=1}^N \cos p_j. \quad (\text{A.10})$$

Using this together with (A.8) we obtain

$$\frac{A_P}{A_Q} = -\frac{t + t e^{i(p+q)} + V e^{ip}}{t + t e^{i(p+q)} + V e^{iq}} \quad (\text{A.11})$$

for the ratio of two amplitudes A_P and A_Q , where A_P belongs to a permutation $\dots p, q, \dots$ and A_Q to the same permutation where only p and q are switched. This equation can also be expressed as

$$A_P = -e^{-i\Theta} A_Q, \quad (\text{A.12})$$

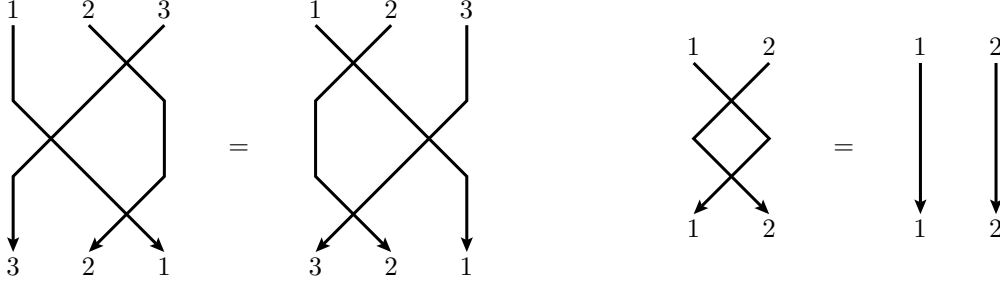


Figure A.1: Graphical representation of the Yang-Baxter equations.

where

$$\Theta(p, q) = 2 \arctan \frac{-\frac{V}{2t} \sin \frac{p-q}{2}}{\cos \frac{p+q}{2} + \frac{V}{2t} \cos \frac{p-q}{2}}. \quad (\text{A.13})$$

So far we have only considered permutations of two neighboring particles. To generalize this finding we need to decompose an arbitrary permutation into a set of two-particle permutations. This only works if the Yang-Baxter equations [116]

$$\begin{aligned} (12)(13)(23) &= (23)(13)(12) \\ (12)(21) &= 1 \end{aligned} \quad (\text{A.14})$$

are fulfilled. The first equation requires that all different decompositions of a general permutation are equivalent. The second states that interchanging two particles twice should have no effect. These equations are depicted in Figure A.1. So in general we get

$$A_P = (-1)^{\#\text{Perm.}} \exp \left\{ -i \sum_{(j,l)} \Theta(p_j, p_l) \right\} A_Q, \quad (\text{A.15})$$

where the sign is determined by the number of needed 2-particle permutations and the sum in the exponential goes over the set of permutations between A_Q and A_P . If we assume periodic boundary conditions

$$\psi(\dots x_j \dots) = \psi(\dots x_j + L \dots) = \psi(\dots x_j \dots) e^{ip_j L} \quad (\text{A.16})$$

we get from (A.15) an equation for the momenta p_j

$$1 = (-1)^{N-1} \exp \left\{ -i \sum_{i=1}^N \Theta(p_j, p_i) \right\} \exp \{-ip_j L\}. \quad (\text{A.17})$$

After taking the logarithm we find

$$p_j L = 2\pi \left(-\frac{N-1}{2} + j - 1 \right) - \sum_{i=1}^N \Theta(p_j, p_i) \quad j = 1 \dots N, \quad (\text{A.18})$$

where the first term is found by taking the logarithm of the factor $(-1)^N = e^{i\pi N + 2\pi j}$. The values of j are chosen such that the solution of this equation gives the ground state. Since the function Θ depends on the momenta this equation has to be solved self-consistently. The ground state energy of the system can then be calculated from (A.10).

If we are investigating a system with a magnetic flux through the one-dimensional ring, this flux leads to an additional phase at the boundary. It is therefore easy to incorporate into the formalism just by introducing an additional phase factor $e^{i\Phi}$ into equation (A.16). This leads to an additional term, Φ , which has to be added to the right hand side of equation (A.18).

B Hohenberg-Kohn theorem

The Hohenberg-Kohn theorem marks the birth of density functional theory [1] by stating that the ground state energy of an interacting many-body system is a unique functional of the density. If such a system is described by the Hamiltonian

$$\hat{H} = \hat{T} + \hat{V} + \int dr v(r) \hat{n}(r), \quad (\text{B.1})$$

where \hat{T} and \hat{V} describe the kinetic and interaction energy and $v(r)$ is the potential, the theorem reads [1]:

The potential $v(r)$ is (up to a trivial additive constant) a unique functional of the density $n(r) = \langle \hat{n}(r) \rangle$.

It is elegantly proofed for nondegenerate ground states by reductio ad absurdum:

Assume that two potentials $v(r), v'(r)$, which differ by more than a constant, lead to the same density $n(r)$. Then the corresponding ground states Ψ and Ψ' are different, because they are the eigenstates of the different Hamiltonian H and H' . Since the ground state minimizes the eigenenergy, we find

$$E' = \langle \Psi' | H' | \Psi' \rangle < \langle \Psi | H' | \Psi \rangle = \langle \Psi | H | \Psi \rangle + \int dr [v'(r) - v(r)] n(r). \quad (\text{B.2})$$

Thus we get

$$E' < E + \int dr [v'(r) - v(r)] n(r), \quad (\text{B.3})$$

and similarly by exchanging primed and unprimed variables

$$E < E' + \int dr [v(r) - v'(r)] n(r). \quad (\text{B.4})$$

Addition of these two expression leads to

$$E + E' < E' + E, \quad (\text{B.5})$$

which contradicts itself.

So we can conclude that a potential $v(r)$ is uniquely determined by the density $n(r)$. Furthermore, since the potential determines the Hamiltonian the density also determines the ground state energy, i. e. it is a unique functional of the density, $E = E[n]$. If the ground state is degenerate, the above reasoning would lead to $E + E' \leq E' + E$, which is no contradiction. In this case or, for example, in spin-density functional theory

the uniqueness is no longer guaranteed. A discussion of this problem can be found for example in [117, 118, 119].

C Legendre transformations within DFT

C.1 Definition

The Legendre transform $g(p)$ of a function $f(x)$ can be defined as [120]

$$g(p) = \max_x \{px - f(x)\}. \quad (\text{C.1})$$

Clearly, a necessary condition for the maximum of this expression is given by

$$\frac{\partial}{\partial x} (px - f(x)) \stackrel{!}{=} 0, \quad (\text{C.2})$$

from where the usual expression for p ,

$$p = \frac{\partial f(x)}{\partial x}, \quad (\text{C.3})$$

follows. However, this condition alone is not sufficient, furthermore we need the convexity of $f(x)$ to ensure the existence of the maximum.

C.2 Existence within the DFT context

Within the context of static density functional theory, the existence of the Legendre transform of the ground state energy can be proved by a variant of the Hohenberg-Kohn theorem [1]. In order to do so we rewrite (C.1) as

$$F[n] = \max_v \left\{ E[v] - \sum_l v_l n_l \right\}, \quad (\text{C.4})$$

where $E[v]$ is the ground state energy as a functional of the potential $v = v_l$ and the densities $n_l = \partial E / \partial v_l$. Please note that we changed the sign ($-f \rightarrow E$), so that $E[v]$ must be concave for the Legendre transform to exist. Concavity is ensured by the condition

$$(1 - \lambda)E[v] + \lambda E[u] < E[(1 - \lambda)v + \lambda u] \quad (\text{C.5})$$

with two different potentials v and u for all parameters λ between 0 and 1. Rewriting the energies as expectation values this condition becomes

$$(1 - \lambda) \langle \Psi_v | H_v | \Psi_v \rangle + \lambda \langle \Psi_u | H_u | \Psi_u \rangle < \langle \Psi_\lambda | H_\lambda | \Psi_\lambda \rangle, \quad (\text{C.6})$$

where the H_v and H_u are the Hamiltonian corresponding to the potentials v and u . Ψ_v and Ψ_u are the respective eigenstates. The Hamiltonian H_λ belongs to the potential

$(1 - \lambda)v + \lambda u$ with the eigenstate Ψ_λ . Rewriting the right hand side in terms of the Hamiltonian H_v and H_u one finds that the functional $E[v]$ is convex if

$$(1 - \lambda) \langle \Psi_v | H_v | \Psi_v \rangle + \lambda \langle \Psi_u | H_u | \Psi_u \rangle < (1 - \lambda) \langle \Psi_\lambda | H_v | \Psi_\lambda \rangle + \lambda \langle \Psi_\lambda | H_u | \Psi_\lambda \rangle. \quad (\text{C.7})$$

On the other hand, assuming nondegenerate ground states, we have $\langle \Psi_v | H_v | \Psi_v \rangle < \langle \Psi_\lambda | H_v | \Psi_\lambda \rangle$ and $\langle \Psi_u | H_u | \Psi_u \rangle < \langle \Psi_\lambda | H_u | \Psi_\lambda \rangle$. Therefore this condition is fulfilled and thus the Legendre transform exists. A similar proof can be found for example in [76].

C.3 V-representability

Given a potential v that leads to a density n , the Hohenberg-Kohn theorem provides that this potential can be uniquely determined by the density. It does not, however, provide the existence of such a potential, i. e. given a certain density it is possible that there exists no potential that leads to this density. The question of v-representability of static systems has been studied for example in [72, 61, 121]. In the noninteracting spinless fermion model a not v-representable density is for example given by

$$n_l = \begin{cases} 0 & \text{if } l \text{ even} \\ 1 & \text{if } l \text{ odd} \end{cases}. \quad (\text{C.8})$$

If for a given density a potential exists the corresponding density is v-representable. The question of v-representability is important for practical applications of DFT since one uses a mapping between the interacting many-particle system and a noninteracting one [2], which should yield the same density as the interacting one. Thus if the interacting density is not v-representable in the noninteracting system density functional theory cannot be applied.

Within the formulation by means of Legendre transformations the problem of v-representability transforms to the questions, whether the functional $F^s[n^s]$ (cf. Eq. (3.6)) exists at the density of the many-body system, $n^s = n$, or in other words, whether the back-transformation $F^s[n] \rightarrow E^s[v^s]$ exists.

D Properties of the dynamical susceptibility

The density and current density response functions obey Onsager's relations:

$$\begin{aligned}\chi_{nn}(l, l', \omega; \{\phi_l\}) &= \chi_{nn}(l', l, \omega; \{-\phi_l\}) \\ \chi_{nj}(l, l', \omega; \{\phi_l\}) &= -\chi_{jn}(l', l, \omega; \{-\phi_l\}) \\ \chi_{jj}(l, l', \omega; \{\phi_l\}) &= \chi_{jj}(l', l, \omega; \{-\phi_l\})\end{aligned}\tag{D.1}$$

The minus sign in the second relation reflects that the current is odd under time reversal. Considering a homogeneous situation we obtain

$$\begin{aligned}\chi_{nn}(q, \omega; \phi) &= \chi_{nn}(-q, \omega; -\phi) \\ \chi_{nj}(q, \omega; \phi) &= -\chi_{jn}(-q, \omega; -\phi) \\ \chi_{jj}(q, \omega; \phi) &= \chi_{jj}(-q, \omega; -\phi)\end{aligned}\tag{D.2}$$

where q is the wave vector. For the single-particle system the explicit results are as follows:

$$\chi_{\mu\nu}^s(q, \omega; \phi) = -\frac{1}{L} \sum_k \frac{n_k - n_{k+q}}{\omega + \epsilon_k - \epsilon_{k+q} + i0} \kappa_{\mu\nu}\tag{D.3}$$

where $\kappa_{nn} = 1$, $\kappa_{nj} = \kappa_{jn} = v_{k+q/2}$, and $\kappa_{jj} = v_{k+q/2}^2$. In addition, $\epsilon_k = -2t \cos(k + \phi)$ is the free-particle dispersion, $v_k = \partial\epsilon_k/\partial k$ the corresponding velocity, and n_k denotes the Fermi function. We note also that

$$\chi_{nj}(q, \omega; \phi) = \chi_{jn}(q, \omega; \phi)\tag{D.4}$$

due to parity symmetry. Particle conservation implies

$$\begin{aligned}\omega \chi_{nn} &= 2 \sin \frac{q}{2} \chi_{nj} \\ \omega^2 \chi_{nn} &= \left[2 \sin \frac{q}{2}\right]^2 \chi_{jj}\end{aligned}\tag{D.5}$$

where we suppressed the argument $(q, \omega; \phi)$ for simplicity. These relations allow writing the density and current response in gauge-invariant form, for example

$$\delta n(q, \omega) = \frac{\chi_{nn}(q, \omega)}{2i \sin \frac{q}{2}} e(q, \omega)\tag{D.6}$$

where $e(q, \omega) = -i\omega \phi(q, \omega) - 2i \sin \frac{q}{2} v(q, \omega)$. Equivalently

$$\delta j(q, \omega) = \frac{\chi_{jj}(q, \omega)}{i\omega} e(q, \omega)\tag{D.7}$$

such that $\omega \delta n(q, \omega) = 2 \sin \frac{q}{2} \delta j(q, \omega)$.

E Transparent boundaries

To calculate transport through a finite system it would be optimal if one could model an open system in such a way that the boundaries are transparent, i. e. that there is no backscattering. In general, this is difficult to achieve. However, if we require only that a particle at the Fermi energy is not backscattered and use an small imaginary potential at the leads, thereby implying a finite lifetime of a particle, we can model our system accordingly.

Consider the Hamiltonian of a lead attached to some real space sites,

$$\hat{H} = -t \sum_l (\hat{c}_l^+ \hat{c}_{l+1} + \hat{c}_{l+1}^+ \hat{c}_l) - \sum_k t_k (\hat{c}_0^+ \hat{c}_k + \hat{c}_k^+ \hat{c}_0) + \sum_k \epsilon_k \hat{c}_k^+ \hat{c}_k. \quad (\text{E.1})$$

The first term describes the hopping on the real space sites, whereas the last term represents the lead. The second terms gives the coupling between the two. In the following we determine the coupling strength t_k to suit our needs. Without backscattering the eigenfunction can be written in the form

$$|\Psi_q\rangle = \sum_l e^{-iql} |l\rangle + \sum_k A_k |k\rangle, \quad (\text{E.2})$$

where $|l\rangle = c_l^+ |0\rangle$ and $|k\rangle = c_k^+ |0\rangle$ with the vacuum state $|0\rangle$. Now applying the Hamiltonian onto this state we find

$$\hat{H} |\Psi_q\rangle = \left(-te^{-iq} - \sum_k t_k A_k \right) |l=1\rangle - 2t \cos q \sum_{l=2,\dots} e^{-iql} |l\rangle + \sum_k (\epsilon_k A_k - t_k) |k\rangle, \quad (\text{E.3})$$

so that $|\Psi_q\rangle$ is an eigenstate if the two conditions

$$\begin{aligned} -te^{-iq} - \sum_k t_k A_k &\stackrel{!}{=} -2t \cos q \\ \epsilon_k A_k - t_k &\stackrel{!}{=} -2t \cos q \end{aligned} \quad (\text{E.4})$$

are fulfilled. If we take the Fermi vector at half filling, $q = \frac{\pi}{2}$, the right hand side becomes zero. Now solving the second equation for A_k and inserting it into the first we get

$$i - \sum_k \frac{t_k^2}{\epsilon_k} = i - \int d\epsilon \mathcal{N}(\epsilon) \frac{t_k^2}{\epsilon} \stackrel{!}{=} 0. \quad (\text{E.5})$$

Here $\mathcal{N}(\epsilon)$ is the density of states at the leads. This condition is fulfilled if

$$\mathcal{N}(\epsilon) \frac{t_k^2}{\epsilon} \stackrel{!}{=} i\delta(\epsilon). \quad (\text{E.6})$$

This equation can be solved if the energy has a small imaginary part which can be set to zero at the end of the calculation. We then see that

$$t_k = \frac{1}{\sqrt{\pi\mathcal{N}(\epsilon_k)}}. \tag{E.7}$$

F Potentials from exact diagonalizations for bulk systems

F.1 Applicability of the exact diagonalization procedure to bulk systems

The main question of this section is, how to generalize the exact diagonalization procedure from Chapter 5.2 to find nonlocal exchange-correlation potentials in bulk systems where the interaction is not confined to a small region. It can be accomplished by using the approximation

$$E^{\text{HXC}}[n] = \sum_l \frac{E_l^{\text{ED}}(n_{l-m}, \dots, n_{l+m})}{M}, \quad (\text{F.1})$$

where $M = 2m + 1$ is the size of the subsystems to be diagonalized exactly. E_l^{ED} is the difference of the ground state energies of the interacting and the noninteracting subsystem evaluated at the densities n_{l-m}, \dots, n_{l+m} , similar to (5.9). The Hartree-exchange-correlation potential is then found to be

$$v_l^{\text{HXC}} = \sum_{i=l-m}^{l+m} \frac{\partial}{\partial n_i} \frac{E_i^{\text{ED}}(n_{i-m}, \dots, n_{i+m})}{M}. \quad (\text{F.2})$$

The most important technical difference to the application of this method to the system with the small interacting region is that now we have to sweep through the complete system and diagonalize a subsystem for every lattice site. Disregarding the limits of numerics, it is obvious that if the size of the subsystem reaches the size of the total system, $M \rightarrow L$, this method becomes exact. However due to numerical limits we have to use small sizes for the subsystem, $M = 3, \dots, 9$. To assess the quality of this approximation we return to our prominent test case of Chapter 3, the static susceptibility, which can be calculated from the density profile of a homogeneous system with a weak impurity at one site. The results for various values of M are shown in Figure F.1. For comparison we also included the results obtained by exact diagonalizations of small systems and results from LDA.

Although this method becomes exact for $M = L$, this approximation is far worse than the local density approximation, for several reasons: The most striking problem is that the static susceptibility in the long-wavelength limit $q \rightarrow 0$ reaches not the correct value but the value of the noninteracting system, $\frac{1}{v_F \pi}$. One also observes that the susceptibility oscillates as a function of q which is also an artifact of the approximation. A more thorough investigation shows that the intersections of the susceptibility with the exact

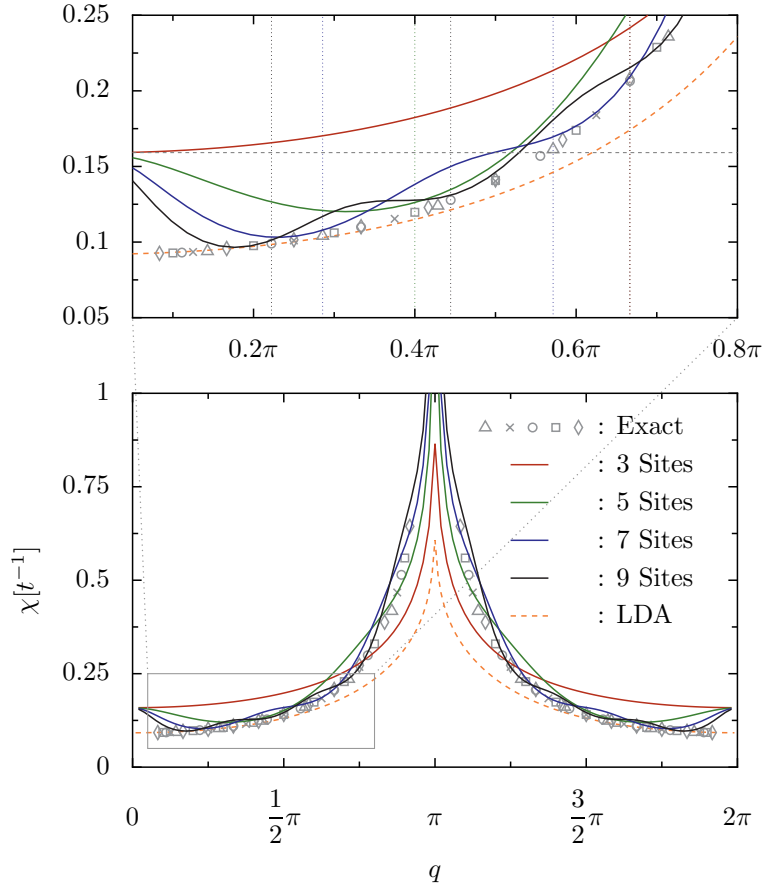


Figure F.1: Static susceptibility of a chain of spinless fermions (size $L = 102$, half filling, interaction $V = 1.0t$) calculated with nonlocal exchange-correlation potentials as defined in equation (F.2). The different colors indicate the system size taken for these diagonalization. The symbols denote values obtained from exact diagonalizations of small systems (sizes: $L = 14, 16, 18, 20, 24$). The upper panel is a detailed view of the region confined by the gray box in the lower panel. The horizontal, dashed grey line in the upper panel at $\chi = \frac{1}{v_F \pi}$ indicates the noninteracting static susceptibility in the $q \rightarrow 0$ limit. The vertical lines are drawn at the q -values of the small systems, depicted with the same color.

values are given by the q -values that exist in the subsystems, $q_S = \frac{2\pi}{M}j$ where $1 \dots M-1$, with the exception of $q_S = 0$.

These peculiarities can be understood as follows: We begin by considering variations of the Hartree-exchange-correlation potential,

$$\delta v_l^{\text{HXC}} = \frac{1}{M} \sum_{x=l-m}^{l+m} [\delta v_l^s(x) - \delta v_l(x)]. \quad (\text{F.3})$$

The parameter x can be understood as the position of the center of a subsystem and thus specifies the subsystem where the potential is taken from. Thus we also have to sum over all subsystems that contain the site l and therefore contribute to the potential. Since we discuss the susceptibility of the homogeneous system in q -space, we need the Fourier transform of δv^{HXC} , which is given by

$$\delta v_q^{\text{HXC}} = \frac{1}{M} \sum_{l=1}^L e^{-iql} \sum_{x=l-m}^{l+m} [\delta v_l^s(x) - \delta v_l(x)]. \quad (\text{F.4})$$

The potentials v_l^s and v_l , determined from a subsystem centered at x depends only on the densities at $x-m, \dots, x+m$. Therefore this expression can be expanded as

$$\delta v_q^{\text{HXC}} = \frac{1}{M} \sum_{l=1}^L e^{-iql} \sum_{x=l-m}^{l+m} \sum_{y=x-m}^{x+m} \left[\frac{\delta v_l^s(x)}{\delta n_y} - \frac{\delta v_l(x)}{\delta n_y} \right] \delta n_y. \quad (\text{F.5})$$

Using the definition of the susceptibility we can replace the two fractions by the inverse of the corresponding susceptibility of the subsystem,

$$\delta v_q^{\text{HXC}} = \frac{1}{M} \sum_{l=1}^L e^{-iql} \sum_{x=l-m}^{l+m} \sum_{y=l-m}^{l+m} \left\{ [\chi_S^s(y-l)]^{-1} - [\chi_S(y-l)]^{-1} \right\} \delta n_y. \quad (\text{F.6})$$

Here we have used the homogeneity of the system twice. First, it is necessary for writing the susceptibility as a function of the difference $y-l$, and second, it enables us to eliminate the index x specifying the subsystem. In particular we choose the subsystem specified by $x=l$. Carrying out the sum over x gives just a factor M and using the substitutions $y \rightarrow y-l$ and $l \rightarrow l+y$ we find

$$\begin{aligned} \delta v_q^{\text{HXC}} &= \sum_{y=-m}^m \left\{ [\chi_S^s(y)]^{-1} - [\chi_S(y)]^{-1} \right\} \sum_{l=1+y}^{L+y} e^{-iq(l-y)} \delta n_l \\ &= \sum_{y=-m}^m e^{iqy} \left\{ [\chi_S^s(y)]^{-1} - [\chi_S(y)]^{-1} \right\} \sum_{l=1}^L e^{-iql} \delta n_l \\ &= \sum_{y=-m}^m e^{iqy} \left\{ [\chi_S^s(y)]^{-1} - [\chi_S(y)]^{-1} \right\} \delta n_q. \end{aligned} \quad (\text{F.7})$$

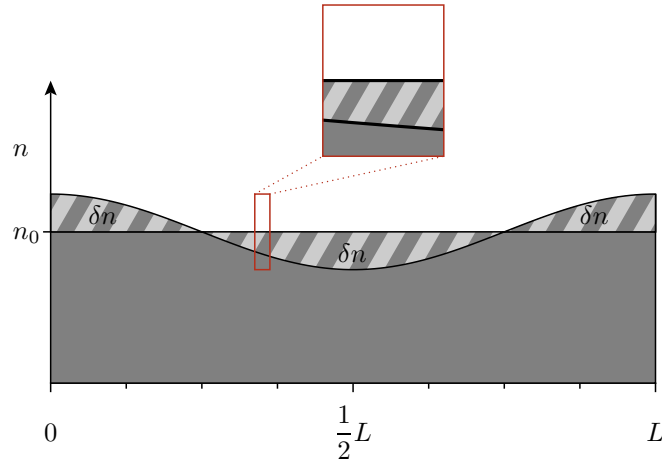


Figure F.2: Schematic of the variations of the homogeneous density in the long-wavelength limit. The magnified region depicts the situation in a small subset of the whole system.

In the step from the first to the second line we used the periodicity of the system and rearranged the elements of the sum, which is then just the Fourier transform of the density-variations. The sum over y also looks like a Fourier transformation but is only in special cases. In general, the values that q can take are determined by the size of the total system, $q = \frac{2\pi}{L}j$ with $j = 0, \dots, L - 1$, whereas the subsystems can take only the values $q_S = \frac{2\pi}{M}j$ with $j = 0, \dots, M - 1$. Thus $q = q_S + q_{\text{remaining}}$ and the sum is a Fourier transformation only if $q_{\text{remaining}} = 0$. In this case we find

$$\delta v_q^{\text{HXC}} = [\chi_S^s(q)]^{-1} - [\chi_S(q)]^{-1} \quad (\text{F.8})$$

and thus for the susceptibility

$$\chi(q) = \frac{\chi^s(q)}{1 + \chi^s(q) \left\{ [\chi_S^s(q)]^{-1} - [\chi_S(q)]^{-1} \right\}}. \quad (\text{F.9})$$

Therefore we expect that χ yields the exact values (except for finite size effects) whenever $q_{\text{remaining}} = 0$. This can be clearly seen in Figure F.1 where vertical lines are plotted at these values. However, according to (F.7), in between those points a crude trigonometric interpolation is used, which is responsible for these oscillations.

Now we are also able to explain the other artifact, χ going to the noninteracting value for $q \rightarrow 0$. The general situation in this limit is depicted in Figure F.2. In this limit the density varies only slowly in real space. Thus, if we choose a particular subsystem, the density profile within this system will be almost constant. On the other hand, as can clearly be seen from the figure, the variations of the density lead to a variation of the number of particles in the subsystems, which is the dominant contribution for $q \rightarrow 0$. Therefore the susceptibilities χ_S^s and χ_S in equation (F.9) are evaluated at $q \equiv 0$ and thus are zero, since the particle numbers are fixed.

F.2 Constructing nonlocal potentials from the exact susceptibility

We have seen that the local density approximation performs poorly when calculating the susceptibility. Now we can ask ourselves, if we can use the exact results of the density response function for small systems to obtain a better exchange-correlation functional. Of course, one may use the exact-exchange approximation, but this method has two problems: First, the inherent instability of the homogeneous system and second, the computational complexity scales very poorly with system size compared to the LDA. It is indeed possible to construct an approximation based on the susceptibility; in fact the limit $q \rightarrow 0$ of such a construction has been used to construct a gradient approximation [74].

We start with the local density approximation for the exchange-correlation energy,

$$E_{\text{LDA}}^{\text{XC}}[n] = \sum_l \epsilon_{\text{LDA}}^{\text{XC}}(n_l) \quad \rightarrow \quad v_l^{\text{XC}} = \left. \frac{\partial \epsilon_{\text{LDA}}^{\text{XC}}}{\partial n} \right|_{n=n_l}. \quad (\text{F.10})$$

Since this approximation is exact in the homogeneous case we construct our approximation around the LDA. Unlike the various flavors of the gradient approximation we do not use the local densities and their gradients but pairs of densities,

$$E^{\text{XC}}[n] = \sum_l \epsilon_1^{\text{XC}}(n_l) + \frac{1}{2} \sum_{l,l'} \epsilon_2^{\text{XC}}(n_l, n_{l'}; l-l'). \quad (\text{F.11})$$

The exchange-correlation potential is then

$$v_l^{\text{XC}} = \frac{\partial \epsilon_1^{\text{XC}}(n_l)}{\partial n_l} + \sum_{l'} \frac{\partial \epsilon_2^{\text{XC}}(n_l, n_{l'}; l-l')}{\partial n_l}. \quad (\text{F.12})$$

Here we have assumed that ϵ_2^{XC} is symmetric under the exchange of l and l' . Earlier we stated that we construct the nonlocal potential around the local density approximation. Hence we choose $\epsilon_1^{\text{XC}} = \epsilon_{\text{LDA}}^{\text{XC}}$. Since the LDA is exact for the homogeneous system we have to construct ϵ_2^{XC} such that it is zero if n_l and $n_{l'}$ are equal to the density of the homogeneous system $\bar{n} = \frac{N}{L}$. The most simple expression satisfying this condition is

$$\epsilon_2^{\text{XC}}(n_l, n_{l'}; l-l') = f_2^{\text{XC}}(\bar{n}, l-l') \cdot (n_l - \bar{n})(n_{l'} - \bar{n}), \quad (\text{F.13})$$

where the quantity f_2^{XC} depends only on the average density (or the particle number) and the distance $l-l'$. As the name suggests this quantity is part of the exchange-correlation kernel of the susceptibility as can be seen in the usual way of writing the variations of the effective single-particle potential in q -space as

$$\delta v_q^s = \delta v_q + \delta v_q^{\text{H}} + \delta v_q^{\text{LDA}} + \delta v_q^{\text{LR}}. \quad (\text{F.14})$$

v_q^{LR} is the Fourier transform of the second term in (F.12) and $f_2^{\text{XC}}(\bar{n}, q) = \frac{\partial v_q^{\text{LR}}}{\partial n_q}$. The acronym LR stands for *linear response*, which is used to determine f_2^{XC} as we will see.

The susceptibility can then be written as

$$\chi(q) = \frac{\chi^s(q)}{1 + \chi^s(q) [2V \cos q + f_{\text{LDA}}^{\text{XC}} + f_2^{\text{XC}}(q)]}. \quad (\text{F.15})$$

If we have an approximation for $\chi(q)$, we can calculate the prefactor of our nonlocal potential

$$f_2^{\text{XC}}(q) = [\chi(q)]^{-1} - [\chi^s(q)]^{-1} - 2V \cos q - f_{\text{LDA}}^{\text{XC}}, \quad (\text{F.16})$$

or in real space

$$f_2^{\text{XC}}(\bar{n}, l - l') = \frac{1}{L} \sum_q e^{iq(l-l')} f_2^{\text{XC}}(\bar{n}, q). \quad (\text{F.17})$$

Using the homogeneous system as input, this exchange-correlation potential should be fairly good even for inhomogeneous systems, as long as the inhomogeneities are within the linear response regime of the homogeneous system.

The connection of this approximation to the gradient expansions can be seen on the basis of equation (F.11), where the second term can be written as

$$E_2^{\text{XC}}[n] = \frac{1}{2} \sum_{l,l'} f_2^{\text{XC}}(l - l') \cdot (n_l - \bar{n})(n_{l'} - \bar{n}) = \frac{1}{2L} \sum_{q \neq 0} f_2^{\text{XC}}(q) \cdot n_{-q} n_q. \quad (\text{F.18})$$

The last equality can be found by inserting the Fourier representation of f_2^{XC} and the densities. Thereby the $q = 0$ term of n_l and \bar{n} cancel each other. Please also note that $f_2^{\text{XC}}(q)$ goes to zero for $q \rightarrow 0$ since this limit is already described by the local density approximation. Using the symmetry $f_2^{\text{XC}}(q) = f_2^{\text{XC}}(-q)$ we see that the lowest order expansion of $f_2^{\text{XC}}(q)$ in powers of q is proportional to q^2 . On the other hand if we use the lowest order gradient expansion (see for example [74]) we have

$$\tilde{E}_2^{\text{XC}}[n] = -\frac{1}{2} \sum_l B \cdot (\nabla n_l)^2 = -\frac{1}{2L} \sum_q q^2 B \cdot n_{-q} n_q, \quad (\text{F.19})$$

where again we inserted the Fourier representation for the densities. Thus we see that the gradient expansion is given by the lowest order term of our nonlocal exchange-correlation potential. On the other hand it is clear that we need an infinite sum of higher order terms to reproduce the singularity at $q = 2k_F$.

Bibliography

- [1] P. Hohenberg, W. Kohn, *Inhomogeneous Electron Gas*, Phys. Rev. **136**, B864 (1964).
- [2] W. Kohn, L. J. Sham, *Self-Consistent Equations Including Exchange and Correlation Effects*, Phys. Rev. **140**, A1133 (1965).
- [3] A. K. Rajagopal, J. Callaway, *Inhomogeneous Electron Gas*, Phys. Rev. B **7**, 1912 (1973).
- [4] G. Vignale, M. Rasolt, *Density-Functional Theory in Strong Magnetic Fields*, Phys. Rev. Lett. **59**, 2360 (1987).
- [5] G. Vignale, M. Rasolt, *Current- and spin-density-functional theory for inhomogeneous electronic systems in strong magnetic fields*, Phys. Rev. B **37**, 10685 (1988).
- [6] G. Diener, *Current-density-functional theory for a non-relativistic electron gas in a strong magnetic field*, J. Phys.: Condens. Matter **3**, 9417 (1991).
- [7] E. Runge, E. K. U. Gross, *Density-Functional Theory for Time-Dependent Systems*, Phys. Rev. Lett. **52**, 997 (1984).
- [8] E. K. U. Gross, W. Kohn, *Local Density-Functional Theory of Frequency-Dependent Linear Response*, Phys. Rev. Lett. **55**, 2850 (1985).
- [9] G. Vignale, W. Kohn, *Current-Dependent Exchange-Correlation Potential for Dynamical Linear Response Theory*, Phys. Rev. Lett. **77**, 2037 (1996).
- [10] R. van Leeuwen, *Causality and Symmetry in Time-Dependent Density-Functional Theory*, Phys. Rev. Lett. **80**, 1280 (1998).
- [11] M. Petersilka, U. J. Gossmann, E. K. U. Gross, *Excitation Energies from Time-Dependent Density-Functional Theory*, Phys. Rev. Lett. **76**, 1212 (1996).
- [12] R. T. Sharp, G. K. Horton, *A Variational Approach to the Unipotential Many-Electron Problem*, Phys. Rev. **90**, 317 (1953).
- [13] J. D. Talman, W. F. Shadwick, *Optimized effective atomic central potential*, Phys. Rev. A **14**, 36 (1976).
- [14] A. Görling, M. Levy, *Exact Kohn-Sham scheme based on perturbation theory*, Phys. Rev. A **50**, 196 (1994).

- [15] T. Grabo, E. K. U. Gross, *Density-functional theory using an optimized exchange-correlation potential*, Chem. Phys. Lett. **240**, 141 (1995).
- [16] M. Städele, M. Moukara, J. A. Majewski, P. Vogl, A. Görling, *Exact exchange Kohn-Sham formalism applied to semiconductors*, Phys. Rev. B **59**, 10031 (1999).
- [17] D. C. Langreth, J. P. Perdew, *Theory of nonuniform electronic systems. I. Analysis of the gradient approximation and a generalization that works*, Phys. Rev. B **21**, 5469 (1980).
- [18] K. Schönhammer, O. Gunnarson, *Difference between the quasiparticle and the Kohn-Sham-Fermi surface*, Phys. Rev. B **37**, 3128 (1988).
- [19] L. J. Sham, M. Schlüter, *Density Functional Theory of the Energy Gap*, Phys. Rev. Lett. **51**, 1888 (1983).
- [20] J. F. Janak, *Proof that $\partial E/\partial n_i = \epsilon_i$ in density-functional theory*, Phys. Rev. B **18**, 7165 (1978).
- [21] J. P. Perdew, M. Levy, *Physical Content of the Exact Kohn-Sham Orbital Energies: Band Gaps and Derivative Discontinuities*, Phys. Rev. Lett. **51**, 1884 (1983).
- [22] O. Gunnarson, K. Schönhammer, *Density-Functional Treatment of an Exactly Solvable Semiconductor Model*, Phys. Rev. Lett. **56**, 1968 (1986).
- [23] K. Schönhammer, O. Gunnarson, *Discontinuity of the exchange-correlation potential in density functional theory*, J. Phys. C: Solid State Phys. **20**, 3675 (1987).
- [24] K. Schönhammer, O. Gunnarson, R. M. Noack, *Density-functional theory on a lattice: Comparison with exact numerical results for a model with strongly correlated electrons*, Phys. Rev. B **52**, 2504 (1995).
- [25] N. A. Lima, M. F. Silva, L. N. Oliveira, K. Capelle, *Density Functionals Not Based on the Electron Gas: Local-Density Approximation for a Luttinger Liquid*, Phys. Rev. Lett. **90**, 146402 (2003).
- [26] C. Verdozzi, *Time-Dependent Density-Functional Theory and Strongly Correlated Systems: Insight from Numerical Studies*, Phys. Rev. Lett. **101**, 166401 (2008).
- [27] G. Xianlong, M. Polini, M. P. Tosi, J. Vivaldo L. Campo, K. Capelle, M. Rigol, *Bethe ansatz density-functional theory of ultracold repulsive fermions in one-dimensional optical lattices*, Phys. Rev. B **73**, 165120 (2006).
- [28] G. Xianlong, M. Rizzi, M. Polini, R. Fazio, M. P. Tosi, J. V. L. Campo, K. Capelle, *Luther-Emery Phase and Atomic-Density Waves in a Trapped Fermion Gas*, Phys. Rev. Lett. **98**, 030404 (2007).
- [29] J. Sólyom, *The Fermi gas model of one-dimensional conductors*, Adv. Phys. **28**, 201 (1979).

-
- [30] H. J. Schulz, *Fermi liquids and non-Fermi liquids*, in Proceedings of Les Houches Summer School LXI, edited by E. Akkermans, G. Montambaux, J. Pichard and J. Zinn-Justin (Elsevier, Amsterdam, 1995), p. 533.
- [31] J. Voit, *One-dimensional Fermi liquids*, Rep. Prog. Phys. **58**, 977 (1995).
- [32] S. J. Tans, M. H. Devoret, H. Dai, A. Thess, R. E. Smalley, L. J. Geerligs, C. Dekker, *Individual single-wall carbon nanotubes as quantum wires*, Nature **386**, 474 (1997).
- [33] M. Bockrath, D. H. Cobden, J. Lu, A. G. Rinzler, R. E. Smalley, L. Balents, P. L. McEuen, *Luttinger-liquid behaviour in carbon nanotubes*, Nature **397**, 598 (1999).
- [34] H. Moritz, T. Stöferle, K. Günter, M. Köhl, T. Esslinger, *Confinement Induced Molecules in a 1D Fermi Gas*, Phys. Rev. Lett. **94**, 210401 (2005).
- [35] I. Bloch, J. Dalibard, W. Zwerger, *Many-body physics with ultracold gases*, Rev. Mod. Phys. **80**, 885 (2008).
- [36] S. Giorgini, L. P. Pitaevskii, S. Stringari, *Theory of ultracold atomic Fermi gases*, Rev. Mod. Phys. **80**, 1215 (2008).
- [37] A. M. Chang, *Chiral Luttinger liquids at the fractional quantum Hall edge*, Rev. Mod. Phys. **75**, 1449 (2003).
- [38] X. Duan, Y. Huang, Y. Cui, J. Wang, C. M. Lieber, *Indium phosphide nanowires as building blocks for nanoscale electronic and optoelectronic devices*, Nature **409**, 66 (2001).
- [39] S. J. Tans, A. R. M. Verschueren, C. Dekker, *Room-temperature transistor based on a single carbon nanotube*, Nature **393**, 49 (1998).
- [40] A. Aviram, M. A. Ratner, *Molecular Rectifiers*, Chem. Phys. Lett. **29**, 277 (1974).
- [41] M. A. Reed, C. Zhou, C. J. Muller, T. P. Burgin, J. M. Tour, *Conductance of a Molecular Junction*, Science **278**, 252 (1997).
- [42] C. Kergueris, J.-P. Bourgoin, S. Palacin, D. Esteve, C. Urbina, M. Magoga, C. Joachim, *Electron transport through a metal-molecule-metal junction*, Phys. Rev. B **59**, 12505 (1999).
- [43] X. D. Cui, A. Primak, X. Zarate, J. Tomfohr, O. F. Sankey, A. L. Moore, T. A. Moore, D. Gust, G. Harris, S. M. Lindsay, *Reproducible Measurement of Single-Molecule Conductivity*, Science **294**, 571 (2001).
- [44] J. Reichert, R. Ochs, D. Beckmann, H. B. Weber, M. Mayor, H. v. Löhneysen, *Driving Current through Single Organic Molecules*, Phys. Rev. Lett. **88**, 176804 (2002).
- [45] A. Nitzan, *Electron transmission through molecules and molecular interfaces*, Annu. Rev. Phys. Chem. **52**, 681 (2001).

- [46] S. Kohler, J. Lehman, P. Hänggi, *Driven quantum transport on the nanoscale*, Phys. Rep. **406**, 379 (2005).
- [47] F. J. Kaiser, P. Hänggi, S. Kohler, *Coulomb repulsion effects in driven electron transport*, Eur. Phys. J. B **54**, 201 (2006).
- [48] F. J. Kaiser, P. Hänggi, S. Kohler, *Molecular electronics in junctions with energy disorder*, New J. Phys. **10**, 065013 (2008).
- [49] S. Kurth, G. Stefanucci, C.-O. Almbladh, A. Rubio, E. K. U. Gross, *Time-dependent quantum transport: A practical scheme using density functional theory*, Phys. Rev. B **72**, 035308 (2005).
- [50] A. Arnold, F. Weigend, F. Evers, *Quantum chemistry calculations for molecules coupled to reservoirs: Formalism, implementation, and application to benzenedithiol*, J. Chem. Phys. **126**, 174101 (2007).
- [51] F. Evers, F. Weigend, M. Koentopp, *Conductance of molecular wires and transport calculations based on density-functional theory*, Phys. Rev. B **69**, 235411 (2004).
- [52] C. Toher, A. Filippetti, S. Sanvito, K. Burke, *Self-Interaction Errors in Density-Functional Calculations of Electronic Transport*, Phys. Rev. Lett. **95**, 146402 (2005).
- [53] M. Koentopp, K. Burke, F. Evers, *Zero-bias molecular electronics: Exchange-correlation corrections to Landauer's formula*, Phys. Rev. B **73**, 121403 (2006).
- [54] S.-H. Ke, H. U. Baranger, W. Yang, *Role of the exchange-correlation potential in ab initio electron transport calculations*, J. Chem. Phys. **126**, 201102 (2007).
- [55] S. M. Lindsay, M. A. Ratner, *Molecular Transport Junctions: Clearing Mists*, Adv. Mater. **19**, 23 (2007).
- [56] P. Schmitteckert, F. Evers, *Exact ground state density functional theory for impurity models coupled to external reservoirs and transport calculations*, Phys. Rev. Lett. **100**, 086401 (2008).
- [57] C. N. Yang, C. P. Yang, *One-Dimensional Chain of Anisotropic Spin-Spin Interactions. I. Proof of Bethe's Hypothesis for Ground State in a Finite System*, Phys. Rev. **150**, 321 (1966).
- [58] F. D. M. Haldane, *'Luttinger liquid theory' of one-dimensional quantum fluids: I. Properties of the Luttinger model and their extension to the general 1D interacting spinless Fermi gas*, J. Phys. C: Solid State Phys. **14**, 2585 (1981).
- [59] S. R. White, *Density Matrix Formulation for Quantum Renormalization Groups*, Phys. Rev. Lett. **69**, 2863 (1992).

-
- [60] S. R. White, *Density-matrix algorithms for quantum renormalization groups*, Phys. Rev. B **48**, 10345 (1993).
- [61] E. H. Lieb, *Density Functionals for Coulomb Systems*, Int. J. Quant. Chem. **24**, 243 (1983).
- [62] R. Fukuda, T. Kotani, Y. Suzuki, S. Yokojima, *Density Functional Theory through Legendre Transformation*, Prog. Theo. Phys. **92**, 833 (1994).
- [63] U. Eckern, P. Schwab, *Normal persistent currents*, Adv. Phys. **44**, 387 (1995).
- [64] C. N. Yang, C. P. Yang, *One-Dimensional Chain of Anisotropic Spin-Spin Interactions. II. Properties of the Ground-State Energy Per Lattice Site for an Infinite System*, Phys. Rev. **150**, 327 (1966).
- [65] C. N. Yang, C. P. Yang, *One-Dimensional Chain of Anisotropic Spin-Spin Interactions. III. Applications*, Phys. Rev. **151**, 258 (1966).
- [66] P. Jordan, E. Wigner, *Über das Paulische Äquivalenzverbot*, Z. Phys. **47**, 631 (1928).
- [67] H.-J. Mikeska, A. K. Kolezhuk, *One-Dimensional Magnetism*, Lect. Notes Phys. **645**, 1 (2004).
- [68] F. D. M. Haldane, *General Relation of Correlation Exponents and Spectral Properties of One-Dimensional Fermi-Systems: Application to the Anisotropic $S = \frac{1}{2}$ Heisenberg Chain*, Phys. Rev. Lett. **45**, 1358 (1980).
- [69] N. Ishimura, H. Shiba, *Dynamical Correlation Functions of One-Dimensional Anisotropic Heisenberg Model with Spin 1/2*, Phys. Rev. **136**, B864 (1964).
- [70] V. E. Korepin, N. M. Bogoliubov, A. G. Izergin, *Quantum Inverse Scattering Method and Correlation Functions* (Cambridge University Press, 1993).
- [71] A. Luther, I. Peschel, *Calculation of critical exponents in two dimensions from quantum field theory in one dimension*, Phys. Rev. B **12**, 3908 (1975).
- [72] M. Levy, *Universal variational functional of electron densities, first-order density matrices, and natural spin-orbitals and solution of the v -representability problem*, Proc. Nat. Acad. Sci. USA **76**, 6062 (1979).
- [73] M. Levy, *Electron densities in search of Hamiltonians*, Phys. Rev. A **26**, 1200 (1982).
- [74] G. F. Giuliani, G. Vignale, *Quantum Theory of the Electron Liquid*, chapter 7, 327–404 (Cambridge University Press, 2005).
- [75] J. Kohanoff, N. I. Gidopoulos, *Density Functional Theory: Basics, New Trends and Applications*, volume 2, chapter 26, 532–568 (John Wiley & Sons, Ltd, Chichester, 2003).

- [76] H. Eschrig, *The Fundamentals of Density Functional Theory* (B. G. Teubner Verlagsgesellschaft Leipzig, 1996).
- [77] M. Dzierzawa, U. Eckern, S. Schenk, P. Schwab, *Current density functional theory for one-dimensional fermions*, in Proceedings of Coherence and Correlations in Nanostructures, Ustron, Polen, Phys. Status Solidi B **246**, 941 (2009).
- [78] J. P. Perdew, A. Zunger, *Self-interaction correction to density functional approximations for many-electron systems*, Phys. Rev. B **23**, 5048 (1981).
- [79] D. Ceperley, *Ground state of the fermion one-component plasma: A Monte Carlo study in two and three dimensions*, Phys. Rev. B **18**, 3126 (1978).
- [80] B. Sutherland, B. S. Shastry, *Adiabatic Transport Properties of an Exactly Soluble One-Dimensional Quantum Many-Body Problem*, Phys. Rev. Lett. **65**, 1833 (1990).
- [81] J. P. Perdew, K. Burke, M. Ernzerhof, *Generalized Gradient Approximation Made Simple*, Phys. Rev. Lett. **77**, 3865 (1996).
- [82] A. Görling, *Orbital- and state-dependent functionals in density-functional theory*, J. Chem. Phys. **123**, 062203 (2005).
- [83] R. O. Jones, O. Gunnarson, *The density functional formalism, its application and prospects*, Rev. Mod. Phys. **61**, 689 (1989).
- [84] N. W. Ashcroft, N. D. Mermin, *Solid State Physics* (Thomson Learning, 1976).
- [85] D. W. Hess, J. W. Serene, *Quasiparticle band structure and density-functional theory: Single-particle excitations and band gaps in lattice models*, Int. J. Quant. Chem. **69**, 265 (1998).
- [86] S. Schenk, M. Dzierzawa, P. Schwab, U. Eckern, *Successes and failures of Bethe Ansatz Density Functional Theory*, Phys. Rev. B **78**, 165102 (2008).
- [87] A. Görling, *Exact Exchange Kernel for Time-Dependent Density-Functional Theory*, Int. J. Quant. Chem. **69**, 265 (1998).
- [88] A. Görling, *Exact exchange-correlation kernel for dynamic response properties and excitation energies in density-functional theory*, Phys. Rev. A **57**, 3433 (1998).
- [89] P. Schmitteckert, T. Schulze, C. Schuster, P. Schwab, U. Eckern, *Anderson Localization versus Delocalization of Interacting Fermions in One Dimension*, Phys. Rev. Lett. **80**, 560 (1998).
- [90] C. L. Kane, M. P. A. Fisher, *Transport in a One-Channel Luttinger Liquid*, Phys. Rev. Lett. **68**, 1220 (1992).
- [91] K. A. Matveev, D. Yue, L. I. Glazman, *Tunneling in One-Dimensional Non-Luttinger Electron Liquid*, Phys. Rev. Lett. **71**, 3351 (1993).

-
- [92] W. Kohn, *Theory of the Insulating State*, Phys. Rev. **133**, A171 (1964).
- [93] B. S. Shastry, B. Sutherland, *Twisted Boundary Conditions and Effective Mass in Heisenberg-Ising and Hubbard Rings*, Phys. Rev. Lett. **65**, 243 (1990).
- [94] R. A. Molina, P. Schmitteckert, D. Weinmann, R. A. Jalabert, G.-L. Ingold, J.-L. Pichard, *Residual conductance of correlated one-dimensional nanosystems: A numerical approach*, Eur. Phys. J. B **39**, 107 (2004).
- [95] M. A. L. Marques, C. A. Ullrich, F. Nogueira, A. Rubio, K. Burke, E. K. U. Gross, editors, *Time-Dependent Density Functional Theory, Lecture Notes in Physics*, volume 706 (Springer, Berlin Heidelberg, 2006).
- [96] R. van Leeuwen, *Key Concepts in Time-Dependent Density-Functional Theory*, Int. J. Mod. Phys. B **15**, 1969 (2001).
- [97] L. V. Keldysh, *Diagram Technique for nonequilibrium processes*, Sov. Phys. JETP **20**, 1018 (1965).
- [98] J. Rammer, H. Smith, *Quantum field-theoretical methods in transport theory of metals*, Rev. Mod. Phys. **58**, 323 (1986).
- [99] E. K. U. Gross, C. A. Ullrich, U. J. Gossmann, *Density Functional Theory, NATO ASI Series*, volume B337 (Plenum Press, New York, 1995).
- [100] E. K. U. Gross, J. F. Dobson, M. Petersilka, *Density Functional Theory* (Springer, 1996).
- [101] G. Vignale, C. A. Ullrich, S. Conti, *Time-Dependent Density Functional Theory Beyond the Adiabatic Local Density Approximation*, Phys. Rev. Lett. **79**, 4878 (1997).
- [102] P. L. de Boeji, F. Kootstra, J. A. Berger, R. van Leeuwen, J. G. Snijders, *Current density functional theory for optical spectra: A polarization functional*, J. Chem. Phys. **115**, 1995 (2001).
- [103] M. Petersilka, E. K. U. Gross, *Excitation energies from Time-Dependent Density Functional Theory Using Exact and Approximate Potentials*, Int. J. Quant. Chem. **80**, 534 (2000).
- [104] F. Aryasetiawan, O. Gunnarson, A. Rubio, *Excitation energies from time-dependent density-functional formalism for small systems*, Europhys. Lett. **57**, 683 (2002).
- [105] M. Hellgren, U. von Barth, *Linear density response function within the time-dependent exact-exchange approximation*, Phys. Rev. B **78**, 115107 (2000).
- [106] H. O. Wijewardane, C. A. Ullrich, *Real-Time Electron Dynamics with Exact-Exchange Time-Dependent Density-Functional Theory*, Phys. Rev. Lett. **100**, 056404 (2008).

- [107] Y. Shigeta, K. Hirao, S. Hirata, *Exact-exchange time-dependent density-functional theory with the frequency-dependent kernel*, Phys. Rev. A **73**, 010502 (2006).
- [108] Y.-H. Kim, A. Görling, *Excitonic Optical Spectrum of Semiconductors Obtained by Time-Dependent Density-Functional Theory with the Exact-Exchange Kernel*, Phys. Rev. Lett. **89**, 096402 (2002).
- [109] R. G. Pereira, S. R. White, I. Affleck, *Exact Edge Singularities and Dynamical Correlations in Spin-1/2 Chains*, Phys. Rev. Lett. **100**, 027206 (2008).
- [110] J. P. Perdew, R. G. Parr, M. Levy, J. Jose L. Balduz, *Density-Functional Theory for Fractional Particle Number: Derivative Discontinuities of the Energy*, Phys. Rev. Lett. **49**, 1691 (1982).
- [111] E. H. Lieb, F. Y. Wu, *Absence of Mott Transition in an Exact Solution of the Short-Range, One-Band Model in One Dimension*, Phys. Rev. Lett. **68**, 1445 (1968).
- [112] H. Bethe, *Zur Theorie der Metalle. I. Eigenwerte und Eigenfunktionen der linearen Atomkette*, J. Phys.: Condens. Matter **3**, 9417 (1931).
- [113] E. H. Lieb, W. Liniger, *Exact Analysis of an Interacting Bose Gas. I. The General Solution and the Ground State*, Phys. Rev. **130**, 1605 (1963).
- [114] E. H. Lieb, *Exact Analysis of an Interacting Bose Gas. II. The Excitation Spectrum*, Phys. Rev. **130**, 1616 (1963).
- [115] R. J. Baxter, *One-Dimensional Anisotropic Heisenberg Chain*, Phys. Rev. Lett. **26**, 834 (1971).
- [116] C. N. Yang, *S-Matrix for the One-Dimensional N-Body Problem with Repulsive or Attractive δ -Functions Interaction*, Phys. Rev. **168**, 1920 (1968).
- [117] K. Capelle, G. Vignale, *Nonuniqueness of the Potentials of Spin-Density-Functional Theory*, Phys. Rev. Lett. **86**, 5546 (2001).
- [118] C. A. Ullrich, *Nonuniqueness in spin-density-functional theory on lattices*, Phys. Rev. B **72**, 073102 (2005).
- [119] K. Capelle, C. A. Ullrich, G. Vignale, *Degenerate ground states and nonunique potentials: Breakdown and restoration of density functionals*, Phys. Rev. A **76**, 012508 (2007).
- [120] R. T. Rockafellar, *Convex Analysis* (Princeton University Press, 1970).
- [121] W. Kohn, *v -Representability and Density Functional Theory*, Phys. Rev. Lett. **51**, 1596 (1983).

Acknowledgements

At this point I would like to thank all the people that contributed in one way or another to this thesis.

Especially, I would like to thank *Prof. Dr. Ulrich Eckern* for giving me the opportunity to join his group and work on such an interesting field as the foundations of density functional theory.

A great many thanks go to *Priv.-Doz. Dr. Peter Schwab* for supervising this thesis. His advice and the many discussions have been very helpful for my understanding of physics in general and the intricacies of density functional theory in particular.

I would also like to thank *Prof. Dr. Gert-Ludwig Ingold* for acting as second referee of this thesis.

I am also obliged to *Dr. Michael Dzierzawa* for sharing his deep knowledge of numerics and for double-checking some of my numerical results.

My special thanks go to *Franz Kaiser* for many stimulating discussions about physics and the rest of life.

Many thanks to *Dr. Cosima Schuster* for her insight into the DFT calculations for real world materials.

I would also like to thank *Ralf Utermann* for keeping the compute cluster in good shape.

Finally, I would like to thank the members of both groups, *Theoretische Physik I* and *Theoretische Physik II*, for a most pleasant atmosphere.

Curriculum vitae

Name: Stefan Schenk

Geburtsdatum: 21.09.1979

Geburtsort: Starnberg

Ausbildung:

Seit 2006: Wissenschaftlicher Mitarbeiter bei Prof. Dr. U. Eckern am
Lehrstuhl für Theoretische Physik II, Universität Augsburg

2000-2006: Studium der Physik an der Universität Augsburg,
Abschluss als Diplom-Physiker

1999-2000: Zivildienst

1990-1999: Besuch des Gymnasiums Donauwörth,
Abschluss mit Abitur

